Doctoral Dissertation

博士論文

Frequency response data-driven disturbance observer design by convex optimization -Experimental verification with a non-minimum phase motion stage

（外乱オブザーバの凸最適化を用いた周波数応答データ駆動設計法の研究
-非最小位相系の位置決めステージによる実験検証）

by

37-177269 汪暁柯 **(Xiaoke Wang)**

Dissertation Submitted to

Department of Electrical Engineering and Information Systems

for the Degree of

Doctor of Philosophy

at

The University of Tokyo

Submitted: December 01, 2020

Supervisor:
Professor Takafumi Koseki

Abstract

Unavoidable disturbances that include external disturbances as well as the unmodeled dynamics downgrade the performance of industrial control systems and thus, disturbance rejection has been an essential objective in control field. Compared to feedback scheme of disturbance rejection, a feedforward method which directly counteracts the influence of disturbance but requires its dynamics acts faster and disturbance can be well-rejected. However, since the dynamics of disturbance are normally unknown, observer-based disturbance rejection methods, which utilize the estimation of disturbances, have been well-established among which disturbance observer is an efficient tool.

Disturbance observer-based disturbance rejection system utilizes the estimated disturbance created by the nominal plant inversion to compensate the influence of real disturbances. Simple structure yet efficient disturbance rejection performance has made disturbance observer be applied to many engineering applications. Despite its wide application, the design of a disturbance observer tends to be intuitive and relies on designers' experience to a large extent. Furthermore, for non-minimum phase systems which consist of unstable zeros and/or time delay that leads to special characteristics, such as unstable inversion or limitation on sensitivity function, disturbance observer design has become more difficult.

Frequency response data-based controller design, which is an alternative of model-based controller design and considers all the information of frequency response data rather than identified parametric model, has appeared as a promising way of designing larger bandwidth controllers. By formulating the controller design specification into optimization constraints, parameters of the controller can be tuned by optimization algorithms.

Inspired by the above analysis, frequency response data-based low pass filter design has been conducted and further extended to identify the nominal plant model and design low pass filter simultaneously in both continuous domain and discrete domain.

Disturbance observer design has been firstly formulated into a non-linear optimization problem in which non-convex constraints, such as constraint for guaranteeing stability margins, has been represented by mathematical equations. Then the transformation process from non-convex optimization problem to convex optimization problem, more specifically, conic optimization problem, has been given in detail. During this process, techniques such as Schur Complement as well as the linear approximation have been extensively employed and since the transformation process is mathematical calculation-based and transformed constraints are the sufficient condition of original non-convex constraints, the optimal point of newly-obtained convex optimization problem undoubtedly satisfies the original non-convex optimization also. Additionally, proposed methods set requirements on neither low pass filter nor on the plant model, *i.e.*, it is applicable to both low-order and high-order low pass filter designs for minimum phase as well as non-minimum phase plants.

Extensive case study results have been provided to verify the feasibility of proposal for different design

scenarios which are classified based on the relative order of nominal plant model and whether plant is non-minimum phase as well as whether nominal plant model is to be simultaneously identified or not. Optimized disturbance observers have satisfied all the predefined constraints. Also, identification of plant model simultaneously with design of low pass filter has provided the largest bandwidth which verifies the necessity of adjusting plant model together. Moreover, the comparison with existing methods has been carried out and results have confirmed the superiority of proposal in terms of design effort along with obtained bandwidth.

Finally, experimental applications to a non-minimum phase motion stage have successfully obtained satisfactory disturbance rejection performance and validated the efficacy of proposed methods.

Acknowledgments

My deepest gratitude goes first and foremost to my supervisor, Professor Takafumi Koseki, for his patient guidance and expert suggestions on this research work as well as his constant encouragement and concern related to daily life. I am grateful to him for selecting me to join his prestigious laboratory. He has not only taught me technical knowledge but also a way to become a good researcher and his knowledgeable but modest personality has left an incredible mark in my life. Despite his busy schedule, he has always managed time for technical discussions and for providing personal guidance. Discussions with him have altered my way of thinking about control engineering and electric machines as well as about being a researcher. Without his kind help and encouragement, I could not have completed my doctoral course here.

I am also humbly grateful to Assistant Professor Wataru Ohnishi. He has guided me to enter motion control field and his profound knowledge in control has enlightened me. I want to thank him for the patient guidance and instructions not only in technical discussions but also in paper writing, presentations as well as in technical visits. Even when he was abroad, he still managed to arrange the tele-meeting to help me polish my theoretical research as well as the experiment. Without his consistent and illuminating instructions, this thesis could not have reached its present form.

I am grateful to Professor Yoichi Hori, Professor Hiroshi Fujimoto, Professor Takashi Kubota, Professfor Hitoshi Tsunashima (Nihon Univeristy), who are members of the evaluation committee of my doctoral degree along with Professor Takafumi Koseki. I thank them for their constructive and insightful comments on this work.

I am specially thankful to Dr. Houng-Joong Kim (Kovery Company Ltd.) for his suggestions on the design of my experimental test bench and its manufacturing as well as its setup. The experiment could not have gone smoothly without his generous help.

Special thanks goes to Dr. Ahmed Salman, my senior in Koseki Lab, for not only offering many enlightening suggestions on my research but also on my daily life. Even after his graduation, he continues to help me on hardware knowledge. I am forever grateful to be friends with him and his family in Tokyo.

I want to express my gratitude to other members of Koseki lab who have made my stay at Koseki lab enjoyable. Matsuzaki san has always been kind to provid me with warm support not only in lab activities but also in my daily life. Takada san, Takeda san, Miyoshi san and Mizoguchi san have helped me in dealing with Japanese documents, software problems as well as the experimental setup. Interactions with Varsha san, Saini san, Han Xu and Feng Zhe were always delightful and relaxing. I am grateful to have met such kind and friendly people here and thank them for their help during my stay.

I want to convey my gratitude to China Scholarship Council (CSC) for providing me a chance to experience foreign culture and the financial support during my course study. Additionally, part of this work has been supported by the Japan Society for the Promotion of Sciences (JSPS) KAKENHI Grant Num-

ber 18H05902 and the Telecommunications Advancement Foundation as well as Nagamori Foundation. I extend my sincere gratitude to them also.

Lastly, my love and gratitude goes to my dearest parents for their continuous support and encouragement. Daily conversations with them have helped me in coming out of depression phase and in keeping my stress levels under control.

Contents

List of Figures

List of Tables

Chapter 1

Introduction

1.1 Background of disturbance rejection control

Disturbances including external disturbances as well as plant uncertainties are unavoidable in many engineering applications, such as spacecraft [1], process industry [2]. In the mechanical control community, the system performance can be influenced by disturbances such as variations of load torque, the parameter perturbations caused by the change of operating conditions as well as working environment [3] [4] [5] [6].

Existence of disturbance influences the performance and sometimes stability of control systems [7] [8], thus disturbance rejection is of significant importance and one of the key objectives in control system design. To ensure the performance of system under the influence of disturbances, *e.g.* robust stability and robust performance, generally two types of methods are employed [9].

One way is to design disturbances-tolerant controllers, which means designed controllers should guarantee the required performance if some bounded disturbances appear, such as internal model control [10] and robust control [11]. However, such controllers use feedback scheme to realize disturbance rejection which does not directly react to the disturbance and may not be fast enough when strong disturbance exists.

The other is to counteract disturbances by measuring or estimating the disturbance and further compensating its influences [12]. If a perfect model of disturbance and its effect on the controlled plant are known which are strict settings, feedforward method can reject the influences of disturbance. However, in most of the time, disturbances are unknown and unmeasurable which makes feedforward controller paradigm impractical and leads to the idea of estimating disturbance by observers, *e.g.* extended state observer ([13]), uncertainty and disturbance estimator ([14]) and so on, among which disturbance observer (DOB) proposed in [15] has become one of the most widely used tools and will be further introduced in section 1.3.

1.2 Non-minimum phase system

1.2.1 Definition

Minimum phase (mp) systems, which do not contain any unstable zero or time delay, have the minimum phase lag when the magnitude is given. In contrast, non-minimum phase (nmp) systems, which refer to systems containing unstable zeros and/or time delays, can be found in industrial applications such as hard disk drive (HDD, [16]) and high precision positioning stage [17] [18] and have special characteristics

as introduced in the following section.

1.2.2 Characteristics

① Undershoot

Undershoot has appeared as a typical characteristic of non-minimum phase systems as shown in Fig. 1.1. Furthermore, the number of zero-crossings is same as the number of real unstable zeros [19] [20].

② Unstable inversion caused by unstable zero

If a plant has unstable zero(s), inversion of it is unstable since unstable zero becomes unstable pole which is straightforward. In addition, since time delay can be transformed into Eq. (1.1) by first order *Padé* approximation [21], the inversion of system containing time delays also presents to be unstable.

$$e^{-\tau s} \simeq \frac{1-\tau s}{1+\tau s}, \tag{1.1}$$

in which τ is the time constant [s].

Unstable inversion leads to internal stability problem if the inversion is used in controller design, such as disturbance observer which will be introduced in the following section.

③ Phase delay

Compared to its counterpart, *i.e.* minimum phase systems, non-minimum phase systems have an additional phase delay which can be explained by Eq. (1.2) (take one unstable zero case as an example).

$$G_{nmp} = G_{mp} \times \underbrace{\frac{-s+\alpha}{s+\alpha}}_{\substack{\text{allpass} \\ \text{function}}}, \ \angle G_{nmp} = \angle G_{mp} - 2\angle(s+a), \tag{1.2}$$

in which α is the unstable zero of G_{nmp}; G_{mp} and G_{nmp} represent for random transfer functions of a non-minimum phase plant and the corresponding minimum phase plant respectively.

In order to build a straightforward impression, G_{mp} and G_{nmp} has been selected as the following example and Nyqusit plots are shown in Fig. 1.2.

$$G_{nmp} = \frac{2}{s(s+2)} \times \frac{-s+6}{s+6}, \ \angle G_{nmp} = \angle G_{mp} - 2\angle(s+6). \tag{1.3}$$

Phase delay caused by unstable zeros and/or time delay sets an upper limit for feedback bandwidth ($\omega_c > 2|\alpha_0|$ ([22]) in which α_0 is an unstable zero).

④ Sensitivity function limitation

The Bode integral formula or waterbed effect ([23]), which represents the limitation for sensitivity function for minimum phase systems as well as non-minimum phase systems are shown in Eq. (1.4). For minimum phase systems, area of $|S(j\omega)| < 1$ should be equal to the area of $|S(j\omega)| > 1$ (blue area equals to pink area in Fig. 1.3) while in non-minimum phase systems, the existence of unstable zeros adds the weight of $|S(j\omega)| > 1$ area which can be understood from the example in Fig. 1.4. The influence caused by existence of unstable zeros limits the disturbance rejection performance.

$$\text{minimum phase system case} : \int_0^\infty log|S(j\omega)|d\omega = 0, \tag{1.4}$$

$$\text{non-minimum phase system case} : \int_0^\infty log|S(j\omega)|d\omega = \pi \sum \alpha_{nmp}. \tag{1.5}$$

in which α_{nmp} are unstable zeros.

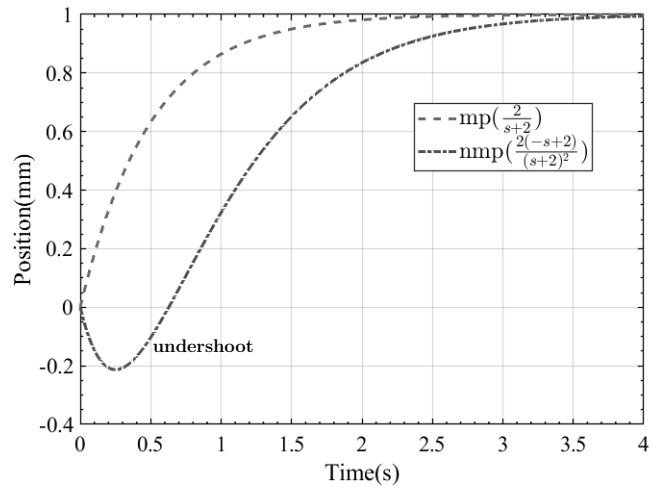

Figure 1.1 Examples of step responses for a minimum phase system and a non-minimum phase system

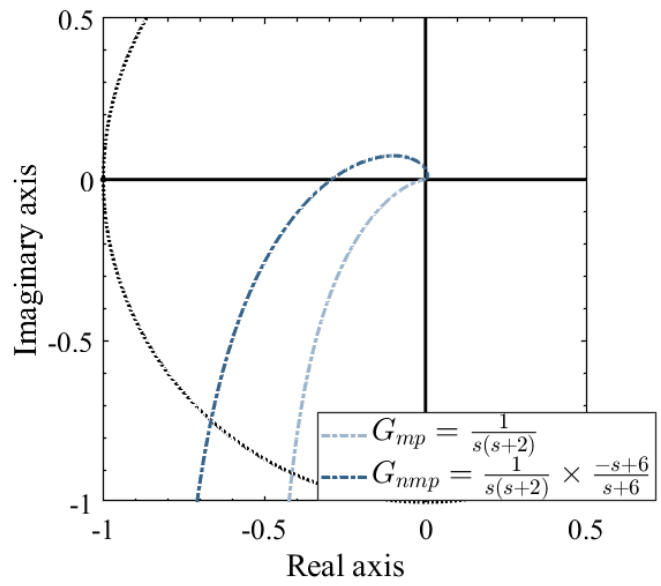

Figure 1.2 Locally enlarged Nyquist plots of G_{mp} and G_{nmp}

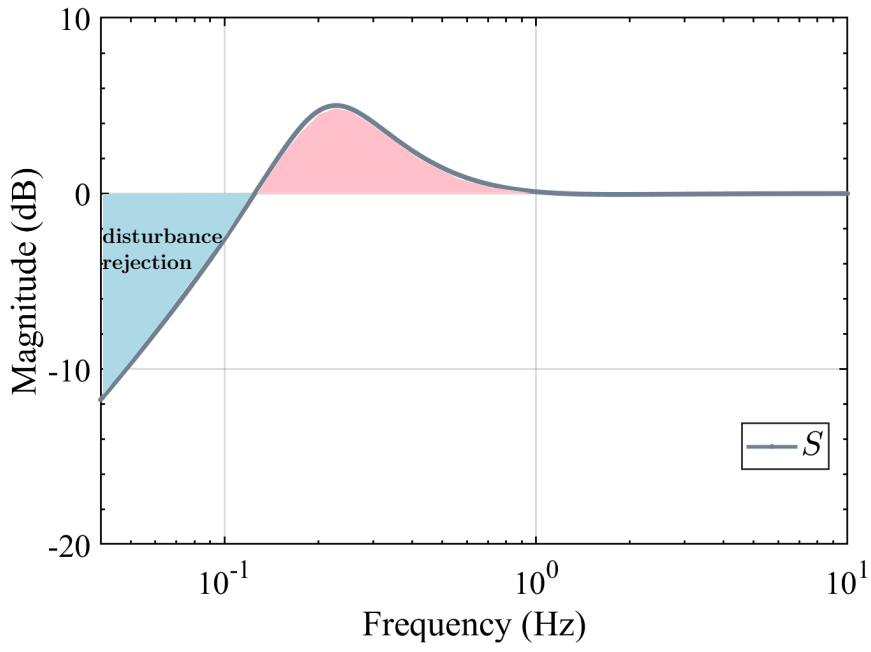

Figure 1.3 Explanation for Bode integral formula

1.3 Review on disturbance observer

Despite the simple structure which will be introduced in detail in the following section, disturbance observer (DOB) has been widely applied to engineering systems spanning from automation [24] [25], hard disk drive [26], mechatronics [27], aircraft [28] to cutting-edge robots [29] [30] and so on. Furthermore, several commercial motion control products based on DOB are available in the market [31] [32], such as Panasonic's MINAS-A5 series motor drivers [31].

1.3.1 Basic idea of disturbance observer control system

In Fig. 1.5 that showing the basic idea of DOB, P_r and P_n represent the real physical plant and nominal plant model. Signals u_a, u_p and y are the control input, plant input and system output, respectively. Signal d is the lumped external disturbance and $\hat{d}$ is the estimated disturbance which is the difference between reproduced plant input ($\hat{u_p}$) ,which is obtained by utilizing P_n^{-1}, and input signal u.

Since P_n^{-1} is not causal, low pass filter, which is generally called as Q filter, is employed to guarantee the causality of the whole system in practical. The reason for choosing low pass filter is because the to-be-rejected disturbance is usually of low or medium frequency, whereas the sensor noise is of medium or high frequency.

The following analysis can be obtained from Fig. 1.5.

1. disturbance estimation

$$\hat{d} = \frac{(P_r P_n^{-1} - 1)Q}{1 - Q + P_r P_n^{-1} Q} u + \frac{P_r P_n^{-1} Q}{1 - Q + P_r P_n^{-1} Q} d. \tag{1.6}$$

   (a) When no external disturbance works on the system and nominal plant is exactly the real plant, estimated disturbance is 0.

   (b) When nominal plant is accurate but external disturbance exists, $\hat{d} = Qd$ holds which means disturbance estimation is precise within the bandwidth of Q filter.

2. transfer functions $G_{u_a y}$ (from u_a to y) and G_{dy} (from d to y)

$$G_{u_a y} = \frac{P_r P_n}{Q(P_r - P_n) + P_n}, G_{dy} = \frac{P_r P_n (1 - Q)}{Q(P_r - P_n) + P_n}. \tag{1.7}$$

   (a) In the frequency range of $Q \cong 1$ (low frequency), $G_{u_a y} = P_n$ and $G_{dy} = P_n(1 - Q)$ hold which indicates that the system behaves as the nominal plant [3] [33].

   (b) In the frequency range of $Q \cong 0$ (high frequency), $G_{u_a y} = P_r$ and $G_{dy} = P_r(1 - Q)$ hold which shows the system works as real plant.

3. sensitivity function S and complementary sensitivity function T

$$S = \frac{P_n(1 - Q)}{Q(P_r - P_n) + P_n}, T = \frac{P_r Q}{Q(P_r - P_n) + P_n}. \tag{1.8}$$

   (a) When nominal plant is accurate, $S = 1 - Q$ and $T = Q$ hold.

   (b) In the frequency range of $Q \cong 1$ (low frequency), $S \cong 0$ and $T \cong 1$ hold whereas when $Q \cong 0$, $S \cong 1$ and $T \cong 0$.

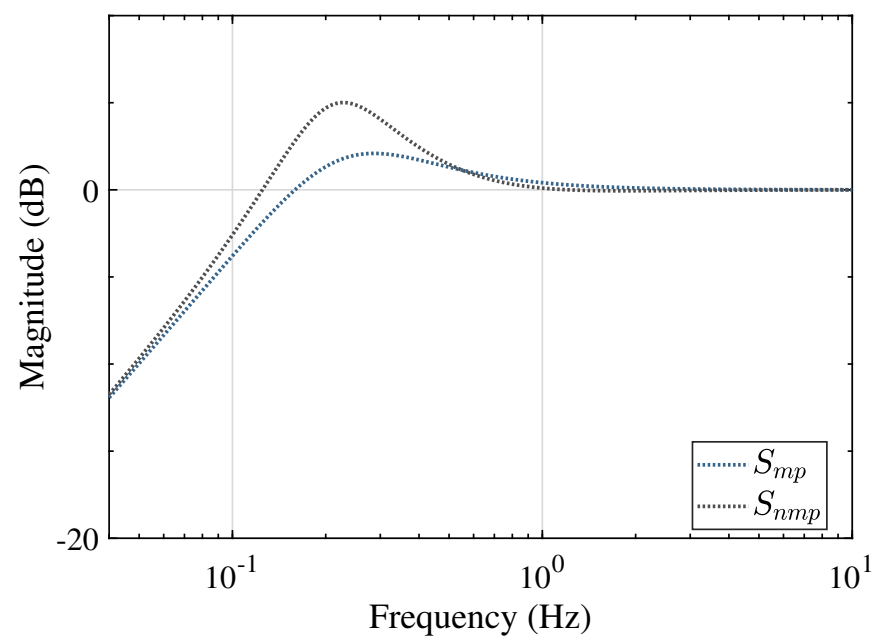

Figure 1.4 Magnitude plots of sensitivity function S_{mp} (sensitivity function for minimum phase system) and S_{nmp} (sensitivity function for non-minimum phase system) in which S_{nmp} has larger peak than S_{mp}.

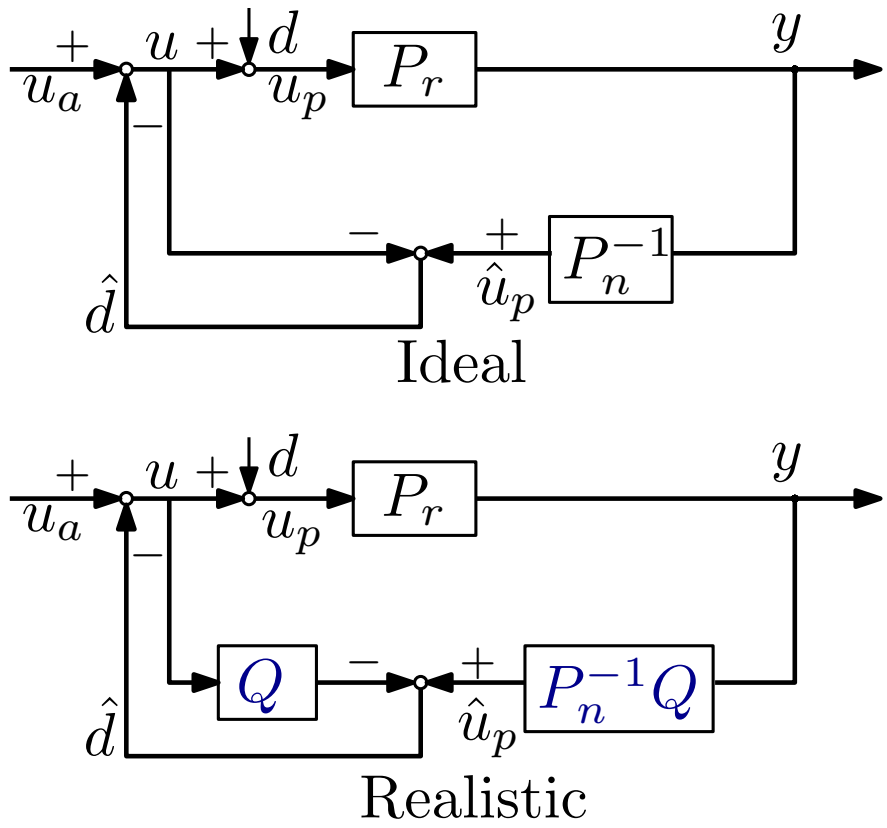

Figure 1.5 Explanation of idea of disturbance observer

Based on the above analysis, Q filter is essential in designing disturbance observer and its bandwidth should be as large as possible to guarantee the satisfactory disturbance rejection performance. However, robustness [12] and noises [34] limit the bandwidth of a DOB. Furthermore, when a DOB is applied to a non-minimum phase plant, internal stability problem and additional limitation on sensitivity function caused by unstable zero(s) need to be considered [35] [36] [37].

1.3.2 Introduction of previous studies on disturbance observer design

DOB for linear systems or for non-linear systems can all be found but since this thesis focuses on linear system, research works on DOB for non-linear system, such as [38]- [41], will not be introduced in detail. Although DOB has been applied to various applications, the design of it highly depends on designers' experience and parameters of DOB are normally tuned intuitively. Trial-and-error method and $\mathcal{H}_\infty$ methods have been extensively employed in the design of DOB, see survey [9] [42] and book [43].

Based on the analysis of robustness, *e.g.* robust stability analysis as well as robust performance, the design of DOB has been investigated [3] [44]- [47]. In [44], an almost necessary and sufficient stability condition of DOB based control systems has been given. In [45]- [47], disturbance observers have been designed by trial-and-error method while in [49]- [52], $\mathcal{H}_\infty$ optimization methods have been employed. Paper [50] investigated the design of DOB based on the closed loop system robustness analysis. In [51], a new robust stability analysis tool, which depends on the real parametric uncertainty analysis methods, is proposed for the control systems based on DOB. The DOB can also be designed from the perspective of noise suppression [53] [54] in which authors have proposed a noise suppression DOB and time constant of Q filter, which guarantees good noise suppression performance, is selected by trial-and-error.

Design of DOB in discrete domain has been investigated in [55]- [58]. Paper [55] discussed improvement of robustness for DOB-based discrete control algorithm by shaping the true plant with a cascaded frequency shaping filter. Paper [56] has provided guidelines in deciding parameters and [57] presents a generalized framework for robust stability analysis of control systems based on the discrete-time DOB. Applications of different discretization methods of continuous DOB has been discussed in [58].

Compared to its counterpart, due to the limitation (unstable inversion and waterbed effect) introduced by unstable zeros, DOB design for non-minimum phase systems becomes more challenging. Existing methods can be classified into two categories: One is to transform the non-minimum phase system into minimum phase system so that various methods for minimum phase systems can be employed [59]. In [60] [61] [62], authors have managed to show the bandwidth range according to the analysis based on Bode/Poisson integral formula after the non-minimum phase plant has been approximated. In [37], an approximate inverse system for non-minimum phase system has been obtained by least-square approximation method. In [63] [64], the controlled plant is in parallel with a filter to make it become a minimum phase one and then $\mathcal{H}_\infty$ methods have been employed.

The other is to make Q filter contain the same unstable zero or the time delay as nominal plant does, such as [65]- [70]. In [66] [67] [68], DOB-based model predictive control scheme were proposed in which time delay or unstable zeros can be considered as part of Q filter and trial-and-error was used to tune the parameters. In [69] [70], $\mathcal{H}_\infty$ optimization problems have been formulated to tune Q parameters.

Bases on the above analysis, the DOB design is more of intuitive process rather than mathematical-calculation based auto-tuning process, even in $\mathcal{H}_\infty$ methods, the selection of weighting functions needs

to be repeated. Therefore, a systematic and mathematical-calculation based auto-tuning method which can realize satisfactory disturbance rejection process is investigated in this thesis.

Furthermore, for non-minimum phase plants, in order to eliminate the influence of unstable zeros appeared in non-minimum phase plant, pole-zero analysis, such as coprime factorization [65] [69] [70], is always employed which necessitates the usage of parametric model. Since parametric plant model (transfer function or state space representation) is identified from experimental frequency response data, model uncertainty introduced in the fitting process should be considered in designing a robust controller which is prone to obtaining a conservative controller since worst case is considered. In this thesis, the direct use of frequency response data for DOB design is explored which is inspired by research works in the following section.

1.4 Review on frequency response data-based controller design

For classical model-based controller design, identifying the plant model and designing the controller based on the obtained model with the consideration of modeling uncertainty is the ordinary process. Thus the identification of the plant model is essential to model-based control theory.

However, industries which have large-scale production technologies and equipment, *e.g.* machinery, electronics, and transportation, identifying the plant model has become more difficult. Furthermore, for a system whose model is available but not adapted to control design because of too high order or a model is unavailable or too difficult to obtain, model-based control design methods are not as efficient as data-based controller design methodologies [71].

Under such circumstances, data-based controller design has been an attractive alternative way of designing controller, including time domain data-based design and frequency response data-based design. ([72], [73] and [74]). A parametric model is not required in data-based design framework, thus identification effort can be decreased. Since this thesis is about frequency domain data-based approach, time domain data-based studies are briefly-introduced while frequency response data-based studies are discussed in detail.

Time domain data-based design approaches employ time domain input and output data to design controller so that model reference criterion can be satisfied. The Virtual Reference Tracking (VRFT, [75]), Unfalsified Control (UC, [76]), Iterative Feedback Tuning (IFT, [77]), Model-Free Adaptive Control (MFAC, [78]) and Iterative Learning Control (ILC, [79]), Correlation-based Tuning (CbT, [80]) all belong to this category.

Compared to various time domain data-based design, a few methods employ frequency domain data directly. Frequency domain data-based controller design methods have been used in classical loop-shaping to compute simple controllers, *e.g.* Quantitative Feedback Theory (QFT, [81]). In [82], desired closed-loop poles are computed by frequency response data (FRD) although authors have pointed out their proposal is only applicable to systems with low damping. A set of proportional-integral-derivative (PID) controllers which satisfy the desired performance can be obtained from proposal in [83].

The aforementioned research works are not automatic optimization process and other researchers have turned frequency response data-based controller design problem into an optimization problem and solved it by optimization software. By converting performance limitations and necessary trade-offs in controller design into mathematical constraints either by graphical tools, *e.g.* Nyquist plot, or $\mathcal{H}_\infty$ framework,

and selecting an appropriate criterion as the optimization objective, *e.g.* integrator gain, parameters of desired controller can be tuned.

In [84] [85], a robust fixed order linearly parameterized controller design method using linear programming is proposed. Constraints in this paper, such as gain margin and phase margin, have all been approximated to its linear form. In [86], given an loop-shaping objective and $\mathcal{H}_\infty$ performance criteria, FRD-based design methodology for linearly-parameterized controllers are proposed for single-input-single-output (SISO) systems. Robust performance conditions are expressed as linear or convex constraints around the desired open-loop on the Nyquist diagram. Specially, the design of PID controllers for SISO systems were investigated in [87] [88] by interpreting the concept in [86] as a convex-concave optimization problem. In [89], compared to [86], no linearization around a given desired open loop transfer function is required and global minimum can be obtained and the application to a power converter can be found in [90].

The extension to PID controllers design for multi-input-multi-output (MIMO) system has been done in [91] (toolbox has been developed in [92]). Linearly parameterized controller design for MIMO systems has been discussed in [93] and fully parameterized controller design by convex optimization has been conducted in [94] [95].

Some techniques based on non-convex optimization have also been proposed. In [96], fixed order controllers are defined using Q parameterization and designed by a non-convex optimization. In [97], a nonlinear programming problem has been formulated based on the concept of bounded error to compute fixed order controllers for SISO system only.

1.5 Thesis structure

This thesis is organized as shown in Fig. 1.5. On the whole, the thesis has been divided into three parts: theoretical analysis (Chapter 3 and 4), numerical case study results (Chapter 5 and 6) as well as experimental results (Chapter 7).

Firstly, mathematical preliminaries in Chapter 2 has laid the foundation for theoretical discussion. The necessary mathematical preliminaries have been introduced starting from the definition of convex optimization problem as well as conic optimization problem since this thesis has transformed the original non-convex DOB design problem into a conic optimization problem. The required mathematical knowledge in the transformation process, such as Schur Complement and Linear Matrix Inequality have also been shown. Furthermore, in order to transform original nonlinear constraints which are represented by the difference between two convex functions into convex form, the lower bound of a convex function is always needed which is found by linear approximation.

In the second part or the theoretical part, the theoretical analysis of DOB design problem has been elaborated. Based on the block diagram of DOB-based control system, the original non-convex problem formulation process including the introduction of constraints, such as constraint for guaranteeing stability margins, has been given for both continuous domain and discrete domain design. Subsequently, the detailed mathematical transformation process from non-convex constraints to convex constraints has been present. Importantly, not only the low pass filter design (Chapter 3) but also the design of low pass filter along with identification of plant model (Chapter 4) has been investigated. The newly-obtained convex optimization problem can be easily solved by off the shelf toolboxes.

Extensive case study results, which are classified into design for a minimum phase system (Chapter 5) case and design for a non-minimum phase system (Chapter 6) case, have been shown to verify the feasibility of proposed methods. For both cases, low pass filter design result as well as results of design plant model and low pass filter together have been analyzed in continuous domain and discrete domain. In addition, resultant Nyquist plots and magnitude plots of sensitivity function as well as complementary sensitivity function, which are for ensuring the satisfaction of constraints, have all been exhibited. Moreover, the proposal has been compared with previous studies and its superiority has been proven in terms of optimized bandwidth. Particularly, for the DOB design for a non-minimum phase plant which contains unstable zero, special case study, such as low pass filter contains the same unstable zero as nominal plant does, has been conducted.

The experimental verification has been presented in chapter 7. To start with, the structure of experimental test bench, which is a non-minimum phase motion stage, and the system identification process for obtaining frequency response data have been introduced. After setting up the machine, proposed FRD-based DOBs and DOBs designed by methods in previous research have been implemented. Output responses, which are position signals, have been recorded and compared with each other. Proposed methods have achieved satisfactory disturbance rejection performance which demonstrates the efficacy of proposal.

Finally, concluding remarks as well as the prospective research in future have been given in Chapter 8.

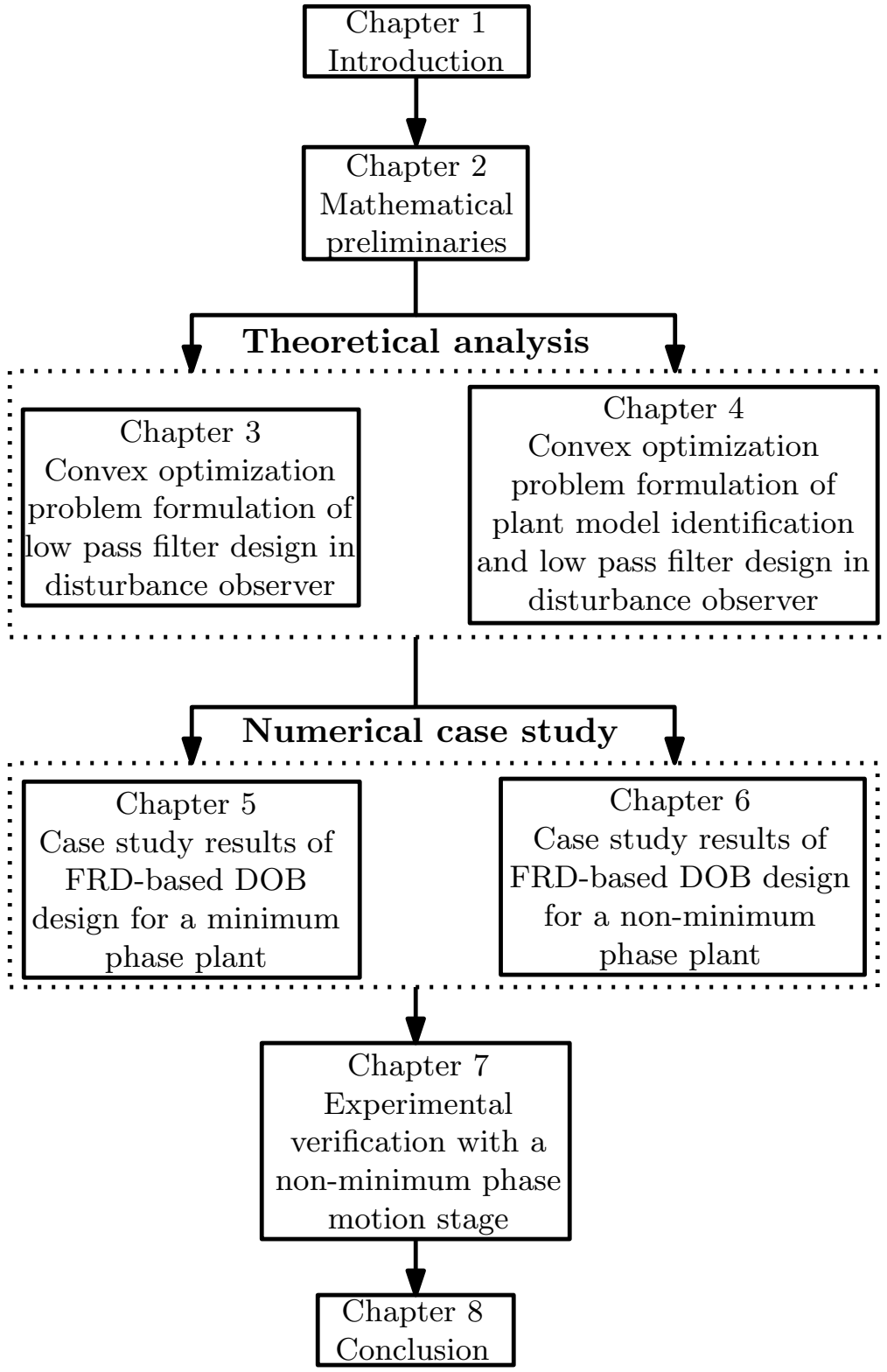
Chapter 1
Introduction
Chapter 2
Mathematical
preliminaries
Theoretical analysis
Chapter 3
Convex optimization
problem formulation of
low pass filter design in
disturbance observer
Chapter 4
Convex optimization
problem formulation of
plant model identification
and low pass filter design in
disturbance observer
Numerical case study
Chapter 5
Case study results of
FRD-based DOB
design for a minimum
phase plant
Chapter 6
Case study results of
FRD-based DOB design
for a non-minimum
phase plant
Chapter 7
Experimental
verification with a
non-minimum phase
motion stage
Chapter 8
Conclusion

Chapter 2

Mathematical preliminaries

2.1 Overview

This chapter is to introduce the necessary mathematical preliminaries used in following chapters including the definition of convex optimization problem as well as conic optimization and introduction of Schur complement along with linear approximation and some special mathematical techniques used in the discussion afterwards. Finally, some frequently-used mathematical notations have been summarized.

2.2 Mathematical preliminaries

2.2.1 Definitions and theorems

A function f is convex means it satisfies Eq. (2.1) and a simple example would be a quadratic function.

$$f(\beta_1 x + \beta_2 y) \leq \beta_1 f(x) + \beta_2 f(y). \tag{2.1}$$

for all $x, y \in R^{\bar{n}}$ with $\beta_1 + \beta_2 = 1, \beta_1 \geq 0, \beta_2 \geq 0$.

A standard form of convex optimization problem can be shown as follows ([98]).

$$\begin{aligned} \text{minimize} \quad & f_0(x) && (2.2)\\ \text{subject to} \quad & f_{k^*}(x) \leq 0, k^* = 1, \cdots, \gamma && (2.3)\\ & \kappa_{k^*}^T x = \xi_{k^*}, k^* = 1, \cdots, \lambda && (2.4) \end{aligned}$$

in which $f_0, f_1, \cdots, f_\gamma$ are convex; equality constraints are affine.

For example, the following problem is a convex optimization problem.

$$\begin{aligned} \text{minimize} \quad & f_0(x) = x_1^2 + x_2^2 && (2.5)\\ \text{subject to} \quad & x_1 \leq 0, && (2.6)\\ & x_1 + x_2 = 0 && (2.7) \end{aligned}$$

This thesis has succeeded in transforming the disturbance observer design problem into a convex optimization problem, specifically, a conic optimization problem. A conic optimization problem is the subfield of convex optimization and the explanation of it is shown as follows.

A conic optimization problem has one or more cone constraints. A cone constraint specifies that the vector formed by a set of decision variables is constrained to lie within a closed convex pointed cone. Many different cones exist, such as norm cones (Fig. 2.1), positive semi-definite cones.

In order to approximate the original non-convex optimization problem into a conic optimization problem, following three techniques are utilized in the next chapter.

1) Schur Complement ([99]) is introduced as follows:

$$\begin{bmatrix} Y(x) & M(x) \\ (M(x))^T & R(x) \end{bmatrix} > 0, \tag{2.8}$$

where $Y(x) = Y(x)^T, R(x) = R(x)^T$ and $M(x)$ depends affinely on x, is equivalent to

$$Y(x) > 0, R(x) - M(x)Y(x)^{-1}M(x)^T > 0. \tag{2.9}$$

Schur Complement can be used to obtain Matrix Inequality form, specially, Linear Matrix Inequality (LMI) form ([99]) which can be represented by the following equation:

$$F(x) = F_0 + \sum_{i^*=1}^{\bar{m}} x_{i^*} F_{i^*} > 0, \tag{2.10}$$

in which $x \in R^{\bar{m}}$ is the variable and symmetric matrices $F_{i^*} = F_{i^*}^T \in R^{\bar{n}\times\bar{n}}$, $i^* = 0, \cdots, \bar{m}$ are given.

For example, if $x > 0$, $y > 0$, then $xy > 1$ can be changed into the following LMI form by using Schur Complement.

$$x > 0, y > 0, xy > 1 \Leftrightarrow \begin{bmatrix} x & 1 \\ 1 & y \end{bmatrix} > 0. \tag{2.11}$$

2) Linear approximation

For a convex function, linear approximation is extensively employed in finding the lower bound of it. The basic concept is to estimate the value of a function, $f(x)$, near a point $x_0 = [x_{0(1)}, x_{0(2)}, ..., x_{0(\hat{n})}]^T$, using the following formula.

$$f(x) \approx f(x_0) + \nabla f(x_0)(x - x_0), \tag{2.12}$$

in which

$$\nabla f(x_0) = \left[\frac{\partial f(x_0)}{\partial x_{0(1)}}, \frac{\partial f(x_0)}{\partial x_{0(2)}}, \cdots, \frac{\partial f(x_0)}{\partial x_{0(\hat{n})}} \right]. \tag{2.13}$$

Especially, for the difference between two convex functions $f(x)$ and $g(x)$,

$$f(x) - \underbrace{g(x)}_{\text{original}} \leq 0 \Leftarrow f(x) - \underbrace{(g(x_0) + \nabla g(x_0)(x - x_0))}_{\text{lower bound of } g(x)} \leq 0 \tag{2.14}$$

This technique is used in convex-concave optimization problem [100] [101] which is a procedure where the optimization criterion and constraints are written as a difference between two convex functions:

$$\text{minimize } f_0(x) - g_0(x) \tag{2.15}$$

$$\text{subject to } f_{i'}(x) - g_{i'}(x) \leq 0, i' = 1, \cdots, \hat{m} \tag{2.16}$$

Such optimization problem can be solved efficiently by the iterative procedure and finally converges to a saddle point or a local minimum [101]. Even though there is no guarantee of convergence to a global minimum, experience has shown that this method is often effective in producing good solutions [87].

3) Technique in finding lower bound for $m_1^{-2}(m_1 > 0)$

For a concave function, linear approximation can only find the upper bound of it. In this thesis, the lower bound of a specific case $m_1^{-2}(m_1 > 0)$ is needed and the following method is used. By using an

known positive scalar m_2 and building the following equation, the lower bound of m_1^{-2} can be found successfully [102].

$$\begin{aligned}&(m_1^{-2}-m_2^{-2})(m_1^{-2}-m_2^{-2})\geq 0(\text{forever hold equation})\\&\Leftrightarrow m_1^{-4}\geq 2m_1^{-2}m_2^{-2}-m_2^{-4}\\&\xLeftrightarrow{\text{multiply } m_1^{-2}\text{to both sides}} m_1^{-2}\geq 2m_2^{-2}-m_2^{-4}m_1^2.\end{aligned}\tag{2.17}$$

If the LMI form of the lower bound is needed, by introducing a positive variable ϕ and making $m_1^{-2}\geq 2m_2^{-2}-m_2^{-4}m_1^2\geq\phi>0$, the following LMI form can be obtained.

$$\begin{bmatrix}2m_2^2-\phi_1 m_2^4 & m_1\\ m_1 & 1\end{bmatrix}>0,\phi>0.\tag{2.18}$$

2.2.2 Nomenclature

In this section, extensively-used notations have been listed while explanations for notations not mentioned here are present in the place where notations appear for the first time.

2.3 Summary

This chapter has introduced the mathematical knowledge that is used in following chapters. This chapter is the basis of mathematical transformation from nonlinear optimization problem to convex optimization problem which will be discussed thoroughly from next chapter.

Table 2.1 Summary of notations

Notations	meaning
DOB	disturbance observer
FRD	frequency response data
mp	minimum phase
nmp	non-minimum phase
j	imaginary unit
ω_k	frequency ([rad/s]) (k: index)
L^*	open loop function
S^*	sensitivity function
T^*	complementary sensitivity function
W_p	weighting function for sensitivity function
W_m	weighting function for complementary sensitivity function
P_r	real plant
P_n	nominal plant
Q	low pass filter in disturbance observer
g_m	gain margin
ϕ_m	phase margin
$(-\sigma,0)$	center point of stability circle
r_m	radius of stability circle
i	iteration index in the optimization process
d	disturbance
$\hat{d}$	estimated disturbance
y	position signal
u_p	plant input
u_a	control input
r	reference signal
e	error signal

$*$: In the thesis, different subscripts are used to represent L, S, T for different systems.

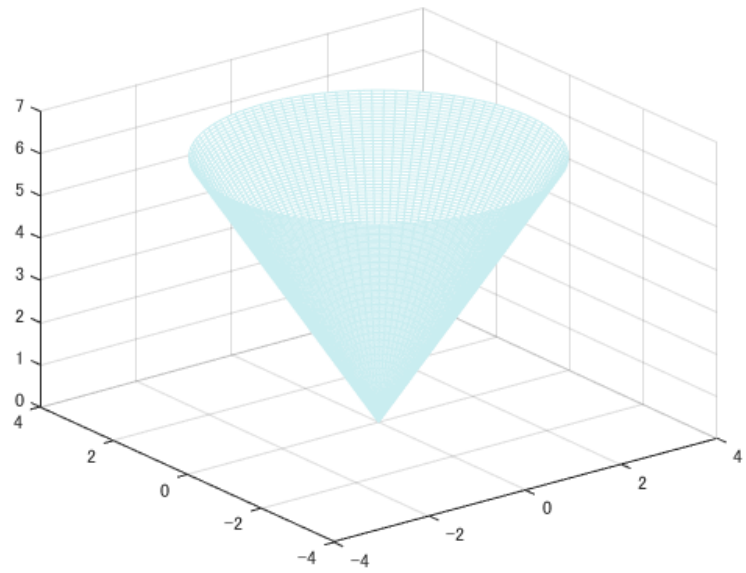

Figure 2.1 An example of norm cone

Chapter 3

Convex optimization problem formulation of low pas filter design in disturbance observer

3.1 Overview

This chapter is dedicated to the theoretical analysis of FRD-based low pass filter design in disturbance observer including continuous domain (s domain) and discrete domain (z domain) design.

Firstly, the FRD-based low pass filter design when the nominal plant is given regardless of its type (minimum phase or non-minimum phase) has been explored. More specifically, for either of the following cases, parameters of Q filter can be tuned automatically and bandwidth-maximized DOB can be obtained.

1. Minimum phase nominal plant model is employed in the design.
2. Non-minimum phase nominal plant is used in the design.
   In this case, to guarantee the internal stability, Q should also contain the same unstable zeros as plant does [65] [69].
3. The minimum phase approximation of a non-minimum phase plant is used in the design.

The original non-convex optimization problem formulation of low pass filter design including the introduction of constraints have been given and the detailed transformation process from non-convex constraints to convex constraints based on the mathematical preliminaries in Chapter 2 has been presented.

Subsequently, in this chapter, the low pass filter design in discrete domain has been present. Although design in continuous domain is convenient and straightforward, the implementation of DOB is in discrete domain and direct design in discrete domain is more of practical meaning. Furthermore, even the constraints have been satisfied for the design result in continuous domain, the discrete DOB which is discretized from continuous domain result may break the constraints. Therefore, the design of DOB in discrete domain has been investigated.

Finally, procedures of proposed methods have been summarized.

3.2 Low pass filter design in continuous domain

3.2.1 Block diagram analysis

In the disturbance observer control system as shown in Fig. 3.1, P_r and $P_n(s)$ denote real plant and nominal plant (known), defined by FRD and transfer function (s domain), respectively. $Q(s)$ represents

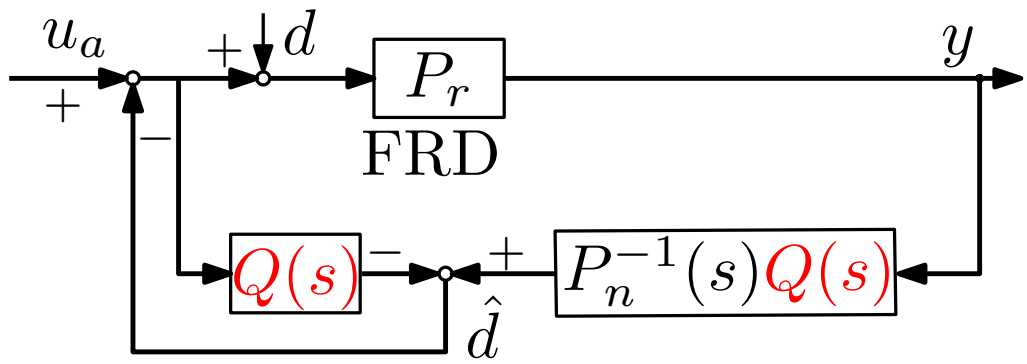

Figure 3.1 Block diagram of disturbance observer system in continuous domain for low pass filter design

the to-be-designed low pass filter. Signals $d, \hat{d}, u_a, y$ are real external disturbance, estimated disturbance, control input and output, respectively. The selection of $Q(s)$ filter, which includes the form as well as the relative order, depends on the nominal plant which can be classified as follows:

1. Nominal plant $P_n(s)$ is minimum phase:

$$Q(s, a.b) = \frac{a_m s^m + \cdots + a_1 s + 1}{b_n s^n + \cdots + b_1 s + 1}. \tag{3.1}$$

2. Nominal plant $P_n(s)$ is a minimum phase approximation of a non-minimum phase model and $Q(s)$ is minimum phase:

$$Q(s, a, b) = \frac{a_m s^m + \cdots + a_1 s + 1}{b_n s^n + \cdots + b_1 s + 1}. \tag{3.2}$$

3. Nominal plant $P_n(s)$ is non-minimum phase and $Q(s)$ is non-minimum phase:

$$Q(s, b) = \frac{(s + z_{nmp(1)}) \cdots (s + z_{nmp(m)})}{b_n s^n + \cdots + b_1 s + \prod_{k'=0}^{m} z_{nmp(k')}}. \tag{3.3}$$

in which $a \triangleq [a_1, \cdots, a_m]^T$ and $b \triangleq [b_1, \cdots, b_n]^T$ are to-be-decided parameter vectors and the order $n-m$ should be no smaller than the relative order of the inversion (or approximated inversion) of $P_n(s)$. When $P_n(s)$ is of non-minimum phase, $z_{nmp(1)}, \cdots, z_{nmp(m)}$ are unstable zeros of nominal plant.

The loop gain $L(j\omega_k, a, b)$, sensitivity function $S(j\omega_k, a, b)$ and complementary function $T(j\omega_k, a, b)$ for Fig. 3.1 can be obtained as follows:

$$L(j\omega_k, a, b) = P_n^{-1}(s)Q(s, a, b)(1 - Q(s, a, b))^{-1}P_r(j\omega_k) = \frac{N(j\omega_k, a)}{D(j\omega_k, a, b)}, \tag{3.4a}$$

$$S(j\omega_k, a, b) = \frac{1}{1 + (1 - Q(s, a, b))^{-1}Q(s, a, b)P_n^{-1}(s)P_r(j\omega_k)} = \frac{D(j\omega_k, a, b)}{D(j\omega_k, a, b) + N(j\omega_k, a)}, \tag{3.4b}$$

$$T(j\omega_k, a.b) = \frac{(1 - Q(s, a, b))^{-1}Q(s, a, b)P_n^{-1}(s)P_r(j\omega_k)}{1 + (1 - Q(s, a, b))^{-1}Q(s, a, b)P_n^{-1}(s)P_r(j\omega_k)} = \frac{N(j\omega_k, a)}{D(j\omega_k, a, b) + N(j\omega_k, a)}. \tag{3.4c}$$

in which $D(s, a, b)$ is a linear function in terms of a, b.

In the following section, several constraints has been designed to obtain satisfactory disturbance rejection performance. Thereafter, the design of DOB has been formulated into an optimization problem in which a as well as b are optimization parameters and the bandwidth of DOB is the optimization objective.

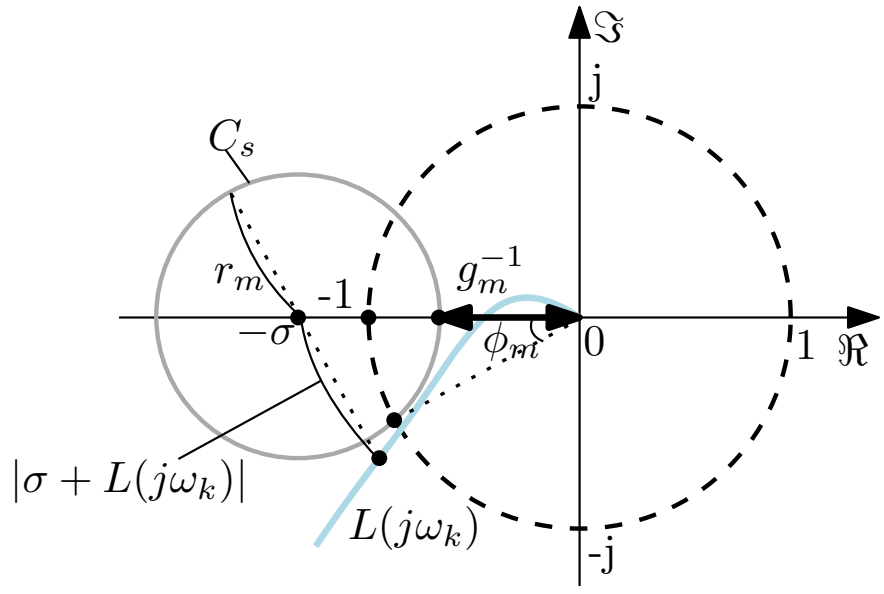

Figure 3.2 Circle condition description for prospective Nyquist plot

3.2.2 Constraints formulation

① **Constraint for guaranteeing stability margins**

The circle condition ([88]), which is shown in Fig. 3.2, should be met to guarantee the desired gain margin g_m and phase margin ϕ_m. Black dashed line denotes unit circle and gray line is a circle whose center $(-\sigma,0)$ and radius r_m can be obtained by following equations when $0 < \phi_m < \frac{\pi}{2}, \frac{1}{g_m} < \cos\phi_m, 0 < r_m < \sigma$ and $(\sigma-1)^2 < r^2$ hold.

$$\sigma = \frac{g_m^2 - 1}{2g_m(g_m\cos\phi_m - 1)}, r_m = \frac{(g_m-1)^2 + 2g_m(1-\cos\phi_m)}{2g_m(g_m\cos\phi_m - 1)}. \tag{3.5}$$

The mathematical representation of this constraint is shown as follows:

$$|\sigma + L(j\omega_k, a, b)| - r_m \geq 0, \tag{3.6}$$

in which $L(j\omega_k, a, b)$ is the loop gain in Eq. (3.4a).

② **Constraints for sensitivity function and complementary sensitivity function**

Weighting function $W_p(s,\omega_p)$ and $W_m(s,\omega_t)$, which are shown in Eq. (3.7), are selected for $S(j\omega_k, a, b)$ and $T(j\omega_k, a, b)$ respectively to establish the constraints for sensitivity function and complementary sensitivity function as shown in Fig. 3.3 and Fig. 3.4. ω_p is selected as the optimization objective since the blue part in Fig. 3.3 represents for disturbance rejection area. When the optimal point $\omega_{p(opt)}$ is found, a and b are obtained simultaneously.

$$W_p(j\omega_k, \omega_p) = \frac{\omega_p}{j\omega_k}, |W_p(j\omega_k, \omega_t)S(j\omega_k, a, b)| \leq 1. \tag{3.7}$$

$$W_m(j\omega_k, \omega_t) = \frac{j\omega_k + \omega_t}{M_t\omega_t},\ |W_m(j\omega_k, \omega_t)T(j\omega_k, a, b)| \leq 1. \tag{3.8}$$

③ **Constraint for guaranteeing stability of low pass filter**

If the Q filter is of second order, as long as $b_1 > 0$ and $b_2 > 0$ hold, Q must be stable.

If the Q filter is of high order, given that the initial Q filter is stable, when the Nyquist plot of $L_q(s, b_i)$ (ith iteration), which is the open loop function defined as follows, never encircles (-1,0) as shown in

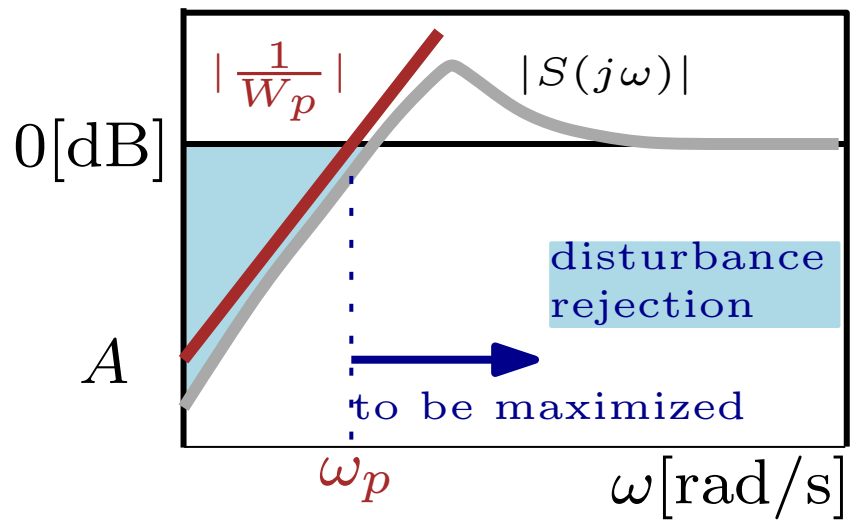

Figure 3.3 Figure of constraint for sensitivity function

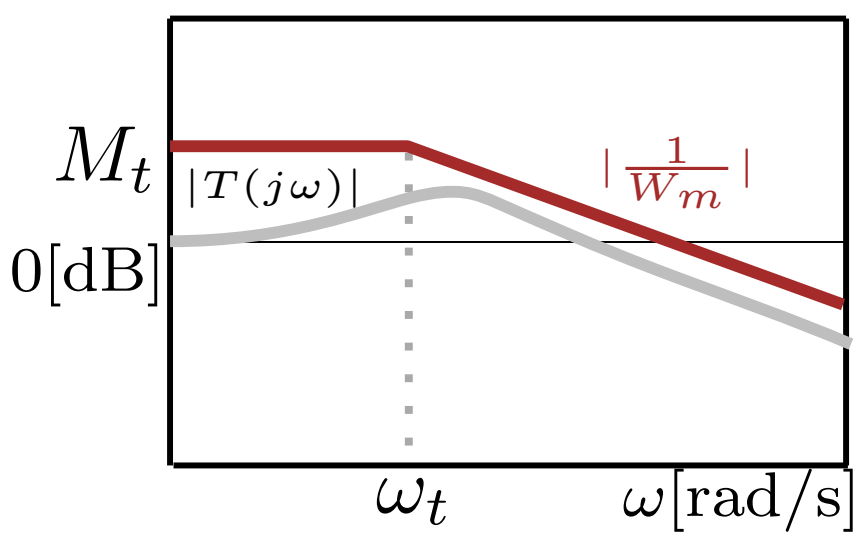

Figure 3.4 Figure of constraint for complementary sensitivity function

Fig. 3.5, the stability of Q filter which simultaneously means the stability of closed loop function H_q, is guaranteed during the optimization process.

$$L_q(s, b_i) = \frac{1}{b_{n(i)}s^n + \cdots + b_{1(i)}s} = \frac{1}{D_q(s, b_i)}, \tag{3.9}$$

$$H_q(s, b_i) = \frac{L_q(s, b_i)}{1 + L_q(s, b_i)} = \frac{1}{b_{n(i)}s^n + \cdots + b_{1(i)}s + 1}. \tag{3.10}$$

The mathematical interpretation is given as Eq. (3.11) which means the distance $|L_q(j\omega_k, b_i) - L_q(j\omega_k, b_{i-1})|$ should be no larger than the distance between $L_q(j\omega_k, b_{i-1})$ and $(-1, 0)$ at every frequency point after every iteration.

$$|L_q(j\omega_k, b_i) - L_q(j\omega_k, b_{i-1})| \leq |L_q(j\omega_k, b_{i-1}) + 1|. \tag{3.11}$$

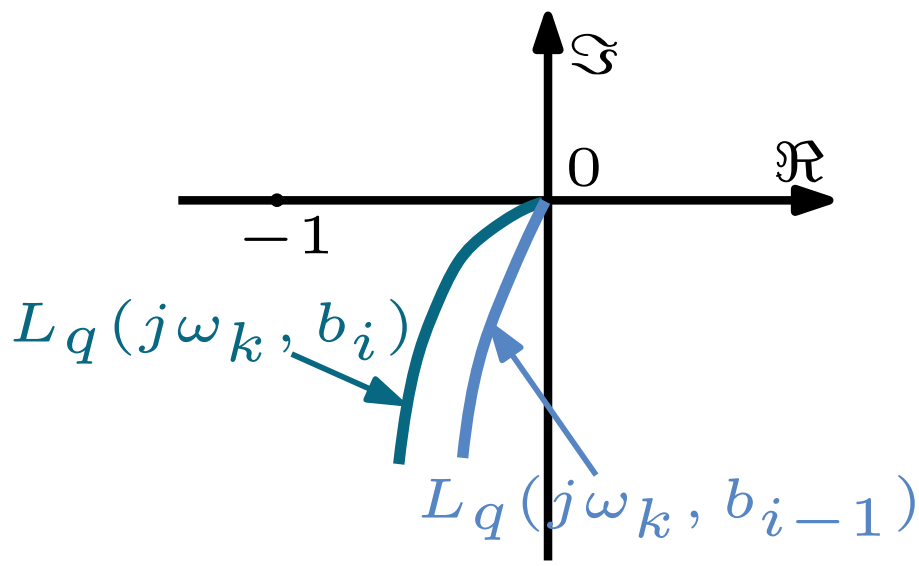

Figure 3.5 Explanation of constraint for guaranteeing the stability of high order low pass filter

In summary, the Q filter design is formulated into the following optimization problem.

$$\underset{a,b,\omega_t}{\text{Maximize}} \quad \omega_p \tag{3.12a}$$

$$\text{Subject to} \quad 0 < b_1, \cdots, b_n, 0 < \omega_p < \omega_t, \tag{3.12b}$$

$$|L(j\omega_k, a, b) + \sigma| \geq r_m, \tag{3.12c}$$

$$|W_p(j\omega_k, \omega_p) S(j\omega_k, a, b)| \leq 1, \tag{3.12d}$$

$$|W_m(j\omega_k, \omega_t) T(j\omega_k, a, b)| \leq 1, \tag{3.12e}$$

$$|L_q(j\omega_k, b_i) - L_q(j\omega_k, b_{i-1})| \leq |L_q(j\omega_k, b_{i-1}) + 1|. \tag{3.12f}$$

Especially, if the Q filter is of second order, the optimization problem can be formulated as follows:

$$\underset{a,b,\omega_t}{\text{Maximize}} \quad \omega_p \tag{3.13a}$$

$$\text{Subject to} \quad 0 < b_1, b_2, 0 < \omega_p \leq \frac{1}{\sqrt{b_2}} \leq \omega_t, \tag{3.13b}$$

$$|L(j\omega_k, a, b) + \sigma| \geq r_m, \tag{3.13c}$$

$$|W_p(j\omega_k, \omega_p) S(j\omega_k, a, b)| \leq 1, \tag{3.13d}$$

$$|W_m(j\omega_k, \omega_t) T(j\omega_k, a, b)| \leq 1, \tag{3.13e}$$

3.2.3 Convex constraints derivation

Constraint for guaranteeing stability margins

In this subsection, constraint Eq. (3.12c), which is for guaranteeing margins, is converted to a convex constraint in the following way.

$$\begin{aligned} &|L(j\omega_k, a_i, b_i) + \sigma| - r_m = \left| \frac{N(j\omega_k, a_i)}{D(j\omega_k, a_i, b_i)} + \sigma \right| - r_m \geq 0 \\ &\Leftrightarrow |N(j\omega_k, a_i) + D(j\omega_k, a_i, b_i)\sigma| \triangleq \underbrace{F(j\omega_k, a_i, b_i) \geq r_m |D(j\omega_k, a_i, b_i)|}_{\text{original}} \Leftarrow \underbrace{\Psi \geq r_m |D(j\omega_k, a_i, b_i)|}_{\text{newly-obtained}}, \end{aligned} \tag{3.14}$$

where

$$\Psi = F(j\omega_k, a_{i-1}, b_{i-1}) + \nabla F(j\omega_k, a_{i-1}, b_i)(a_i - a_{i-1}) + \nabla F(j\omega_k, a_i, b_{i-1})(b_i - b_{i-1}),$$

$$\nabla F(j\omega_k, a_{i-1}, b_i) = \begin{bmatrix} \frac{\partial(|N(j\omega_k, a_{i-1}) + D(j\omega_k, a_{i-1}, b_i)\sigma|)}{\partial a_{1(i-1)}} \\ \vdots \\ \frac{\partial(|N(j\omega_k) + D(j\omega_k, a_{i-1}, b_i)\sigma|)}{\partial a_{m(i-1)}} \end{bmatrix}^T,$$

$$\nabla F(j\omega_k, a_i, b_{i-1}) = \begin{bmatrix} \frac{\partial(|N(j\omega_k, a_i) + D(j\omega_k, a_i, b_{i-1})\sigma|)}{\partial b_{1(i-1)}} \\ \vdots \\ \frac{\partial(|N(j\omega_k, a_i) + D(j\omega_k, a_i, b_{i-1})\sigma|)}{\partial b_{n(i-1)}} \end{bmatrix}^T. \tag{3.15}$$

with $a_i(b_i)$ and $a_{i-1}(b_{i-1})$ denoting the current value and the previous value in the iterative optimization process, respectively.

Constraint for sensitivity function

For the sensitivity function constraint Eq. (3.12d), the following method is used to obtain LMI form.

$$\left|W_p(j\omega_k, \omega_{p(i)})S(j\omega_k, a_i, b_i)\right| \le 1 \Leftrightarrow \left|\frac{\omega_{p(i)}}{j\omega_k} D(j\omega_k, a_i, b_i)\right| \le |D(j\omega_k, a_i.b_i) + N(j\omega_k, a_i)|. \tag{3.16}$$

Squaring both sides of Eq. (3.16), the following matrix inequality form can be obtained by using Schur Complement.

$$\begin{aligned} &\left|\frac{\omega_{p(i)}}{j\omega_k}\right|^2 |D(j\omega_k, a_i, b_i)|^2 \le |D(j\omega_k, a_i, b_i) + N(j\omega_k, a_i)|^2 \\ \Leftrightarrow &\begin{bmatrix} \left|\frac{\omega_k}{\omega_{p(i)}}\right|^2 & D(j\omega_k, a_i, b_i) \\ (D(j\omega_k, a_i, b_i))^* & |D(j\omega_k, a_i, b_i) + N(j\omega_k, a_i)|^2 \end{bmatrix} := \begin{bmatrix} S_{11} & S_{12} \\ (S_{12})^* & S_{22} \end{bmatrix} \ge 0. \end{aligned} \tag{3.17}$$

To obtain the sufficient condition of original constraint, the lower bound of S_{11} and S_{22} are required. For $S_{11} = \frac{(\omega_k)^2}{\omega_{p(i)}^2}$, the lower bound of $\omega_{p(i)}^{-2}$ is obtained by using the technique introduced in Chapter 2.

$$\begin{aligned} &(\omega_{p(i)}^{-2} - \omega_{p(i-1)}^{-2})(\omega_{p(i)}^{-2} - \omega_{p(i-1)}^{-2}) \ge 0 \Leftrightarrow \omega_{p(i)}^{-4} \ge 2\omega_{p(i-1)}^{-2}\omega_{p(i)}^{-2} - \omega_{p(i-1)}^{-4} \\ &\Leftrightarrow \omega_{p(i)}^{-2} \ge 2\omega_{p(i-1)}^{-2} - \omega_{p(i-1)}^{-4}\omega_{p(i)}^{2} \ge \phi_{s(i)} > 0, \end{aligned} \tag{3.18}$$

in which $\phi_{s(i)}$ is newly-introduced variable and constraints for it can be expressed in the following form:

$$\begin{bmatrix} 2\omega_{p(i-1)}^2 - \phi_{s(i)}\omega_{p(i-1)}^4 & \omega_{p(i)} \\ \omega_{p(i)} & 1 \end{bmatrix} > 0, \phi_{s(i)} > 0. \tag{3.19}$$

with $\omega_{p(i)}$ and $\omega_{p(i-1)}$ representing the current value and the previous value in the iterative optimization process, respectively.

After the lower bound of $\omega_{p(i)}^{-2}$ has been found, a lower bound of S_{11} is expressed as follows:

$$S_{11} = \underbrace{\frac{\omega_k^2}{\omega_{p(i)}^2}}_{\text{original}} \ge \underbrace{\omega_k^2\phi_{s(i)}}_{\text{newly-obtained}}. \tag{3.20}$$

As for S_{22}, the linear approximation is employed.

$$\begin{aligned} S_{22} &= |D(j\omega_k, a_i, b_i) + N(j\omega_k, a_i)|^2 \triangleq \underbrace{(M(j\omega_k, a_i, b_i))^2}_{\text{original}} \geq \Phi \\ &:= \underbrace{(M(j\omega_k, a_{i-1}, b_{i-1}))^2 + \nabla(M(j\omega_k, a_{i-1}, b_i))^2(a_i - a_{i-1}) + \nabla(M(j\omega_k, a_i, b_{i-1}))^2(b_i - b_{i-1})}_{\text{newly-obtained}}, \end{aligned} \tag{3.21}$$

in which $\nabla M(j\omega_k, a_{i-1}, b_i)^2$ as well as $\nabla M(j\omega_k, a_i, b_{i-1})^2$ are calculated similarly to Eq. (3.15).

In summary, the original nonlinear constraint Eq. (3.12d) is transformed into following LMIs by combining Eq. (3.17), Eq. (3.19), Eq. (3.20) and Eq. (3.21).

$$\phi_{s(i)} > 0, \begin{bmatrix} \omega_k^2 \phi_{s(i)} & D(j\omega_k, a_i, b_i) \\ (D(j\omega_k, a_i, b_i))^* & \Phi \end{bmatrix} \geq 0, \begin{bmatrix} 2\omega_{p(i-1)}^2 - \phi_{s(i)}\omega_{p(i-1)}^4 & \omega_{p(i)} \\ \omega_{p(i)} & 1 \end{bmatrix} > 0. \tag{3.22}$$

Constraint for complementary sensitivity function

By following the similar process as used in dealing with Eq. (3.12d), the complementary sensitivity function constraint Eq. (3.12e) is changed into the following form.

$$\begin{aligned} &\left|W_m(j\omega_k, \omega_{t(i)})T(j\omega_k, a_i, b_i)\right| \leq 1 \Leftrightarrow \left|\frac{j\omega_k + \omega_{t(i)}}{M_t\omega_{t(i)}}\right|^2 \leq \left|\frac{D(j\omega_k, a_i, b_i) + N(j\omega_k, a_i)}{N(j\omega_k, a_i)}\right|^2, \\ &\Leftrightarrow \begin{bmatrix} \omega_{t(i)}^2 & \dfrac{(N(j\omega_k, a_i)(j\omega_k + \omega_{t(i)}))}{M_t} \\ \dfrac{(N(j\omega_k, a_i)(j\omega_k + \omega_{t(i)}))^*}{M_t} & |D(j\omega_k, a_i, b_i) + N(j\omega_k, a_i)|^2 \end{bmatrix} := \begin{bmatrix} T_{11} & T_{12} \\ (T_{12})^* & T_{22} \end{bmatrix} \geq 0. \end{aligned} \tag{3.23}$$

Since $T_{22} = S_{22}$, its transformation is omitted due to the repetition. For T_{11}, following two different cases are considered.

If the numerator of L does not contain to-be-optimized parameters, e.g., the numerator of Q is 1 and the numerator of L is $P_r(j\omega_k)P_n^{-1}$, the ω_t can also be selected as the optimization variable. In such case, T_{11} needs to be transformed as shown in Eq. (3.24).

$$\underbrace{\omega_{t(i)}^2}_{\text{original}} \geq \underbrace{2\omega_{t(i-1)}\omega_{t(i)} - \omega_{t(i-1)}^2}_{\text{newly-obtained}}, \tag{3.24}$$

in which $\omega_{t(i)}$ means the current value and $\omega_{t(i-1)}$ means the previous value in the iterative optimization process.

By combining Eq. (3.20), Eq. (3.23) and Eq. (3.24), the original non-convex constraint is changed into

$$\begin{bmatrix} 2\omega_{t(i-1)}\omega_{t(i)} - \omega_{t(i-1)}^2 & \dfrac{|N(j\omega_k)|(j\omega_k + \omega_{t(i)})}{M_t} \\ \dfrac{|N(j\omega_k)|(j\omega_k + \omega_{t(i)})^*}{M_t} & \Phi \end{bmatrix} \geq 0. \tag{3.25}$$

If the numerator of L contains to-be-optimized parameters, ω_t should be a pre-defined fixed number in order to make the constraint into a convex form.

$$\begin{bmatrix} \omega_t^2 & \dfrac{(N(j\omega_k, a_i)(j\omega_k + \omega_{t(i)}))}{M_t} \\ \dfrac{(N(j\omega_k, a_i)(j\omega_k + \omega_{t(i)}))^*}{M_t} & \Phi \end{bmatrix} \geq 0. \tag{3.26}$$

Constraint for guaranteeing stability of high order low pass filter

For constraint Eq. (3.12f), the transformation process is given as follows.

$$\begin{aligned} &|L_q(j\omega_k, b_i) - L_q(j\omega_k, b_{i-1})| \le |L_q(j\omega_k, b_{i-1}) + 1| \\ \Leftrightarrow &\left| \frac{1}{D_q(j\omega_k, b_i)} - \frac{1}{D_q(j\omega_k, b_{i-1})} \right| \le \left| \frac{1}{D_q(j\omega_k, b_{i-1})} + 1 \right|. \end{aligned} \tag{3.27}$$

By defining ΔD_q to represent $D_q(j\omega_k, b_{i-1}) - D_q(j\omega_k, b_i)$, one can derive

$$|\Delta D_q| \le |D_q(j\omega_k, b_i)||D_q(j\omega_k, b_{i-1}) + 1|. \tag{3.28}$$

By squaring the above equation and using the Schur Complement, the following equation is obtained.

$$\begin{bmatrix} |D_q(j\omega_k, b_{i-1}) + 1|^2 & \Delta D_q \\ (\Delta D_q)^* & |D_q(j\omega_k, b_i)|^2 \end{bmatrix} := \begin{bmatrix} Q_{11} & Q_{12} \\ (Q_{12})^* & Q_{22} \end{bmatrix} \ge 0. \tag{3.29}$$

The convex form lower bound of Q_{22} is found by using linear approximation as shown in Eq. (3.30).

$$Q_{22} = \underbrace{|D_q(j\omega_k, b_i)|^2}_{\text{original}} \ge \Phi_q := \underbrace{(D_q(j\omega_k, b_{i-1}))^2 + \nabla(D_q(j\omega_k, b_{i-1}))^2(b_i - b_{i-1})}_{\text{newly-obtained}}, \tag{3.30}$$

in which $\nabla(D(j\omega_k, a_{i-1}))^2$ can be obtained by the similar method of Eq. (3.15).

In conclusion, the convex form sufficient condition of Eq. (3.12f) is obtained as follows.

$$\begin{bmatrix} |D_q(j\omega_k, b_{i-1}) + 1|^2 & \Delta D_q \\ (\Delta D_q)^* & \Phi_q \end{bmatrix} \ge 0. \tag{3.31}$$

Constraint for bandwidth in second order low pass filter case

The left side of Eq. (3.13b) ($\omega_p \le \frac{1}{\sqrt{b_2}}$) is changed into the following form by using linear approximation of $\frac{1}{\sqrt{b_2}}$:

$$\underbrace{\omega_{p(i)} \le \frac{1}{\sqrt{b_{2(i)}}}}_{\text{original}} \Leftarrow \underbrace{\omega_{p(i)} \le \frac{1}{\sqrt{b_{2(i-1)}}} - \frac{b_{2(i-1)}^{\frac{-3}{2}}}{2}(b_{2(i)} - b_{2(i-1)})}_{\text{newly-obtained}}. \tag{3.32}$$

The Schur complement is used to deal with the right side of Eq. (3.13b) ($\frac{1}{\sqrt{b_2}} \le \omega_t$):

$$\begin{aligned} &\underbrace{\frac{1}{b_{2(i)}} \le \omega_{t(i)}^2}_{\text{original}} \Leftarrow \frac{1}{b_{2(i)}} \le 2\omega_{t(i-1)}\omega_{t(i)} - \omega_{t(i-1)}^2 \\ &\Leftrightarrow \underbrace{\begin{bmatrix} 2\omega_{t(i-1)}\omega_{t(i)} - \omega_{t(i-1)}^2 & 1 \\ 1 & b_{2(i)} \end{bmatrix} \ge 0}_{\text{newly-obtained}}. \end{aligned} \tag{3.33}$$

3.2.4 Problem reformulation

By summarizing Eq. (3.14), Eq. (3.22), Eq. (3.25) and Eq. (3.31), the original problem is reformulated as follows.

$$
\begin{aligned}
&\underset{a,b,\omega_t,\phi_s}{\text{Maximize}} && \omega_p \\
&\text{Subject to} && 0 < a, 0 < b, && \text{(3.34a)}\\
& && 0 < w_{p(i)} < w_{t(i)}, 0 < \phi_{s(i)}, && \text{(3.34b)}\\
& && \Psi - r_m D(j\omega_k, a_i, b_i) \geq 0, && \text{(3.34c)}\\
& && \begin{bmatrix} |D_q(b_{i-1}) + 1|^2 & \Delta D_q \\ (\Delta D_q)^* & \Phi_q \end{bmatrix} \geq 0, && \text{(3.34d)}\\
& && \begin{bmatrix} \omega_k^2 \phi_{s(i)} & D(j\omega_k, a_i, b_i) \\ (D(j\omega_k, a_i, b_i))^* & \Phi \end{bmatrix} \geq 0, && \text{(3.34e)}\\
& && \begin{bmatrix} 2\omega_{p(i-1)}^2 - \phi_{s(i)}\omega_{p(i-1)}^4 & \omega_{p(i)} \\ \omega_{p(i)} & 1 \end{bmatrix} \geq 0, && \text{(3.34f)}\\
& && \begin{bmatrix} 2\omega_{t(i-1)}\omega_{t(i)} - \omega_{t(i-1)}^2 & \dfrac{|N(j\omega_k)|(j\omega_k + \omega_{t(i)})}{M_t} \\ \dfrac{|N(j\omega_k)|(j\omega_k + \omega_{t(i)})^*}{M_t} & \Phi \end{bmatrix} \geq 0. && \text{(3.34g)}
\end{aligned}
$$

If Q is a second order filter, Eq. (3.34d) is not needed and can be replaced by Eq. (3.32) and Eq.(3.33). If Q does not contain any variables in the numerator, the constraint Eq. (3.34g) is needed to be modified to Eq. (3.26).

The new optimization problem is a convex optimization problem and can be solved by commercial solvers.

Remark: Although complex mathematical transformation process has been employed in the transformation process, the comparison with Genetic Algorithm has shown that limited conservatism has been introduced [109].

3.2.5 Procedures of designing low pass filter in continuous domain

Based on the previous analysis, procedures of designing low pass filter in continuous domain can be summarized as follows.

1. Select the form and relative order of Q filter based on the nominal plant
   (a) The relative order of Q filter should be no smaller than relative order of nominal plant.
   (b) The form of Q filter depends on the type of nominal plant model.
   For an ordinary minimum phase nominal plant, a minimum phase Q filter is used. Importantly, if the nominal plant model is of non-minimum phase, Q filter should also contain the same unstable zeros as plant model does. However, if the minimum phase approximation of non-minimum phase plant is used, a minimum phase Q filter should be selected.
2. Define desired gain margin as well as phase margin and formulate the design problem as introduced in previous section.
3. Solve the convex optimization in optimization software and confirm defined constraints have been satisfied.

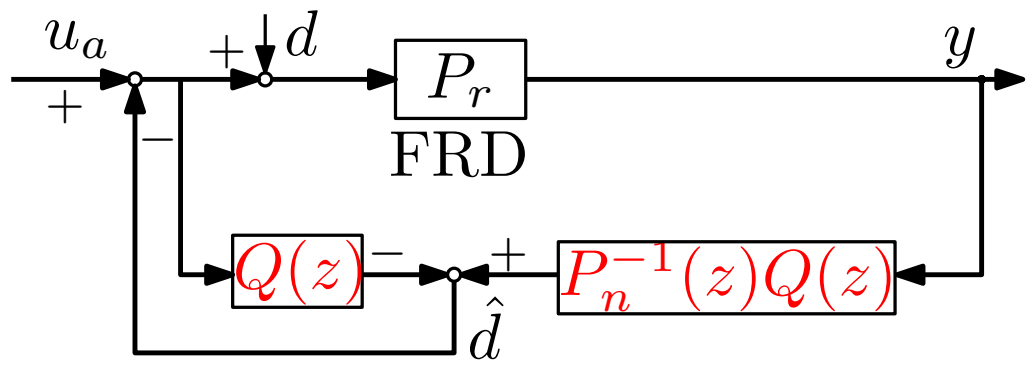

Figure 3.6 Block diagram of disturbance observer system in discrete domain for low pass filter design

3.3 Low pass filter design in discrete domain

3.3.1 Block diagram analysis

In the discrete disturbance observer control system as shown in Fig. 3.6, P_r and $P_n(z)$ denote real plant and nominal plant , defined by FRD and transfer function in discrete domain, respectively. $Q(z)$ represents the to-be-designed low pass filter. Same as in s domain block diagram Fig. 3.1, signals $d, \hat{d}, u_a, y$ are real external disturbance, estimated disturbance, control input and output, respectively.

$Q(z)$ is selected as the following fixed form in which $a_d \triangleq [a_{d(1)}, \cdots, a_{d(m^*)}]^T$ and $b_d \triangleq [b_{d(1)}, \cdots, b_{d(n^*)}]^T$ are parameter vectors to be decided and the order $n^* - m^*$ should be no smaller than the relative order of the inversion (or approximated inversion) of P_n.

$$Q_d(z, a_d, b_d) = \frac{a_{d(m^*)} z^{m^*} + \cdots + a_{d(1)}}{b_{d(n^*)} z^{n^*} + \cdots + b_{d(1)} z + 1}, \tag{3.35}$$

in which $a_{d(m*)} + \cdots + a_{d(1)} = b_{d(n*)} + + \cdots + b_{d(1)} + 1$.

Same as in s domain, the selection of $Q_d(z)$ depends on the nominal plant. But when the relative order of discrete nominal plant is 0, the order of $Q_d(z)$ filter is decided by the designer. The loop gain L_d, sensitivity function S_d and complementary function T_d for Fig. 3.6 are obtained as follows.

$$L_d(j\omega_k, a_d, b_d) = P_n^{-1}(z) Q(z, a_d, b_d)(1 - Q(z, a_d, b_d))^{-1} P_r(j\omega_k) = \frac{N_d(j\omega_k, a_d)}{D_d(j\omega_k, a_d, b_d)}, \tag{3.36a}$$

$$S_d(j\omega_k, a_d, b_d) = \frac{1}{1 + P_n^{-1}(z) Q(z, a_d, b_d)(1 - Q(z, a_d, b_d))^{-1} P_r(j\omega_k)} = \frac{D_d(j\omega_k, a_d, b_d)}{D_d(j\omega_k, a_d, b_d) + N_d(j\omega_k, a_d)}, \tag{3.36b}$$

$$T_d(j\omega_k, a_d, b_d) = \frac{P_n^{-1}(z) Q(z, a_d, b_d)(1 - Q(z, a_d, b_d))^{-1} P_r(j\omega_k)}{1 + P_n^{-1}(z) Q(z, a_d, b_d)(1 - Q(z, a_d, b_d))^{-1} P_r(j\omega_k)}. \tag{3.36c}$$

Constraints for designing low pass filter in discrete domain are introduced in the next section.

3.3.2 Constraints formulation

The constraints for guaranteeing stability margins as well as the constraints for sensitivity function and complementary sensitivity function are the same as in continuous domain design. To avoid repetition, only mathematical representations are shown in this section.

① **Constraint for guaranteeing stability margins**

The same circle condition ([88]), which is shown in Fig. 3.2, should be met to guarantee the desired gain margin g_m and phase margin ϕ_m. The mathematical representation is given as follows:

$$|\sigma + L_d(j\omega_k, a_d, b_d)| - r_m \geq 0, \tag{3.37}$$

in which

$$\sigma = \frac{g_m^2 - 1}{2g_m(g_m \cos\phi_m - 1)}, r_m = \frac{(g_m - 1)^2 + 2g_m(1 - \cos\phi_m)}{2g_m(g_m \cos\phi_m - 1)}. \tag{3.38}$$

② **Constraints for sensitivity function and complementary sensitivity function**

Constraints for the sensitivity function S and the complementary sensitivity function T, which are graphically shown in Fig. 3.3 and Fig. 3.4, are determined as follows. ω_p is selected as the optimization objective. When the optimal point $\omega_{p(opt)}$ is found, a_d, b_d are obtained simultaneously and Q_d filter can be designed.

$$W_p(j\omega_k, \omega_p) = \frac{\omega_p}{j\omega_k}, |W_p(j\omega_k, \omega_p)S(j\omega_k, a_d, b_d)| \leq 1, \tag{3.39}$$

$$W_m(j\omega_k, \omega_t) = \frac{j\omega_k + \omega_t}{M_t\omega_t}, \ |W_m(j\omega_k, \omega_t)T(j\omega_k, a_d, b_d)| \leq 1. \tag{3.40}$$

③ **Constraint for guaranteeing stability of low pass filter**

In s domain, coefficients of denominator of $Q(s)$ should all be positive to make sure poles are in the left side of imaginary axis. But in z domain, such constraints don't exist even in the second order case which adds the difficulty of formulating the constraint.

The author has followed the same idea as in dealing with the stability of high order Q filter in continuous domain by intentionally designing open loop function $L_{qd}(z, b_{d(i)})$ as follows. When the Nyquist plot of $L_{qd}(z, b_{d(i)})$ (ith iteration), which is the open loop function defined as follows, never encircles (-1,0) as shown in Fig. 3.5, the stability of closed loop function $H_{qd}(z, b_{d(i)})$ which represents for the stability of $Q_d(z)$ filter, is guaranteed during the optimization process.

$$L_{qd}(z, b_{d(i)}) = \frac{b_{dc(i)}}{b_{dn(i)}z^n + \cdots + b_{d1(i)}z + 1 - b_{dc(i)}} = \frac{b_{dc(i)}}{D_{qd}(z, b_{d(i)})}, \tag{3.41}$$

$$H_{qd}(z, b_{d(i)}) = \frac{L_q(z, b_{d(i)})}{1 + L_q(z, b_{d(i)})} = \frac{b_{dc(i)}}{b_{n(i)}z^n + \cdots + b_{1(i)}z + 1}, \tag{3.42}$$

where $b_{dc(i)}$ is the DC gain of $b_{dn(i)}z^n + \cdots + b_{d1(i)}z + 1$.

The mathematical interpretation is given as (3.43) which means the distance $|L_{qd}(j\omega_k, b_{d(i)}) - L_{qd}(j\omega_k, b_{d(i-1)})|$ should be no larger than the distance between $L_{qd}(j\omega_k, b_{d(i-1)})$ and $(-1, 0)$ at every frequency point after every iteration.

$$|L_{qd}(j\omega_k, b_{d(i)}) - L_{qd}(j\omega_k, b_{d(i-1)})| \leq |L_{qd}(j\omega_k, b_{d(i-1)}) + 1|. \tag{3.43}$$

In summary, the design of filter $Q_d(z)$ is formulated into the following optimization problem:

$$\underset{a_d, b_d, \omega_t}{\text{Maximize}} \quad \omega_p \tag{3.44a}$$

$$\text{Subject to} \quad 0 < \omega_p < \omega_t, \tag{3.44b}$$

$$|L_d(j\omega_k, a_d, b_d) + \sigma| \geq r_m, \tag{3.44c}$$

$$|W_p(j\omega_k, \omega_p)S(j\omega_k, a_d, b_d)| \leq 1, \tag{3.44d}$$

$$|W_m(j\omega_k, \omega_t)T(j\omega_k, a_d, b_d)| \leq 1, \tag{3.44e}$$

$$|L_{qd}(j\omega_k, b_{d(i)}) - L_{qd}(j\omega_k, b_{d(i-1)})| \leq |L_{qd}(j\omega_k, b_{d(i-1)}) + 1|. \tag{3.44f}$$

3.3.3 Convex constraints derivation

The process for transforming constraints are similar to the process in the design of continuous domain. Therefore, only obtained convex constraints are shown in this section.

Constraint for guaranteeing stability margins

In this subsection, the transformed convex form of constraint Eq. (3.44c), which is for guaranteeing margins, is shown as follows.

$$\begin{aligned}
&\left|L_d(j\omega_k, a_{d(i)}, b_{d(i)}) + \sigma\right| - r_m = \left|\frac{N_d(j\omega_k, a_{d(i)})}{D_d(j\omega_k, a_{d(i)}, b_{d(i)})} + \sigma\right| - r_m \geq 0 \\
&\Leftrightarrow \left|N_d(j\omega_k, a_{d(i)}) + D_d(j\omega_k, a_{d(i)}, b_{d(i)})\sigma\right| \triangleq \underbrace{F_d(j\omega_k, a_{d(i)}, b_{d(i)}) \geq r_m \left|D_d(j\omega_k, a_{d(i)}, b_{d(i)})\right|}_{\text{original}} \\
&\Leftarrow \underbrace{\Psi_d \geq r_m \left|D_d(j\omega_k, a_{d(i)}, b_{d(i)})\right|}_{\text{newly-obtained}},
\end{aligned} \tag{3.45}$$

where $\Psi_d = F_d(j\omega_k, a_{d(i-1)}, b_{d(i-1)}) + \nabla F_d(j\omega_k, a_{d(i-1)}, b_i)(a_{d(i)} - a_{d(i-1)}) + \nabla F_d(j\omega_k, a_{d(i)}, b_{d(i-1)})(b_{d(i)} - b_{d(i-1)})$ and ∇F_d can be obtained by using Eq. (3.15).

Constraint for sensitivity function

For the sensitivity function constraint Eq. (3.44d), following results are obtained.

$$\begin{aligned}
&\left|W_p(j\omega_k, \omega_{p(i)}) S(j\omega_k, a_{d(i)}, b_{d(i)})\right| \leq 1 \Leftrightarrow \left|W_p(j\omega_k, \omega_{p(i)}) S(j\omega_k, a_{d(i)}, b_{d(i)})\right|^2 \leq 1 \\
&\Leftarrow \underbrace{\begin{bmatrix} \omega_k^2 \phi_{d(i)} & D(j\omega_k, a_{d(i)}, b_{d(i)}) \\ (D(j\omega_k, a_{d(i)}, b_{d(i)}))^* & \Phi_d \end{bmatrix} \geq 0,\ \phi_{d(i)} > 0, \begin{bmatrix} 2\omega_{p(i-1)}^2 - \phi_{d(i)}\omega_{p(i-1)}^4 & \omega_{p(i)} \\ \omega_{p(i)} & 1 \end{bmatrix} > 0}_{\text{newly-obtained}}.
\end{aligned} \tag{3.46}$$

in which

$$\begin{aligned}
&\left|D_d(j\omega_k, a_{d(i)}, b_{d(i)}) + N_d(j\omega_k, a_{d(i)})\right|^2 \triangleq \underbrace{(M_d(j\omega_k, a_{d(i)}, b_{d(i)}))^2}_{\text{original}} \geq \underbrace{\Phi_d}_{\text{newly-obtained}} \\
&:= (M_d(j\omega_k, a_{d(i-1)}, b_{d(i-1)}))^2 + \nabla(M_d(j\omega_k, a_{d(i-1)}, b_{d(i)}))^2 (a_{d(i)} - a_{d(i-1)}) \\
&+ \nabla(M_d(j\omega_k, a_{d(i)}, b_{d(i-1)}))^2 (b_{d(i)} - b_{d(i-1)}),
\end{aligned} \tag{3.47}$$

in which $\nabla M_d(j\omega_k, a_{d(i-1)}, b_{d(i)})^2$ as well as $\nabla M_d(j\omega_k, a_{d(i)}, b_{d(i-1)})^2$ are calculated similarly to Eq. (3.15).

Constraint for complementary sensitivity function

The complementary sensitivity function constraint Eq. (3.44e) is changed into the following form (Selection of the form depends on whether the numerator of Q_d contains optimization variables or not).

$$\begin{aligned}
&\left|W_m(j\omega_k, \omega_{t(i)}) T(j\omega_k, a_{d(i)}, b_{d(i)})\right| \leq 1 \\
&\Leftrightarrow \begin{bmatrix} \omega_t^2 & \dfrac{(N_d(j\omega_k, a_{d(i)})(j\omega_k + \omega_t))}{M_t} \\ \dfrac{(N_d(j\omega_k, a_{d(i)})(j\omega_k + \omega_t))^*}{M_t} & \Phi_d \end{bmatrix} \geq 0,
\end{aligned} \tag{3.48}$$

or

$$\begin{aligned}&\left|W_m(j\omega_k,\omega_{t(i)})T(j\omega_k,a_{d(i)},b_{d(i)})\right|\le 1\\ \Leftrightarrow&\begin{bmatrix}2\omega_{t(i)}\omega_{t(i-1)}-\omega_{t(i-1)}^2 & \dfrac{(N_d(j\omega_k)(j\omega_k+\omega_t))}{M_t}\\ \dfrac{(N_d(j\omega_k)(j\omega_k+\omega_t))^*}{M_t} & \Phi_d\end{bmatrix}\ge 0,\end{aligned}\tag{3.49}$$

in which Φ_d is the same item as in Eq. (3.47).

Constraint for guaranteeing the stability of low pass filter

For constraint Eq. (3.44f), the following technique is employed to obtain its sufficient condition in convex form.

$$\begin{aligned}&\underbrace{|L_{qd}(j\omega_k,b_{d(i)})-L_{qd}(j\omega_k,b_{d(i-1)})|\le|L_{qd}(j\omega_k,b_{d(i-1)})+1|}_{\text{original}}\\ \Leftrightarrow&\left|\frac{b_{dc(i)}}{D_{qd}(j\omega_k,b_{d(i)})}-\frac{b_{dc(i-1)}}{D_{qd}(j\omega_k,b_{d(i-1)})}\right|\le\left|\frac{b_{dc(i-1)}}{D_{qd}(j\omega_k,b_{d(i-1)})}+1\right|.\end{aligned}\tag{3.50}$$

Using ΔD_{qd} to represent $D_{qd}(j\omega_k,b_{d(i-1)})\times b_{dc(i)}-D_{qd}(j\omega_k,b_{d(i)})\times b_{dc(i-1)}$, the following equation can be derived.

$$|\Delta D_{qd}|\le|D_{qd}(j\omega_k,b_{d(i)})||D_{qd}(j\omega_k,b_{d(i-1)})+b_{dc(i-1)}|.\tag{3.51}$$

By squaring the above equation and using the Schur complement, the following equation is obtained.

$$\underbrace{\begin{bmatrix}|D_{qd}(j\omega_k,b_{d(i-1)})+b_{dc(i-1)}|^2 & \Delta D_{qd}\\ (\Delta D_{qd})^* & \Phi_{qd}\end{bmatrix}\ge 0}_{\text{newly-obtained}},\tag{3.52}$$

in which

$$\underbrace{\left|D_{qd}(j\omega_k,b_{d(i)})\right|^2}_{\text{original}}\ge\Phi_{qd}:=\underbrace{(D_{qd}(j\omega_k,b_{d(i-1)}))^2+\nabla(D_{qd}(j\omega_k,b_{d(i-1)}))^2(b_{d(i)}-b_{d(i-1)})}_{\text{newly-obtained}},\tag{3.53}$$

with $\nabla(D_{qd}(j\omega_k,b_{d(i-1)}))^2$ denoting the differential result of $(D_{qd}(j\omega_k,b_{d(i-1)}))^2$ in terms of $b_{d(i-1)}$.

3.3.4 Problem reformulation

By summarizing Eq. (3.45), Eq. (3.46), Eq. (3.48) (or Eq. (3.49)) and Eq. (3.52), the original problem is reformulated as follows.

$$
\begin{aligned}
\underset{a_d, b_d, \phi_d}{\text{Maximize}} \quad & \omega_p \\
\text{Subject to} \quad & \omega_{t(i)} > \omega_{p(i)} > 0, && \text{(3.54a)} \\
& \phi_{d(i)} > 0, \Psi_d - r_m D_d(j\omega, a_{d(i)}, b_{d(i)}) \geq 0, && \text{(3.54b)} \\
& \begin{bmatrix} \omega_k^2 \phi_{d(i)} & D_d(j\omega_k, a_{d(i)}, b_{d(i)}) \\ (D_d(j\omega_k, a_{d(i)}, b_{d(i)}))^* & \Phi_d \end{bmatrix} \geq 0, && \text{(3.54c)} \\
& \begin{bmatrix} 2\omega_{p(i-1)}^2 - \phi_{d(i)} \omega_{p(i-1)}^4 & \omega_{p(i)} \\ \omega_{p(i)} & 1 \end{bmatrix} \geq 0, && \text{(3.54d)} \\
& \begin{bmatrix} \omega_t^2 & \dfrac{|N_d(j\omega_k, a_{d(i)})|(j\omega_k + \omega_{t(i)})}{M_t} \\ \dfrac{|N_d(j\omega_k, a_{d(i)})|(j\omega_k + \omega_{t(i)})^*}{M_t} & \Phi_d \end{bmatrix} \geq 0, && \text{(3.54e)} \\
& \begin{bmatrix} |D_{qd}(j\omega_k, b_{d(i-1)}) + b_{dc(i-1)}|^2 & \Delta D_{qd} \\ (\Delta D_{qd})^* & \Phi_{qd} \end{bmatrix} \geq 0. && \text{(3.54f)}
\end{aligned}
$$

The new optimization problem is a convex optimization problem and can be solved by commercial solvers.

3.3.5 Procedures of designing low pass filter in discrete domain

Based on the previous analysis, procedures of designing low pass filter in discrete domain can be summarized as follows.

1. Select the form of $Q(z)$ filter and relative order based on the nominal plant
   (a) The relative order of $Q(z)$ filter should be no smaller than relative order of nominal plant. Different from the design in continuous domain, if the Tustin transformation is used, the relative order of discrete form of nominal plant model is 0. In such case, the relative order of $Q(z)$ filter can also be selected as 0.
   (b) The form of $Q(z)$ filter depends on the type of nominal plant model.
   Same as in continuous domain, for an ordinary minimum phase nominal plant or a minimum phase approximation of a non-minimum phase plant, a minimum phase $Q(z)$ filter is used. For a non-minimum phase nominal plant model, $Q(z)$ filter should also contain the same unstable zeros as nominal plant model has.
2. Define desired gain margin as well as phase margin and formulate the design problem as shown in previous section.
3. Solve the convex optimization in optimization software and confirm defined constraints have been satisfied.

3.4 Summary

This chapter has introduced the theoretical analysis on FRD-based low pass filter design in disturbance observer.

1. The problem formulation process of FRD-based low pass filter design in disturbance observer has been illustrated.
2. Original non-convex constraints have been transformed into convex form, which can be solved by convex optimization method by utilizing off the shelf optimization toolboxes. The detailed mathematical transformation process in continuous domain as well as in discrete domain have been present.
3. Obtained convex constraints are the sufficient condition of original constraints which ensures that obtained DOB satisfies original constraints successfully.
4. No limitations on nominal plant or Q filter, *e.g.*, the nominal plant should be minimum phase or the order of Q filter, are required in this method which indicates that the proposal is a general and systematic way of designing DOB system.

Chapter 4

Convex optimization problem formulation of plant model identification and low pass filter design in disturbance observer

4.1 Overview

This chapter has summarized the content of identifying nominal plant model and designing low pass filter simultaneously in DOB in continuous domain as well as in discrete domain.

Same as in low pass filter design, the original non-convex problem formulation as well as the convex optimization problem reformulation process have been discussed. In previous studies of DOB which has been introduced in Introduction (Chapter 1), the nominal plant is given and to the best of our knowledge, for the first time the plant has been simultaneously obtained from the DOB design process. The necessity for design plant and filter simultaneously can be simply summarized as more freedom in tuning DOB loop open loop function if plant is not fixed which will be further discussed in the case study and experimental results.

Since identification of nominal plant model and design of low pass filter have been done simultaneously in the optimization process, the separation of nominal plant model and low pass filter is needed and separation methods have also been present in this chapter.

4.2 Plant model identification and low pass filter design in continuous domain

4.2.1 Block diagram analysis

In the disturbance observer control system as shown in Fig. 4.1, P_r denotes real plant which is defined by FRD. Signals $d, \hat{d}, u_a, y$ denote external disturbance input, estimated disturbance, control input and output, respectively. $P_n(s)$ and $Q(s)$ represent the to-be-decided nominal plant model and low pass filter.

In this chapter, $Q(s)$ and $P_n(s)$ (irreducible) are selected as follows in which $\hat{a} \triangleq [\hat{a}_1, \cdots, \hat{a}_{n_q}]^T$, $\hat{b} \triangleq [\hat{b}_1, \cdots, \hat{b}_{n_q - r^*}]^T$, $\hat{f} \triangleq [\hat{f}_1, \cdots, \hat{f}_{sn}]^T$, $\hat{c} \triangleq [\hat{c}_0, \cdots, \hat{c}_{sd}]^T$ are parameters to be decided and orders n_q, sn, sd are selected by designer but $r^* \geq sd - sn$ should be satisfied to guarantee the causality.

$$Q(s)=\frac{\hat{b}_{n_q-r^*}s^{n_q-r^*}+\cdots+\hat{b}_1 s+1}{\hat{a}_{n_q}s^{n_q}+\cdots+\hat{a}_1 s+1}\triangleq\frac{Q_{Ns}}{Q_{Ds}},P_n(s)=\frac{\hat{f}_{sn}s^{sn}+\cdots+\hat{f}_1 s+1}{\hat{c}_{sd}s^{sd}+\cdots+\hat{c}_1 s+\hat{c}_0}\triangleq\frac{P_{n(Ns)}}{P_{n(Ds)}}. \tag{4.1}$$

The loop gain (L_{fs}), sensitivity function (S_{fs}) and complementary sensitivity function (T_{fs}) are obtained for Fig. 4.1 as follows.

$$L_{fs}(j\omega_k,t,h)=P_n^{-1}(s)Q(s)(1-Q(s))^{-1}P_r(j\omega_k)=\frac{P_r(j\omega_k)(h_{fh}s^{fh}+\cdots+h_0)}{s^{ft}+\cdots+t_1 s+t_0}=\frac{N_{fs}(j\omega_k,h)}{D_{fs}(j\omega_k,t)}, \tag{4.2a}$$

$$S_{fs}(j\omega_k,t,h)=\frac{1}{1+(1-Q(s))^{-1}Q(s)P_n^{-1}(s)P_r(j\omega_k)}=\frac{D_{fs}(t)}{D_{fs}(j\omega_k,t)+N_{fs}(j\omega_k,h)}, \tag{4.2b}$$

$$\frac{y}{d}=\frac{P_r(j\omega_k)}{1+(1-Q(s))^{-1}Q(s)P_n^{-1}(s)P_r(j\omega_k)}=S_{fs}(j\omega_k,t,h)P_r(j\omega_k), \tag{4.2c}$$

$$\frac{\hat{d}}{d}=\frac{(1-Q(s))^{-1}Q(s)P_n^{-1}(s)P_r(j\omega_k)}{1+(1-Q(s))^{-1}Q(s)P_n^{-1}(s)P_r(j\omega_k)}=T_{fs}(j\omega_k,t,h), \tag{4.2d}$$

in which

$$h_{fh}s^{fh}+\cdots+h_0=(P_{n(Ds)})\times(Q_{Ns}),s^{ft}+\cdots+t_1 s+t_0=(P_{n(Ns)})\times(Q_{Ds}-Q_{Ns}), \tag{4.3}$$

$$\text{DC gain of }(h_{fh}s^{fh}+\cdots+h_0)\geq\text{DC gain of }(s^{ft}+\cdots+t_1 s+t_0). \tag{4.4}$$

Remark 1: when the plant is of non-minimum phase and Q filter is selected to contain unstable zeros of plant, pole-zero cancellation exists in Eq. (4.2a).

In the next section, constraints, such as constraint for guaranteeing stability margins, have been designed to achieve satisfactory disturbance rejection performance. However, constraints for guaranteeing margins and (complementary) sensitivity limitation has been introduced briefly due to the repetition of Chapter 3 while internal stability constraints have been discussed in detail. Furthermore, the separation process of $P_n(s)$ and $Q(s)$ from optimized $L_{fs}(j\omega_k,t,h)$ has been present. Subsequently, simultaneous identification of nominal plant model and design of low pass filter has been formulated into an optimization problem in which h as well as t are optimization parameters and the bandwidth of DOB is the optimization objective.

4.2.2 Constraints formulation

① **Constraint for stability margins**

The same circle condition ([88]), which is shown in Fig. 3.2, is defined to guarantee the desired gain margin g_m and phase margin ϕ_m. The same mathematical representation is given as follows:

$$|\sigma+L_{fs}(j\omega_k,h,t)|-r_m\geq 0, \tag{4.5}$$

in which

$$\sigma=\frac{g_m^2-1}{2g_m(g_m\cos\phi_m-1)},r_m=\frac{(g_m-1)^2+2g_m(1-\cos\phi_m)}{2g_m(g_m\cos\phi_m-1)}. \tag{4.6}$$

② **Constraints for sensitivity function and complementary sensitivity function**

Same constraints for the sensitivity function S_{fs} and the complementary sensitivity function T_{fs}, which are graphically shown in Fig. 3.3 and Fig. 3.4, are determined as follows. ω_p is selected as the optimization

objective. When the optimal point $\omega_{p(opt)}$ is found, h, t are obtained simultaneously and nominal plant as well as Q filter can be obtained subsequently.

$$W_p(j\omega_k, \omega_p) = \frac{\omega_p}{j\omega_k}, |W_p(j\omega_k, \omega_p) S_{fs}(j\omega_k, h, t)| \leq 1, \tag{4.7}$$

$$W_m(j\omega_k, \omega_t) = \frac{j\omega_k + \omega_t}{M_t \omega_t}, |W_m(j\omega_k, \omega_t) T_{fs}(j\omega_k, h, t)| \leq 1. \tag{4.8}$$

③ **Constraints for guaranteeing internal stability**

From the perspective of internal stability, $(P_n(s)^{-1}Q(s)(1-Q(s))^{-1})$ should not contain any unstable poles. Moreover, based on Eq. (4.3), the desired nominal plant should not contain any unstable poles which means the numerator of $(P_n(s)^{-1}Q(s)(1-Q(s))^{-1})$ should also not contain any unstable roots.

By intentionally designing open loop function $L_{ld}(s, h_i, t_i)$ as follows, the same strategy as in dealing with continuous domain high order $Q(s)$ filter stability has been employed.

$$L_{ld}(s, t_i) = \frac{t_{0(i)}}{s^{ft} + \cdots + t_{2(i)} s^2 + t_{1(i)} s} = \frac{t_{0(i)}}{D_{ld}}, \tag{4.9}$$

$$H_{ld}(s, t_i) = \frac{L_q(s, t_i)}{1 + L_q(s, t_i)} = \frac{t_{0(i)}}{s^{ft} + \cdots + t_{2(i)} s^2 + t_{1(i)} s + t_{0(i)}}. \tag{4.10}$$

Remark: if $t_0 = 0$, the $L_{ld}(s, t_i)$ can be defined as follows. But since the analysis is similar for different L_{ld}, in this thesis, the above defined one is used in the following discussion.

$$L_{ld}(s, t_i) = \frac{t_{1(i)}}{s^{ft-1} + \cdots + t_{2(i)} s}. \tag{4.11}$$

The mathematical interpretation is given as Eq. (4.12) which means the distance $|L_{ld}(j\omega_k, t_i) - L_{ld}(j\omega_k, t_{i-1})|$ should be no larger than the distance between $L_{ld}(j\omega_k, t_{i-1})$ and $(-1, 0)$ at every frequency point during every iteration.

$$|L_{ld}(j\omega_k, t_i) - L_{ld}(j\omega_k, t_{i-1})| \leq |L_{ld}(j\omega_k, t_{i-1}) + 1|. \tag{4.12}$$

By employing the same method to the constraint of numerator, the following constraint can be obtained.

$$|L_{ln}(j\omega_k, h_i) - L_{ln}(j\omega_k, h_{i-1})| \leq |L_{ln}(j\omega_k, h_{i-1}) + 1|, \tag{4.13}$$

in which

$$L_{ln}(s, h_i) = \frac{h_{0(i)}}{h_{fh(i)} s^{fh} + \cdots + h_{1(i)} s}. \tag{4.14}$$

In summary, the simultaneous identification of nominal plant model and design of low pass filter in disturbance observer is formulated into the following non-convex optimization problem.

$$\underset{h,t,\omega_t}{\text{Maximize}} \quad \omega_p \tag{4.15a}$$

$$\text{Subject to} \quad 0 < h, t, 0 < \omega_p < \omega_t, \tag{4.15b}$$

$$|L_{fs}(j\omega_k, h_i, t_i) + \sigma| \geq r_m, \tag{4.15c}$$

$$|W_p(j\omega_k, \omega_p) S_{fs}(j\omega_k, h_i, t_i)| \leq 1, \tag{4.15d}$$

$$|W_m(j\omega_k) T_{fs}(j\omega_k, h_i, t_i)| \leq 1, \tag{4.15e}$$

$$|L_{ld}(j\omega_k, t_i) - L_{ld}(j\omega_k, t_{i-1})| \leq |L_{ld}(j\omega_k, t_{i-1}) + 1|, \tag{4.15f}$$

$$|L_{ln}(j\omega_k, h_i) - L_{ln}(j\omega_k, h_{i-1})| \leq |L_{ln}(j\omega_k, h_{i-1}) + 1|. \tag{4.15g}$$

The optimization process will produce the maximized ω_p and optimized parameter vectors $h \triangleq [h_0, \cdots, h_{fh}]^T$ as well as $t \triangleq [t_0, t_1, \cdots, t_{ft-1}]^T$. Thereafter parameter vectors $\hat{a} \triangleq [\hat{a}_1, \cdots, \hat{a}_{n_q}]^T$,

$\hat{b} \triangleq [\hat{b}_1, \cdots, \hat{b}_{n_q-r^*}]^T$, $\hat{f} \triangleq [\hat{f}_1, \cdots, \hat{f}_{sn}]^T$, $\hat{c} \triangleq [\hat{c}_0, \cdots, \hat{c}_{sd}]^T$ are separated from optimized vectors t and h.

4.2.3 Separation of $P_n(s)$ and $Q(s)$ from $(P_n^{-1}(s)Q(s)(1-Q(s))^{-1})_{opt}$

① Allocate poles and zeros of $(P_n^{-1}(s)Q(s)(1-Q(s))^{-1})_{opt}$ to $P_n(s)$ and $Q(s)$.

1. Zeros of $(P_n^{-1}(s)Q(s)(1-Q(s))^{-1})_{opt}$ consist of poles of $P_n(s)$ and zeros of $Q(z)(1-Q(z))^{-1}$, see Eq. (4.2a) and Eq. (4.3).
2. Poles of $(P_n^{-1}(s)Q(s)(1-Q(s))^{-1})_{opt}$ are made up of zeros of $P_n(s)$ and poles of $Q(z)(1-Q(z))^{-1}$, see Eq. (4.2a) and Eq. (4.3).
3. Designer may choose among the following three different cases to obtain $P_n(s)$ and $Q(s)$.
   (a) $P_n(s)$ is minimum phase and $Q(s)$ is a minimum phase low pass filter.
   (b) $P_n(s)$ is non-minimum phase and $Q(s)$ has the same unstable zeros as nominal plant has. In this case, pole-zero cancellation exists.
   (c) $P_n(s)$ is the minimum phase approximation of a non-minimum phase plant and $Q(s)$ is a minimum phase low pass filter.
4. The separation of poles and zeros are done by referring to the phase information of FRD and poles' distribution in the optimization initial condition.
   The separation result can be shown as follows:

$$\begin{aligned}
&\frac{(h_{fh}s^{n_{fh}} + \cdots + h_1 s + h_0)}{s^{ft} + \cdots + t_1 s + t_0} _ \frac{G_{pqs}(s+z_1)\cdots(s+z_{fh})}{s(s+p_1)\cdots(s+p_{ft})}, \\
&= \underbrace{\frac{G_{pqs1}(s+z_{q_1})\cdots(s+z_{q_{n_q-r^*}})}{(s+p_{q_1})\cdots(s+p_{q_{n_q}})}}_{Q(1-Q)^{-1}} \times \frac{\overbrace{(s+z_1)\cdots(s+z_{sn})}^{P_n^{-1}(num_s)}}{G_{pqs2}\underbrace{(s+p_{p_1})\cdots(s+p_{sd})}_{P_n^{-1}(den_s)}},
\end{aligned} \tag{4.16}$$

   in which G_{pqs1} and G_{pqs2} are gains to be calculated.

② Calculate G_{pqs1}, G_{pqs2} as well as $Q(s)$.

1. G_{pqs2} is calculated by using FRD information of plant and Eq. (4.17).
   To eliminate the influence of noise, least squares fitting is used.

$$|(P_r(j\omega_k))| = \frac{G_{pqs2}|P_n^{-1}(den_s)(j\omega_k)|}{|P_n^{-1}(num_s)(j\omega_k)|}. \tag{4.17}$$

2. G_{pqs1} is the multiplication of G_{pqs} and G_{pqs2} and $Q(s)$ can be calculated from Eq. (4.16).

$$G_{pqs1} = G_{pqs} \times G_{pqs2}. \tag{4.18}$$

4.2.4 Convex Constraints Derivation

In this section, above-listed non-convex constraints are all transformed into LMI form of variables ω_p, t, h. Derived constraints are sufficient condition of original constraints which implies that if newly-obtained constraints are satisfied, original constraints undoubtedly hold. The process for transforming constraints

for margins and sensitivity function along with complementary sensitivity function is similar to the design in the previous Chapter. Therefore, only obtained convex constraints are shown in this section. As for constraints for guaranteeing internal stability, similar technique as in dealing with the constraint for ensuring stability of high order Q filter is employed.

Constraint for guaranteeing stability margins

In this subsection, Eq. (4.15c) is converted to the following convex constraint.

$$\begin{aligned}
&|L_{fs}(j\omega_k, h_i, t_i) + \sigma| - r_m = \left| \frac{N_{fs}(j\omega_k, h_i)}{D_{fs}(j\omega_k, t_i)} + \sigma \right| - r_m \geq 0 \\
&\Leftrightarrow |N_{fs}(j\omega_k, h_i) + D_{fs}(j\omega_k, t_i)\sigma| \triangleq \underbrace{F_{fs}(j\omega_k, h_i, t_i) \geq r_m \, |D_{fs}(j\omega_k, t_i)|}_{\text{original}} \\
&\Leftarrow \underbrace{\Psi_{fs} \geq r_m \, |D_{fs}(j\omega_k, t_i)|}_{\text{newly-obtained}},
\end{aligned} \tag{4.19}$$

where $\Psi_{fs} = F_{fs}(j\omega_k, h_{i-1}, t_{i-1}) + \nabla F_{fs}(j\omega_k, h_i, t_{i-1})(t_i - t_{i-1}) + \nabla F_{fs}(j\omega_k, h_{i-1}, t_i)(h_i - h_{i-1})$ and $\nabla F_{fs}(j\omega_k, h_i, t_{i-1})$ as well as $\nabla F_{fs}(j\omega_k, h_{i-1}, t_i)$ can be obtained by using Eq. (3.15).

Constraint for sensitivity function

For the sensitivity function constraint Eq. (4.15d), following results are obtained.

$$\begin{aligned}
&\underbrace{\left|W_p(j\omega_k, \omega_{p(i)}) S_{fs}(j\omega_k, h_i, t_i)\right| \leq 1}_{\text{original}} \Leftrightarrow \left|W_p(j\omega_k, \omega_{p(i)}) S_{fs}(j\omega_k, h_i, t_i)\right|^2 \leq 1 \\
&\Leftarrow \underbrace{\begin{bmatrix} \omega_k^2 \phi_{fs(i)} & D_{fs}(j\omega_k, t_i) \\ (D_{fs}(j\omega_k, t_i))^* & \Phi_{fs} \end{bmatrix} \geq 0, \ \phi_{fs(i)} > 0, \begin{bmatrix} 2\omega_{p(i-1)}^2 - \phi_{fs(i)}\omega_{p(i-1)}^4 & \omega_{p(i)} \\ \omega_{p(i)} & 1 \end{bmatrix} > 0}_{\text{newly-obtained}},
\end{aligned} \tag{4.20}$$

in which $\phi_{fs(i)}$ is a variable and

$$\begin{aligned}
&|D_{fs}(j\omega_k, t_i) + N_{fs}(j\omega_k, h_i)|^2 \triangleq \underbrace{(M_{fs}(j\omega_k, h_i, t_i))^2}_{\text{original}} \geq \underbrace{\Phi_{fs}}_{\text{newly-obtained}} \\
&:= (M_{fs}(j\omega_k, h_{i-1}, t_{i-1}))^2 + \nabla(M_{fs}(j\omega_k, h_{i-1}, t_{(i)}))^2 (h_i - t_{i-1}) \\
&+ \nabla(M_{fs}(j\omega_k, h_i, t_{i-1}))^2 (t_i - t_{i-1}),
\end{aligned} \tag{4.21}$$

while $\nabla M_{fs}(j\omega_k, h_{i-1}, t_i)^2$ as well as $\nabla M_{fs}(j\omega_k, h_i, t_{i-1})^2$ are calculated similarly to Eq. (3.15).

Constraint for complementary sensitivity function

For the complementary sensitivity function constraint Eq. (4.15e), the following convex constraint can be obtained.

$$\begin{aligned}
&\underbrace{\left|W_m(j\omega_k, \omega_{t(i)}) T_{fs}(j\omega_k, h_i, t_i)\right| \leq 1}_{\text{original}} \\
&\Leftrightarrow \underbrace{\begin{bmatrix} \omega_t^2 & \dfrac{(N_{fs}(j\omega_k, h_{(i)})(j\omega_k + \omega_t))}{M_t} \\ \dfrac{(N_{fs}(j\omega_k, h_i)(j\omega_k + \omega_t))^*}{M_t} & \Phi_{fs} \end{bmatrix} \geq 0}_{\text{newly-obtained}},
\end{aligned} \tag{4.22}$$

in which Φ_{fs} is the same item as in Eq. (4.21).

Constraints for guaranteeing internal stability

For constraint Eq. (4.15f), same technique as in dealing with Eq. (3.12f) (constraint for high order Q filter's stability) has been utilized to obtain its approximate convex form.

$$\underbrace{|L_{ld}(j\omega_k,t_i)-L_{ld}(j\omega_k,t_{i-1})|\le|L_{ld}(j\omega_k,t_{i-1})+1|}_{\text{original}}$$
$$\Leftrightarrow\underbrace{\begin{bmatrix}|D_{ld}(j\omega_k,t_{i-1})+t_{0(i-1)}|^2 & \Delta D_{ld}\\ (\Delta D_{ld})^* & \Phi_{ld}\end{bmatrix}\ge 0}_{\text{newly-obtained}}, \tag{4.23}$$

where

$$\Delta D_{ld}=D_{ld}(j\omega_k,t_i)\times t_{0(i-1)}-D_{ld}(j\omega_k,t_{i-1})\times t_{0(i)}, \tag{4.24}$$
$$\underbrace{\left|D_{ld}(j\omega_k,t_{(i-1)})\right|^2}_{\text{original}}\ge\Phi_{ld}:=\underbrace{(D_{qd}(j\omega_k,t_{i-1}))^2+\nabla(D_{ld}(j\omega_k,t_{i-1}))^2(t_i-t_{i-1})}_{\text{newly-obtained}}, \tag{4.25}$$

with $\nabla(D_{ld}(j\omega_k,t_{i-1}))^2$ denoting the differential result of $(D_{ld}(j\omega_k,t_{i-1}))^2$ in terms of t_{i-1}.

Similarly, for the constraint Eq. (4.15g), the following convex constraint can be obtained.

$$\underbrace{|L_{ln}(j\omega_k,h_i)-L_{ln}(j\omega_k,h_{i-1})|\le|L_{ln}(j\omega_k,h_{(i-1)})+1|.}_{\text{original}}$$
$$\Leftrightarrow\underbrace{\begin{bmatrix}|D_{ln}(j\omega_k,h_{i-1})+h_{0(i-1)}|^2 & \Delta D_{ln}\\ (\Delta D_{ln})^* & \Phi_{ln}\end{bmatrix}\ge 0}_{\text{newly-obtained}}, \tag{4.26}$$

where

$$D_{ln}=h_{fh(i)}s^{fh}+\cdots+h_{1(i)}s, \tag{4.27}$$
$$\Delta D_{ln}=D_{ln}(j\omega_k,h_i)\times h_{0(i-1)}-D_{ln}(j\omega_k,h_{i-1})\times h_{0(i)}, \tag{4.28}$$
$$\underbrace{|D_{ln}(j\omega_k,h_{i-1})|^2}_{\text{original}}\ge\Phi_{ln}:=\underbrace{(D_{ln}(j\omega_k,h_{i-1}))^2+\nabla(D_{ln}(j\omega_k,h_{i-1}))^2(h_i-h_{i-1})}_{\text{newly-obtained}}, \tag{4.29}$$

with $\nabla(D_{ln}(j\omega_k,h_{i-1}))^2$ denoting the differential result of $(D_{ln}(j\omega_k,h_{i-1}))^2$ in terms of h_{i-1}.

4.2.5 Problem reformulation

After finishing the process mentioned above, the original problem is reformulated as follows.

$$\underset{h,t,\phi_{fs}}{\text{Maximize}} \quad \omega_p \tag{4.30a}$$

$$\text{Subject to} \quad 0 < h, 0 < t \tag{4.30b}$$

$$0 < w_{p(i)} < w_t, 0 < \phi_{fs(i)}, \tag{4.30c}$$

$$\Psi_{fs} - r_m D_{fs}(j\omega_k, t_i) \geq 0, \tag{4.30d}$$

$$\begin{bmatrix} \omega_k^2 \phi_{fs(i)} & D_{fs}(j\omega_k, t_i) \\ (D_{fs}(j\omega_k, t_i))^* & \Phi_{fs} \end{bmatrix} \geq 0, \tag{4.30e}$$

$$\begin{bmatrix} 2\omega_{p(i-1)}^2 - \phi_{fs(i)}\omega_{p(i-1)}^4 & \omega_{p(i)} \\ \omega_{p(i)} & 1 \end{bmatrix} \geq 0, \tag{4.30f}$$

$$\begin{bmatrix} \omega_t^2 & \dfrac{(N_{fs}(j\omega_k, h_i))(j\omega_k + \omega_t)}{M_t} \\ \dfrac{(N_{fs}(j\omega_k, h_i)(j\omega_k + \omega_t))^*}{M_t} & \Phi_{fs} \end{bmatrix} \geq 0, \tag{4.30g}$$

$$\begin{bmatrix} |D_{ld}(j\omega_k, t_{i-1}) + t_{0(i-1)}|^2 & \Delta D_{ld} \\ (\Delta D_{ld})^* & \Phi_{ld} \end{bmatrix} \geq 0, \tag{4.30h}$$

$$\begin{bmatrix} |D_{ln}(j\omega_k, h_{i-1}) + h_{0(i-1)}|^2 & \Delta D_{ln} \\ (\Delta D_{ln})^* & \Phi_{ln} \end{bmatrix} \geq 0. \tag{4.30i}$$

The new optimization problem is a convex optimization problem and can be solved by commercial solvers. After the convex optimization process, $P_n(s)$ and $Q(s)$ can be separated from $L_{fs(opt)}(s)$ and be implemented in real control system.

4.2.6 Procedures of simultaneous identification of nominal plant model and design of low pass filter in continuous domain

1. The order of nominal plant should be determined first by designer.
2. Select the form and relative order for $Q(s)$ filter in order to get the form of $(P_n^{-1}(s)Q(s)(1 - Q(s))^{-1})$.
   (a) The relative order of $Q(s)$ filter should be no smaller than relative order of nominal plant.
   (b) The form of $Q(s)$ filter depends on the type of nominal plant model.
   For an ordinary minimum phase nominal plant or the minimum phase approximation of a non-minimum phase plant, a minimum phase $Q(s)$ filter is used. However, for a non-minimum phase nominal plant model, since $Q(s)$ filter also contains the same unstable zeros as nominal plant model has, pole-zero cancellation appears.
3. Define desired gain margin as well as phase margin and obtain the problem formulation result as shown in section 4.2.5.
4. Solve the convex optimization in optimization software and confirm defined constraints have all been satisfied.
5. Separate $P_n(s)$ and $Q(s)$ from optimized results based on the analysis in section 4.2.3.

4.3 Plant model identification and low pass filter design in discrete domain

4.3.1 Block diagram analysis

In the discrete domain disturbance observer control system as shown in Fig. 4.2, P_r denotes real plant which is defined by FRD. Same as in continuous domain, signals $d, \hat{d}, u_a, y$ are external disturbance input, estimated disturbance, control input and output, respectively. In this section, $Q(z)$ and $P_n(z)$ (irreducible) are selected as follows in which $\bar{a} \triangleq [\bar{a}_0, \cdots, \bar{a}_{zq}]^T$, $\bar{b} \triangleq [\bar{b}_1, \cdots, \bar{b}_{zq-\tilde{r}}]^T$, $\bar{c} \triangleq [\bar{c}_0, \cdots, \bar{c}_{zd}]^T$ and $\bar{f} \triangleq [\bar{f}_1, \cdots, \bar{f}_{zn}]^T$ are to-be-decided parameters and orders $\tilde{r} \geq zd - zn$, zd and zn are selected by designer.

$$Q(z) = \frac{\bar{b}_{zq-\tilde{r}} z^{zq-\tilde{r}} + \cdots + 1}{\bar{a}_{zq} z^{zq} + \cdots + \bar{a}_0} \triangleq \frac{Q_{Nz}}{Q_{Dz}}, P_n(z) = \frac{\bar{f}_{zn} z^{zn} + \cdots + 1}{\bar{c}_{zd} z^{zd} + \cdots + \bar{c}_0} \triangleq \frac{P_{n(Nz)}}{P_{n(Dz)}}. \tag{4.31}$$

in which

$$\bar{b}_{zq-\tilde{r}} + \cdots + \bar{b}_1 + 1 = \bar{a}_{zq} + \cdots + \bar{a}_0. \tag{4.32}$$

The loop gain (L_{fz}), sensitivity function (S_{fz}) and complementary sensitivity function (T_{fz}) can be written as follows for Fig. 4.2.

$$L_{fz}(j\omega_k, \bar{h}, \bar{t}) = P_n^{-1}(z) Q(z) (1 - Q(z))^{-1} P_r(j\omega_k) = \frac{P_r(j\omega_k)(\bar{h}_{zh} z^{zh} + \cdots + \bar{h}_0)}{z^{zt} + \cdots + \bar{t}_0} = \frac{N_{fz}(j\omega_k, \bar{h})}{D_{fz}(j\omega_k, \bar{t})}, \tag{4.33a}$$

$$S_{fz}(j\omega_k, \bar{h}, \bar{t}) = \frac{1}{1 + (1 - Q(z))^{-1} Q(z) P_n^{-1}(z) P_r(j\omega_k)} = \frac{D_{fz}(j\omega_k, \bar{t})}{D_{fz}(j\omega_k, \bar{t}) + N_{fz}(j\omega_k, \bar{h})}, \tag{4.33b}$$

$$\frac{y}{d} = \frac{P_r(j\omega_k)}{1 + (1 - Q(z))^{-1} Q(z) P_n^{-1}(z) P_r(j\omega_k)} = \frac{P_r(j\omega_k)}{1 + L_{fz}(j\omega_k, \bar{h}, \bar{t})}, \tag{4.33c}$$

$$\frac{\hat{d}}{d} = \frac{(1 - Q(z))^{-1} Q(z) P_n^{-1}(z) P_r(j\omega_k)}{1 + (1 - Q(z))^{-1} Q P_n^{-1}(z) P_r(j\omega_k)} = T_{fz}(j\omega_k, \bar{h}, \bar{t}), \tag{4.33d}$$

in which

$$\bar{h}_{zh} z^{zh} + \cdots + \bar{h}_0 = (P_{n(Dz)}) \times (Q_{Nz}), z^{zt} + \cdots + \bar{t}_0 = (P_{n(Nz)}) \times (Q_{Dz} - Q_{Nz}), \tag{4.34}$$

$$\bar{h}_{zh} + \cdots + \bar{h}_0 \geq 1 + \cdots + \bar{t}_0. \tag{4.35}$$

In the following section, same constraints as in continuous domain have been designed to obtain satisfactory disturbance rejection performance. Then the simultaneous identification of nominal plant model and design of low pass filter in discrete domain has been formulated into an optimization problem in which $\bar{h}$ as well as $\bar{t}$ are optimization parameters and the bandwidth of DOB is the optimization objective.

4.3.2 Constraints formulation

② **Constraint for guaranteeing stability margins**

The same circle condition ([88]) for guaranteeing the desired gain margin g_m and phase margin ϕ_m, which is shown in Fig. 3.2, is presented as follows.

$$|\sigma + L_{fz}(j\omega_k, \bar{h}, \bar{t})| - r_m \geq 0. \tag{4.36}$$

in which

$$\sigma = \frac{g_m^2 - 1}{2g_m(g_m \cos\phi_m - 1)}, r_m = \frac{(g_m - 1)^2 + 2g_m(1 - \cos\phi_m)}{2g_m(g_m \cos\phi_m - 1)}. \tag{4.37}$$

② **Constraints for sensitivity function and complementary sensitivity function**

Constraints for the sensitivity function S_{fz} and the complementary sensitivity function T_{fz}, which are graphically shown in Fig. 3.3 and Fig. 3.4, are shown as follows.

$$W_p(j\omega_k, \omega_p) = \frac{\omega_p}{j\omega_k}, |W_p(j\omega_k, \omega_p)S(j\omega_k, \bar{h}, \bar{t})| \leq 1, \tag{4.38}$$

$$W_m(j\omega_k, \omega_t) = \frac{j\omega_k + \omega_t}{M_t\omega_t},\ |W_m(j\omega_k, \omega_t)T(j\omega_k, \bar{h}, \bar{t})| \leq 1, \tag{4.39}$$

in which ω_p is the crossover frequency of weighting function of sensitivity function and selected as the optimization objective.

When the optimal point $\omega_{p(opt)}$ is found, $\bar{h}, \bar{t}$ are obtained simultaneously.

③ **Constraints for guaranteeing internal stability**

Same as in continuous domain, the internal stability should be guaranteed. For the stability of denominator of L_{fz} which is D_{fz}, the Nyquist plot of intentionally defined open loop function $L_{td}(z, \bar{t}_i)$ (ith iteration), which is defined in Eq. (4.40), never encircles (-1,0), the stability of closed loop function H_{td} which is the stability of D_{fz} is guaranteed during the optimization process.

$$L_{td}(z, \bar{t}_i) = \frac{d_{zdc(i)}}{z^{zt} + \cdots + \bar{t}_{1(i)}z + \bar{t}_{0(i)} - d_{dc(i)}} = \frac{d_{zdc(i)}}{D_{td}(z, \bar{t}_i)}, \tag{4.40}$$

$$\begin{aligned} H_{td}(z, \bar{t}_i) &= \frac{L_{td}(z, \bar{t}_i)}{1 + L_{td}(z, \bar{t}_i)} \\ &= \frac{d_{zdc(i)}}{z^{n_{ld}} + \cdots + \bar{t}_{0(i)}} = \frac{d_{zdc(i)}}{D_{fz}(z, \bar{t}_i)}, \end{aligned} \tag{4.41}$$

in which $d_{zdc(i)}$ is the DC gain of $z^{zt} + \cdots + \bar{t}_{0(i)}$.

The mathematical interpretation is given as Eq. (4.42) which means the distance $|L_{td}(j\omega_k, \bar{t}_i) - L_{td}(j\omega_k, \bar{t}_{i-1})|$ should be no larger than the distance between $L_{td}(j\omega_k, \bar{t}_{i-1})$ and $(-1, 0)$ at every frequency point after every iteration.

$$|L_{td}(j\omega_k, \bar{t}_i) - L_{td}(j\omega_k, \bar{t}_{i-1})| \leq |L_{td}(j\omega_k, \bar{t}_{i-1}) + 1|. \tag{4.42}$$

By employing the same method to the constraint of numerator, the following constraint can be obtained.

$$|L_{tn}(j\omega_k, \bar{h}_i) - L_{tn}(j\omega_k, \bar{h}_{i-1})| \leq |L_{tn}(j\omega_k, \bar{h}_{i-1}) + 1|, \tag{4.43}$$

in which

$$L_{tn}(z, \bar{h}_i) = \frac{n_{zdc(i)}}{\bar{h}_{zh(i)}z^{zh} + \cdots + \bar{h}_{0(i)} - n_{zdc(i)}}, n_{zdc(i)} = \bar{h}_{zh(i)} + \cdots + \bar{h}_{0(i)}. \tag{4.44}$$

In summary, the disturbance observer design problem in discrete domain is formulated into the following

optimization problem.

$$\underset{\bar{h},\bar{t}}{\text{Maximize}} \quad \omega_p \tag{4.45a}$$

$$\text{Subject to} \quad 0 < \omega_p < \omega_t, \tag{4.45b}$$

$$|L_{fz}(j\omega_k, \bar{h}_i, \bar{h}_i) + \sigma| \geq r_m, \tag{4.45c}$$

$$|W_p(j\omega_k, \omega_p) S_{fz}(j\omega_k, \bar{h}_i, \bar{t}_i)| \leq 1, \tag{4.45d}$$

$$|W_m(j\omega_k) T_{fz}(j\omega_k, \bar{h}_i, \bar{t}_i)| \leq 1, \tag{4.45e}$$

$$|L_{td}(j\omega_k, \bar{t}_i) - L_{td}(j\omega_k, \bar{t}_{i-1})| \leq |L_{td}(j\omega_k, \bar{t}_{i-1}) + 1|, \tag{4.45f}$$

$$|L_{tn}(j\omega_k, \bar{h}_i) - L_{tn}(j\omega_k, \bar{h}_{i-1})| \leq |L_{tn}(j\omega_k, \bar{h}_{i-1}) + 1|. \tag{4.45g}$$

After the optimization process, ω_p and the loop gain L_{fz} consist of parameter vectors $\bar{h} \triangleq [\bar{h}_0, \cdots, \bar{h}_{zh}]^T$ and $\bar{t} \triangleq [\bar{t}_0, \cdots, \bar{t}_{zt-1}]^T$ are optimized simultaneously. However, $P_n(z)$ and $Q(z)$ need to be separated from the optimized $P_n^{-1}(z)Q(z)(1-Q(z))^{-1}$.

4.3.3 Separation of $P_n(z)$ and $Q(z)$ from $P_n^{-1}(z)Q(z)(1-Q(z))^{-1}$

① Allocate poles and zeros of $P_n^{-1}(z)Q(z)(1-Q(z))^{-1}$ to $P_n(z)$ and $Q(z)$.

1. Zeros of $P_n^{-1}(z)Q(z)(1-Q(z))^{-1}$ are poles of $P_n(z)$ and zeros of $Q(z)(1-Q(z))^{-1}$, see (4.33a).
2. Poles of $P_n^{-1}(z)Q(z)(1-Q(z))^{-1}$ is made up of zeros of $P_n(z)$ and poles of $Q(z)(1-Q(z))^{-1}$, see (4.33a).
3. The separation result of $P_n(z)$ and $Q(z)$ can be classified into following three types.
   (a) $P_n(z)$ is of minimum phase and $Q(z)$ is a minimum phase low pass filter.
   (b) $P_n(z)$ is of non-minimum phase and $Q(z)$ has the same unstable zeros as nominal plant has. In this case, pole-zero cancellation exists.
   (c) $P_n(z)$ is the minimum phase approximation of a non-minimum phase plant and $Q(z)$ is a minimum phase low pass filter.
4. The separation of poles is done by referring to the poles' distribution in the optimization initial condition of $P_n^{-1}(z)Q(z)(1-Q(z))^{-1}$ and phase information of FRD.
   The separation result is shown as follows:

$$\begin{aligned}\frac{(\bar{h}_{zh}z^{zh} + \cdots + \bar{h}_0)}{z^{zt} + \cdots + \bar{t}_1 z + \bar{t}_0} &= \frac{G_{pqz}(z+z_1)\cdots(z+z_{zh})}{(z+p_1)\cdots(z+p_{zt})} \\ &= \underbrace{\frac{G_{pqz1}}{(z+p_{q_1})\cdots(z+p_{q_{zq}})}}_{Q(1-Q)^{-1}} \times \frac{\overbrace{(z+z_1)\cdots(z+z_{zd})}^{P_n^{-1}(num_z)}}{G_{pqz2}\underbrace{(z+p_{p_1})\cdots(z+p_{p_{zn}})}_{P_n^{-1}(den_z)}}.\end{aligned} \tag{4.46}$$

   in which G_{pqz1} and G_{pqz2} are gains to be calculated.

② Calculate G_{pqz1}, G_{pqz2} and $Q(z)$.

1. G_{pqz2} is calculated by using FRD information of plant and Eq. (4.47).

$$G_{pqz2} = \frac{|(P_r(j\omega_k))||P_n^{-1}(num_z)|}{|P_n^{-1}(den_z)|}. \tag{4.47}$$

2. G_{pqz1} is the multiplication of G_{pqz} and G_{pqz2} and $Q(z)$ can be calculated from (4.46).

$$G_{pqz1} = G_{pqz} \times G_{pqz2}. \tag{4.48}$$

Obtained non-convex constraints should be transformed into linear functions or LMI form of variables ω_p, $\bar{h}$, $\bar{t}$ which is introduced in the following section.

4.3.4 Convex constraints derivation

Constraint for guaranteeing stability margins

In this subsection, Eq. (4.45c), which is for ensuring the gain margin and phase margin, is converted to the following convex constraint.

$$\begin{aligned}
&\left|L_{fz}(j\omega_k,\bar{h}_i,\bar{t}_i)+\sigma\right|-r_m=\left|\frac{N_{fz}(j\omega_k,\bar{h}_i)}{D_{fz}(j\omega_k,\bar{t}_i)}+\sigma\right|-r_m\geq 0\\
&\Leftrightarrow\left|N_{fz}(j\omega_k,\bar{h}_i)+D_{fz}(j\omega_k,\bar{t}_i)\sigma\right|\triangleq\underbrace{F_{fz}(j\omega_k,\bar{h}_i,\bar{t}_i)\geq r_m\left|D_{fz}(j\omega_k,\bar{t}_i)\right|}_{\text{original}}\\
&\Leftarrow\underbrace{\Psi_{fz}\geq r_m\left|D_{fz}(j\omega_k,\bar{t}_i)\right|}_{\text{newly-obtained}},
\end{aligned}\tag{4.49}$$

where $\Psi_{fz}=F_{fz}(j\omega_k,\bar{h}_{i-1},\bar{t}_{i-1})+\nabla F_{fz}(j\omega_k,\bar{h}_i,\bar{t}_{i-1})(\bar{t}_i-\bar{t}_{i-1})+\nabla F_{fz}(j\omega_k,\bar{h}_{i-1},\bar{t}_i)(\bar{h}_i-\bar{h}_{i-1})$ and $\nabla F_{fz}(j\omega_k,\bar{h}_i,\bar{t}_{i-1})$ as well as $\nabla F_{fz}(j\omega_k,\bar{h}_{i-1},\bar{t}_i)$ can be obtained by using Eq.(3.15).

Constraint for sensitivity function

For the sensitivity function constraint Eq. (4.45d), following results are obtained.

$$\underbrace{\left|W_p(j\omega_k,\omega_{p(i)})S_{fs}(j\omega_k,\bar{h}_i,\bar{t}_i)\right|\leq 1}_{\text{original}}\Leftrightarrow\left|W_p(j\omega_k,\omega_{p(i)})S_{fz}(j\omega_k,\bar{h}_i,\bar{t}_i)\right|^2\leq 1$$

$$\Leftarrow\underbrace{\begin{bmatrix}\omega_k^2\phi_{fz(i)} & D_{fz}(j\omega_k,\bar{t}_i)\\ (D_{fz}(j\omega_k,\bar{t}_i))^* & \Phi_{fz}\end{bmatrix}\geq 0,\ \phi_{fz(i)}>0,\begin{bmatrix}2\omega_{p(i-1)}^2-\phi_{fz(i)}\omega_{p(i-1)}^4 & \omega_{p(i)}\\ \omega_{p(i)} & 1\end{bmatrix}>0,}_{\text{newly-obtained}}\tag{4.50}$$

in which $\phi_{fz(i)}$ is a variable and

$$\begin{aligned}
&\left|D_{fz}(j\omega_k,\bar{t}_i)+N_{fz}(j\omega_k,\bar{h}_i)\right|^2\triangleq\underbrace{(M_{fz}(j\omega_k,\bar{h}_i,\bar{t}_i))^2}_{\text{original}}\geq\underbrace{\Phi_{fz}}_{\text{newly-obtained}}\\
&:=(M_{fz}(j\omega_k,\bar{h}_{i-1},\bar{t}_{i-1}))^2+\nabla(M_{fz}(j\omega_k,\bar{h}_{i-1},\bar{t}_i))^2(\bar{h}_i-\bar{h}_{i-1})\\
&+\nabla(M_{fz}(j\omega_k,\bar{h}_i,\bar{t}_{i-1}))^2(\bar{t}_i-\bar{t}_{i-1}),
\end{aligned}\tag{4.51}$$

in which $\nabla M_{fz}(j\omega_k,\bar{h}_{i-1},\bar{t}_i)^2$ as well as $\nabla M_{fz}(j\omega_k,\bar{h}_i,\bar{t}_{i-1})^2$ are calculated similarly to Eq. (3.15).

Constraint for complementary sensitivity function

The complementary sensitivity function constraint Eq. (4.45e) can be changed into the following form.

$$\underbrace{\left|W_m(j\omega_k,\omega_{t(i)})T_{fz}(j\omega_k,\bar{h}_i,\bar{t}_i)\right|\leq 1}_{\text{original}}\tag{4.52}$$

$$\Leftrightarrow\underbrace{\begin{bmatrix}\omega_t^2 & \dfrac{(N_{fz}(j\omega_k,\bar{h}_i)(j\omega_k+\omega_t))}{M_t}\\ \dfrac{(N_{fz}(j\omega_k,\bar{h}_i)(j\omega_k+\omega_t))^*}{M_t} & \Phi_{fz}\end{bmatrix}\geq 0,}_{\text{newly-obtained}}\tag{4.53}$$

in which Φ_{fz} is the same item as in Eq. (4.21).

Constraint for guaranteeing internal stability

For constraint Eq. (4.45f), the following technique is used.

$$\underbrace{|L_{td}(j\omega_k,\bar{t}_i)-L_{td}(j\omega_k,\bar{t}_{i-1})|\le|L_{td}(j\omega_k,\bar{t}_{i-1})+1|}_{\text{original}}$$
$$\Leftrightarrow\underbrace{\begin{bmatrix}|D_{td}(j\omega_k,\bar{t}_{i-1})+d_{zdc(i-1)}|^2 & \Delta D_{td}\\ (\Delta D_{td})^* & \Phi_{td}\end{bmatrix}\ge 0,}_{\text{newly-obtained}} \tag{4.54}$$

where

$$\Delta D_{td}=D_{td}(j\omega_k,\bar{t}_i)\times d_{zdc(i-1)}-D_{td}(j\omega_k,\bar{t}_{i-1})\times d_{zdc(i)}, \tag{4.55}$$
$$\underbrace{|D_{td}(j\omega_k,\bar{t}_{i-1})|^2}_{\text{original}}\ge\Phi_{td}:=\underbrace{(D_{td}(j\omega_k,\bar{t}_{i-1}))^2+\nabla(D_{td}(j\omega_k,\bar{t}_{i-1}))^2(\bar{t}_i-\bar{t}_{i-1})}_{\text{newly-obtained}}, \tag{4.56}$$

with $\nabla D_{td}(j\omega_k,\bar{t}_{i-1})^2$ denoting the differential result of $D_{td}(j\omega_k,\bar{t}_{i-1})^2$ in terms of $\bar{t}_{i-1}$.

Similarly, the following convex constraint can be obtained for constraint Eq. (4.45g).

$$\underbrace{|L_{tn}(j\omega_k,\bar{h}_i)-L_{tn}(j\omega_k,\bar{h}_{i-1})|\le|L_{tn}(j\omega_k,\bar{h}_{i-1})+1|}_{\text{original}}$$
$$\Leftrightarrow\underbrace{\begin{bmatrix}|D_{tn}(j\omega_k,\bar{h}_{i-1})+n_{zdc(i-1)}|^2 & \Delta D_{tn}\\ (\Delta D_{tn})^* & \Phi_{tn}\end{bmatrix}\ge 0,}_{\text{newly-obtained}} \tag{4.57}$$

where

$$D_{tn}(j\omega_k,\bar{h}_i)=\bar{h}_{zh(i)}z^{zh}+\cdots+\bar{h}_{0(i)}-n_{zdc(i)}, \tag{4.58}$$
$$\Delta D_{tn}=D_{tn}(j\omega_k,\bar{h}_i)\times n_{zdc(i-1)}-D_{tn}(j\omega_k,\bar{h}_{i-1})\times n_{zdc(i)}, \tag{4.59}$$
$$\underbrace{\left|D_{tn}(j\omega_k,\bar{h}_{i-1})\right|^2}_{\text{original}}\ge\Phi_{tn}:=\underbrace{(D_{tn}(j\omega_k,\bar{h}_{i-1}))^2+\nabla(D_{tn}(j\omega_k,\bar{h}_{i-1}))^2(\bar{h}_i-\bar{h}_{i-1})}_{\text{newly-obtained}}, \tag{4.60}$$

with $\nabla D_{tn}(j\omega_k,\bar{h}_{i-1})^2$ denoting the differential result of $D_{tn}(j\omega_k,\bar{h}_{i-1})^2$ in terms of $\bar{h}_{i-1}$.

4.3.5 Problem reformulation

After finishing all the process mentioned above, the original problem is reformulated as follows.

$$
\begin{aligned}
\underset{\bar{h},\bar{t},\phi_{fz}}{\text{Maximize}} \quad & \omega_p \\
\text{Subject to} \quad & 0 < \omega_{p(i)} < \omega_t, 0 < \phi_{fz(i)}, \\
& \Psi_{fz} - r_m D_{fz}(j\omega_k, \bar{t}_i) \geq 0, \\
& \begin{bmatrix} \omega_k^2 \phi_{fz(i)} & D_{fz}(j\omega_k, \bar{t}_i) \\ (D_{fz}(j\omega_k, \bar{t}_i))^* & \Phi_{fz} \end{bmatrix} \geq 0, \\
& \begin{bmatrix} |D_{td}(j\omega_k, \bar{t}_{(i-1)}) + d_{zdc(i-1)}|^2 & \Delta D_{td} \\ (\Delta D_{td})^* & \Phi_{td} \end{bmatrix} \geq 0, \\
& \begin{bmatrix} |D_{tn}(j\omega_k, \bar{h}_{(i-1)}) + n_{zdc(i-1)}|^2 & \Delta D_{tn} \\ (\Delta D_{tn})^* & \Phi_{tn} \end{bmatrix} \geq 0, \\
& \begin{bmatrix} 2\omega_{p(i-1)}^2 - \phi_{fz(i)} \omega_{p(i-1)}^4 & \omega_{p(i)} \\ \omega_{p(i)} & 1 \end{bmatrix} \geq 0, \\
& \begin{bmatrix} \omega_t^2 & \dfrac{(N_{fz}(j\omega_k, \bar{h}_i))(j\omega_k + \omega_t)}{M_t} \\ \dfrac{(N_{fz}(j\omega_k, \bar{h}_i)(j\omega_k + \omega_t))^*}{M_t} & \Phi_{fz} \end{bmatrix} \geq 0.
\end{aligned}
$$

The new optimization problem is a convex optimization problem and can be solved by commercial solvers.

4.3.6 Procedures of identifying nominal plant model and designing low pass filter altogether in discrete domain

1. Decide the order of desired nominal plant model.
2. Select the form and relative order for $Q(z)$ filter.
   (a) The relative order of $Q(z)$ filter should be no smaller than the relative order of nominal plant.
   (b) The form of $Q(z)$ filter depends on the type of nominal plant model.
   Same as in continuous domain, for an ordinary minimum phase nominal plant or the minimum phase approximation of a non-minimum phase plant, a minimum phase $Q(z)$ filter is used. However, for a non-minimum phase nominal plant model, since $Q(z)$ filter also contains the same unstable zeros as nominal plant model has, pole-zero cancellation exists.
3. Define desired gain margin as well as phase margin and sampling frequency and obtain the problem formulation result as shown in section 4.3.5.
4. Solve the convex optimization in optimization software and confirm all the defined constraints have been satisfied.
5. Separate $P_n(z)$ and $Q(z)$ from optimized results based on the analysis in section 4.3.3.

4.4 Summary

This chapter has present identification of nominal plant model and design of low pass filter altogether in disturbance observer by only employing frequency response data in continuous domain and discrete domain.

1. The original non-convex design problem has been formulated into a convex optimization problem by transforming non-convex constraints into convex form, which can be solved by convex optimization method by utilizing optimization software. The detailed mathematical transformation process has been present.
2. When the plant model and low pass filter are obtained simultaneously, separation methods have been provided.

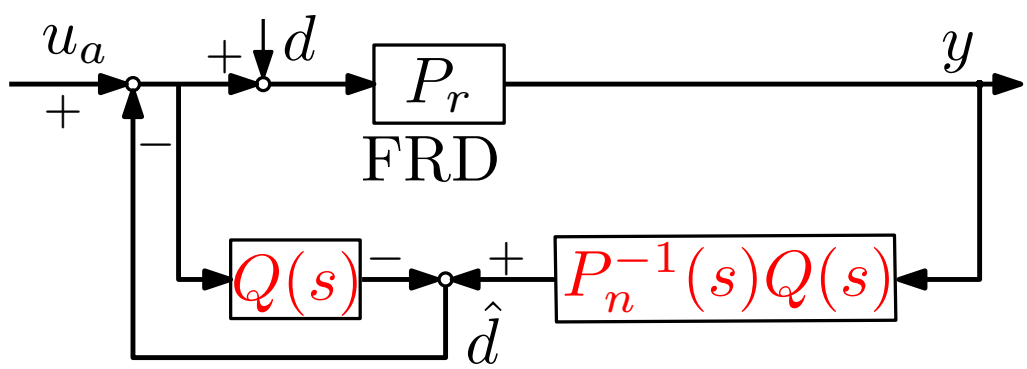

Figure 4.1 Block diagram of disturbance observer system in the simultaneous identification of nominal plant model and design of low pass filter (s domain)

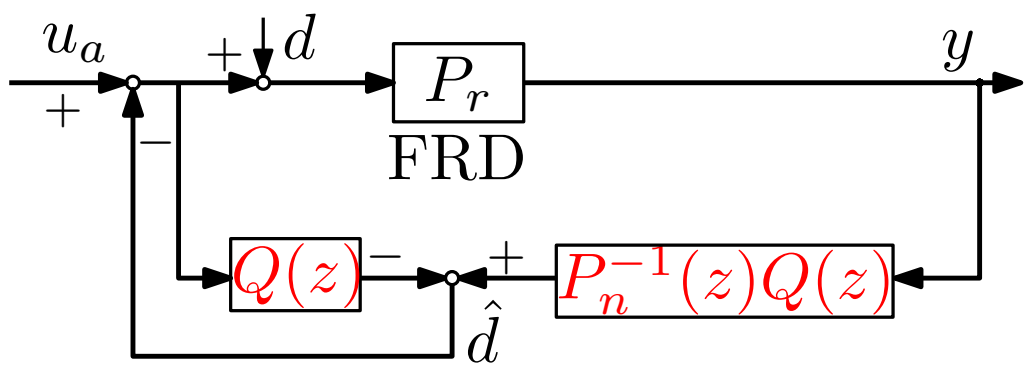

Figure 4.2 Block diagram of disturbance observer system in the simultaneous identification of nominal plant model and design of low pass filter (z domain)

Chapter 5

Numerical case study results of FRD-based DOB design for a minimum phase plant

5.1 Overview

This chapter is to show the case study results of proposed methods in Chapter 3 and Chapter 4 for a minimum phase plant which is a high-precision positioning stage. Results of low pass filter design (relative order of nominal plant model is 2) and simultaneous identification of plant model and design of low pass filter in continuous domain as well as in discrete domain are given. More specifically, case studies can be classified as shown in the following table. For each case, Nyquist plots of open loop function (constraint

Table 5.1 Case study summary for the minimum phase plant employed in this chapter

	section	corresponding section of theoretical analysis	number of to-be-decided parameters
low pass filter design (s domain)	✓ (section 5.3.1)	section 3.2	2 parameters of filter
low pass filter design (z domain)	✓(section 5.3.2)	section 3.3	2 parameters of filter
nominal plant model identification and low pass filter design (s domain)	✓(section 5.3.3)	section 4.2	7 parameters of plant and filter
nominal plant model identification and low pass filter design (z domain)	✓(section 5.3.4)	section 4.3	7 parameters of plant and filter
trial-and-error method	5.4		1 parameter of filter

for guaranteeing margins) and magnitude plots of W_pS and W_mT (constraints for sensitivity function as well as the complementary sensitivity function) are provided to verify the satisfaction of constraints. Furthermore, the comparison between different case studies have been discussed.

Finally, the comparison with trial-and-error method is present which is to show the superiority of the proposed method in terms of design effort along with obtained bandwidth.

5.2 Simulation conditions

1. Software: Matlab R2020a (Yalmip [103] and Mosek [104] toolboxes)
2. Gain margin 6 [dB], phase margin 30°.
   According to Eq. (3.5), $\sigma = 1.03, r_m = 0.525$ and the stability circle C_s in Fig. 3.2 can be decided.
3. Minimum phase plant P_{mp}.
   This plant is a high-precision positioning stage ([105]) and Bode plots of frequency response data and nominal plant model P_{mp} are shown in Fig. 5.1.

$$P_{mp}(s) = \frac{59.275(s^2 + 8.402s + 6.573 \times 10^4)}{s(s + 2.101)(s^2 + 10.89s + 3.665 \times 10^4)}. \tag{5.1}$$

4. Discrete minimum phase plant P_{mpd} (Discretization method: Tustin transformation, 4 [kHz])

$$P_{mpd}(z) = \frac{9.2607 \times 10^{-7}(z + 1)^2(z^2 - 1.994z + 0.9979)}{(z - 1)(z - 0.9995)(z^2 - 1.995z + 0.9973)}. \tag{5.2}$$

5.3 Case study results for a minimum phase plant

5.3.1 Low pass filter design result in continuous domain for a minimum phase plant

Since the relative order of P_{mp} is 2, a second order Q filter is selected and by solving the optimization problem formulated in Chapter 3 section 3.2, the optimized $Q_{mp(qs)}(s)$ and crossover frequency of weighting function of sensitivity function $\omega_{p(qs,mp)}$ are shown as follows ([106]). Resultant Nyquist plots as well as Bode plots of W_pS and W_mT are depicted in Fig. 5.2, Fig. 5.3 Fig. 5.4.

$$P_{mp}(s) = \frac{59.275(s^2 + 8.402s + 6.573 \times 10^4)}{s(s + 2.101)(s^2 + 10.89s + 3.665 \times 10^4)}, \tag{5.3}$$

$$Q_{mp(qs)}(s) = \frac{1}{5.79 \times 10^{-5}s^2 + 0.0071s + 1},\ \omega_{p(qs,mp)} = 88.6\ [\text{rad/s}]. \tag{5.4}$$

5.3.2 Low pass filter design result in discrete domain for a minimum phase plant

For low pass filter design in discrete domain (problem formulation can be found in Chapter 3 section 3.3), a second order low pass filter is selected and the optimized $Q_{mp(qz)}(z)$ and $\omega_{p(qz,mp)}$ are obtained as shown in Eq. (5.6). Corresponding figures are Fig. 5.5, Fig. 5.6 along with Fig. 5.7.

$$P_{mpd}(z) = \frac{9.2607 \times 10^{-7}(z + 1)^2(z^2 - 1.994z + 0.9979)}{(z - 1)(z - 0.9995)(z^2 - 1.995z + 0.9973)}, \tag{5.5}$$

$$Q_{mp(qz)}(z) = \frac{z^2 + 2z + 1}{3904z^2 - 7689z + 3789},\ \omega_{p(qz,mp)} = 87.0\ [\text{rad/s}]. \tag{5.6}$$

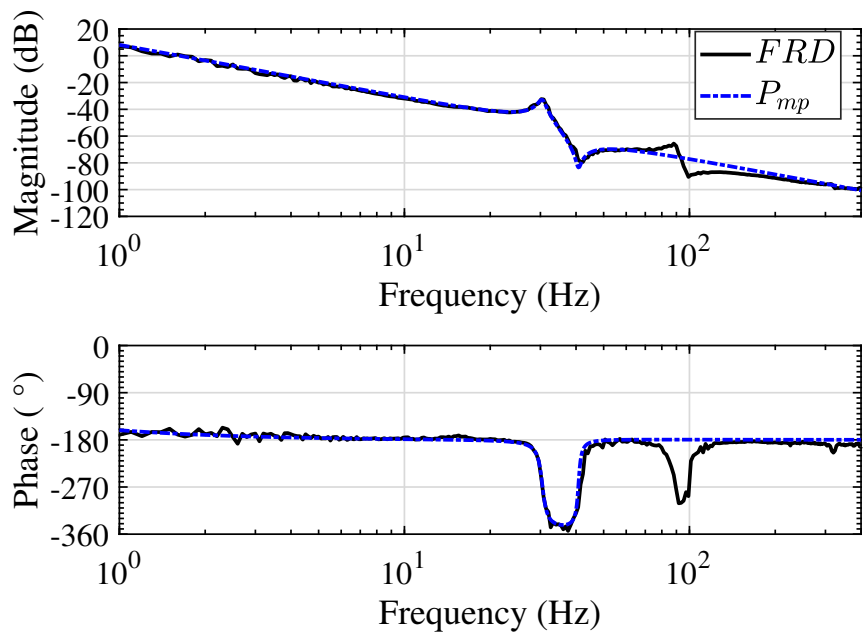

Figure 5.1 Bode plots of frequency response data (FRD) and nominal plant model $P_{mp}(s)$ for a minimum phase high-precision positioning stage

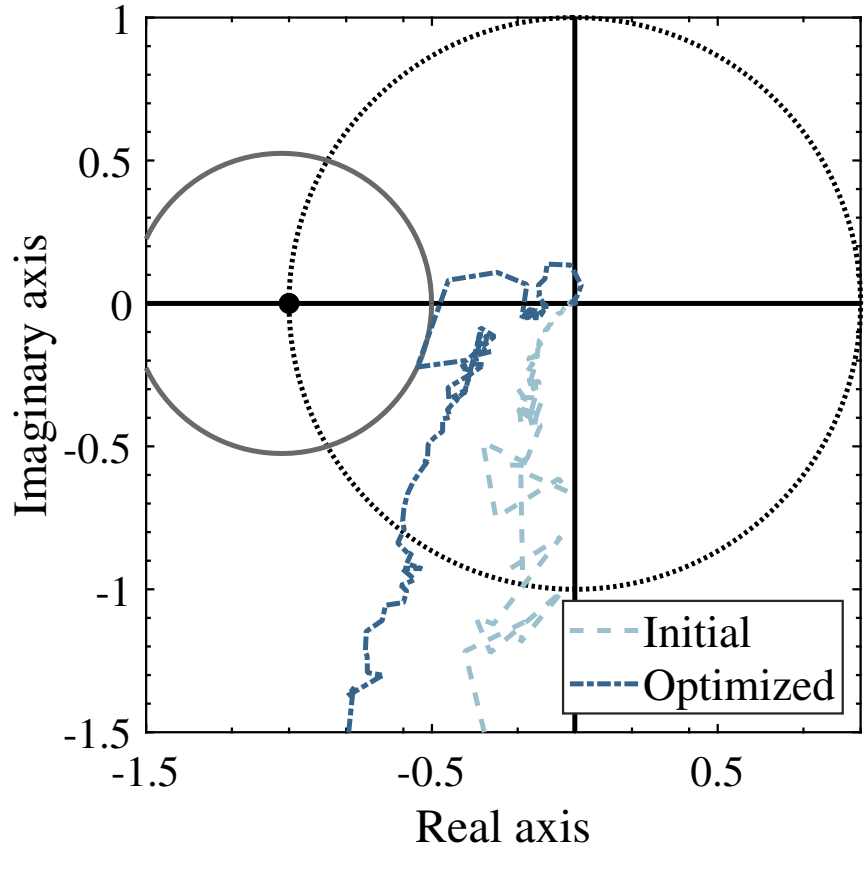

Figure 5.2 Nyquist plots of loop gain (L) (Initial and Optimized) of low pass filter design in continuous domain for a minimum phase plant. The dark blue line, which represents for the optimized case, is tangent to the stability circle (gray line) defined by the gain margin and phase margin.

5.3.3 Identification of nominal plant model and design of low pass filter in continuous domain for a minimum phase plant

Based on the problem formulation process in Chapter 4 section 4.2, low pass filter and nominal plant model can be obtained simultaneously. The bandwidth has been significantly increased compared to design low pass filter only which can be told from Eq. (5.8). Obtained figures are present in Fig. 5.8, Fig. 5.9, Fig. 5.10, and Fig. 5.11.

$$P_{mp(opts)}(s) = \frac{79.795(s^2 + 6.724s + 7.131 \times 10^4)}{s(s + 3.033)(s^2 + 8.258s + 3.522 \times 10^4)}, \tag{5.7}$$

$$Q_{mp(pqs)}(s) = \frac{9.086 \times 10^4}{s^2 + 267.8s + 9.086 \times 10^4},\ \omega_{p(pqs,mp)} = 160.9\ [\text{rad/s}], \tag{5.8}$$

in which $P_{mp(opts)}(s)$ and $Q_{mp(pqs)}(s)$ are the obtained nominal plant model as well as the low pass filter in continuous domain, respectively; $\omega_{p(pqs,mp)}$ is the optimized bandwidth.

5.3.4 Identification of nominal plant model and design of low pass filter in discrete domain for a minimum phase plant

By following the theoretical analysis introduced in Chapter 4 section 4.3, results of designing low pass filter and nominal plant model altogether in discrete domain for a minimum phase plant are given in Eq. (5.10). Acquired figures are present in Fig. 5.12, Fig. 5.13, Fig. 5.14, and Fig. 5.15.

$$P_{mp(optz)}(z) = \frac{1.2462 \times 10^6 (z+1)^2 (z^2 - 1.994z + 0.9983)}{(z - 0.9992)(z-1)(z^2 - 1.996z + 0.9979)}, \tag{5.9}$$

$$Q_{mp(pqz)}(z) = \frac{1.372 \times 10^{-}3(z+1)^2}{(z^2 - 1.93z + 0.9353)},\ \omega_{p(pqz,mp)} = 160.9\ [\text{rad/s}], \tag{5.10}$$

in which $P_{mp(optz)}(z)$ and $Q_{mp(pqz)}(z)$ are optimized nominal plant and low pass filter in discrete domain, respectively; $\omega_{p(pqz,mp)}$ is the optimized bandwidth in discrete domain.

5.3.5 Analysis on simulation results for a minimum phase plant

1. Constraints have been satisfied.
   Nyquist plots of loop gain L (initial and optimized) did not enter the gray circle (stability circle) which implies that the stability margin constraint holds successfully as shown in Fig. 5.2, Fig. 5.5, Fig. 5.9, and Fig. 5.13. With the stability margin constraint satisfied, the peak value of sensitivity function is limited because the closest distance from Nyquist plot to critical point $(-1, 0)$ is the inverse of the peak value of the sensitivity function. Finally, proposed optimization method forces the optimized Nyquist plot to be tangent to the gray circle which implies that the bandwidth of L is maximized under the limitation of constraints. Furthermore, constraints for sensitivity function and complementary sensitivity function are satisfied as $|W_p S|$ and $|W_m T|$ are always under 0 [dB] in Fig. 5.3, Fig. 5.6, Fig. 5.10, and Fig. 5.14.
2. Bandwidth comparison
   (a) Designing low pass filter with identifying plant simultaneously in continuous domain and discrete domain (ω_p : around 160.9 [rad/s]) have obtained larger bandwidth than case of designing low pass filter only (ω_p : no larger than 88.6 [rad/s]).

i. More tuning freedom is in simultaneous design which can be understood from Eq. (5.11) and Eq. (5.12) and thus, better performance has been gained.

A. Design low pass filter only:

$$L_{q,mp}(\text{loop gain}) = \underbrace{P_{(mp,FRD)}P_{mp}^{-1}}_{\text{fixed}}\underbrace{Q(1-Q)^{-1}}_{\text{optimized}}. \tag{5.11}$$

B. Design low pass filter and identify plant simultaneously:

$$L_{pq,mp}(\text{loop gain}) = \underbrace{P_{(mp,FRD)}}_{\text{fixed}}\underbrace{P_{mp(opt)}^{-1}Q(1-Q)^{-1}}_{\text{optimized}}. \tag{5.12}$$

in which $P_{(mp,FRD)}$ is the frequency response data of plant and P_{mp} is the nominal plant model identified from frequency response data while $P_{mp(opt)}$ is the plant model obtained from proposal.

ii. Faster disturbance estimation performance is in simultaneous design which is explained as follows.

The disturbance estimation performance is represented by complementary sensitivity function ($\frac{\hat{d}}{d} = \frac{(1-Q(s))^{-1}Q(s)P_n(s)^{-1}P_r(j\omega_k)}{1+(1-Q(s))^{-1}Q(s)P_n(s)^{-1}P_r(j\omega_k)} = T$). The complementary sensitivity function comparison between design low pass filter only and tune plant model and low pass filter altogether is shown in Fig. 5.16. Larger bandwidth of T means faster estimation which implies that tuning nominal plant model simultaneously with low pass filter has achieved faster estimation performance.

(b) Although discrete domain design is not as convenient as continuous domain, discrete domain design has obtained comparative performance with continuous domain.

i. The design in continuous domain is more straightforward because the meaning of coefficients in low pass filter as well as in nominal plant model is clear and the stability analysis is easier.

ii. Necessity of designing in discrete domain.

A. After discretizing the continuous domain controller into discrete domain, the Bode plot has deviation which can be told from Fig. 5.17 in which the Nyquist plot of discretized open loop function is not strictly same as original open loop function in continuous domain. (The Nyquist plot of discretized open loop function has entered stability circle.).

B. The implementation is in discrete domain.

5.4 Comparison with trial-and-error method

In this section, proposed low pass filter design in continuous domain has been compared with trial-and-error method. In order to compare with the proposal fairly, same gain margin (6 [dB]) and phase margin (30°) have been guaranteed which is shown in Fig. 5.18. The low pass filter in trial-and-error method design has been selected as the following form:

$$Q_{\text{trial}}(s) = \frac{1}{(\tau_{mp}s+1)^{tm}}, \tag{5.13}$$

in which τ_{mp} is the tuning parameter and tm is the relative order.

The tuning process can be summarized as follows when $P_{(mp,FRD)}$ and $P_{mp}(s)$ represent the frequency response data of a minimum phase plant and the nominal plant model which is identified from frequency response data respectively.

1. Give τ_{mp} a value and plot Nyquist plot of $L_{\text{trial}} = P_{(mp,FRD)}P_{mp}(s)Q_{\text{trial}}(s)(1-Q_{\text{trial}}(s))$ to check whether it satisfies the constraint for stability margins or not.
2. If the L_{trial} in previous step satisfies the constraint, decrease the value of τ_{mp} and check new L_{trial} again.
3. If the L_{trial} does not satisfy the constraint, increase the value of τ_{mp} and check new L_{trial} again.
4. Repeat the above steps until the L_{trial} becomes tangent to the stability circle.

Based on the tuning process, $Q_{\text{trial}}(s)$ is obtained as in Eq. (5.14).

$$Q_{\text{trial}}(s) = \frac{1}{(5.4 \times 10^{-3}s + 1)^2},\ \omega_{p(trial)} = 65\ [\text{rad/s}]. \tag{5.14}$$

As can be told from the Fig. 5.18 and Eq. (5.14), proposed method has obtained a larger bandwidth than trial-and-error method.

5.5 Summary

This chapter has enumerated case study results for a minimum phase plant and compared proposed methods with trial-and-error method which can be summarized as Table 3.2.

1. Desired constraints have all been satisfied and bandwidth-maximized DOB has been designed successfully for each case which verified the feasibility of the proposed method for minimum phase plant.
2. Proposed methods has over-performed trial-and-error method in terms of design effort (no trial-and-error process) and design result (bandwidth).
3. Simultaneous identification of plant model and design of low pass filter has obtained larger bandwidth compared with design low pass filter only which shows the necessity of tuning plant model together.
4. Discrete domain design has achieved comparative performance as continuous domain which is promising and convenient in the implementation.

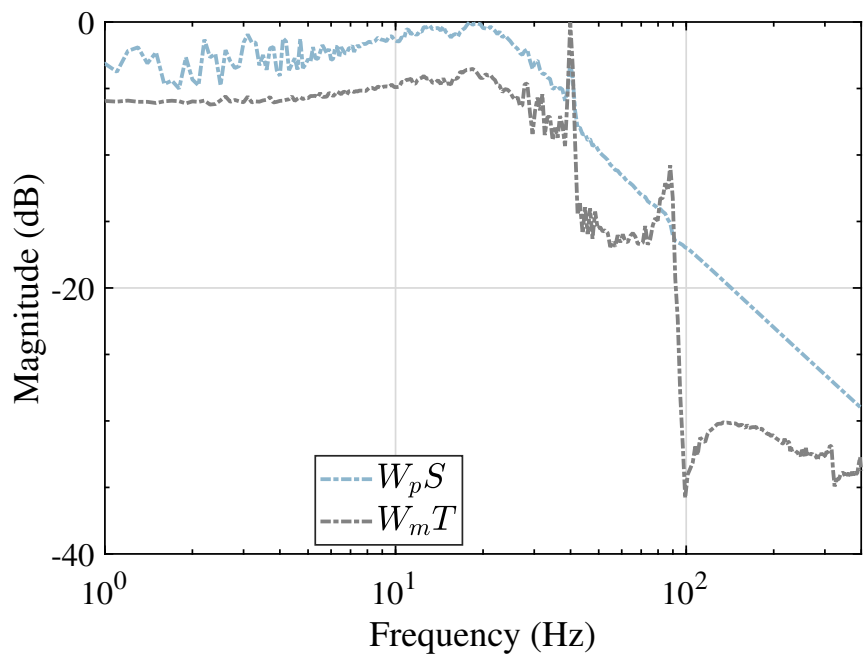

Figure 5.3 Magnitude plots of W_pS and W_mT of low pass filter design in continuous domain for a minimum phase plant. $|W_pS|$ and $|W_mT|$ are under 0 [dB] line which means constraints for sensitivity function and complementary sensitivity function have been satisfied.

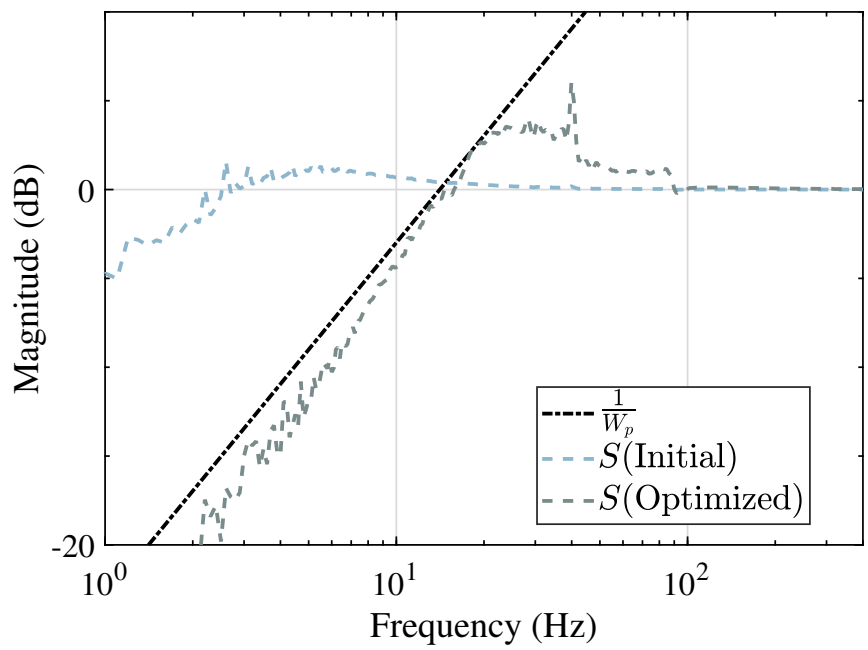

Figure 5.4 Magnitude plots of $\frac{1}{W_p}$, S (initial) and S (optimized) of low pass filter design in continuous domain for a minimum phase plant. This figure shows the crossover frequency of sensitivity function (S) has been increased which means better disturbance rejection performance.

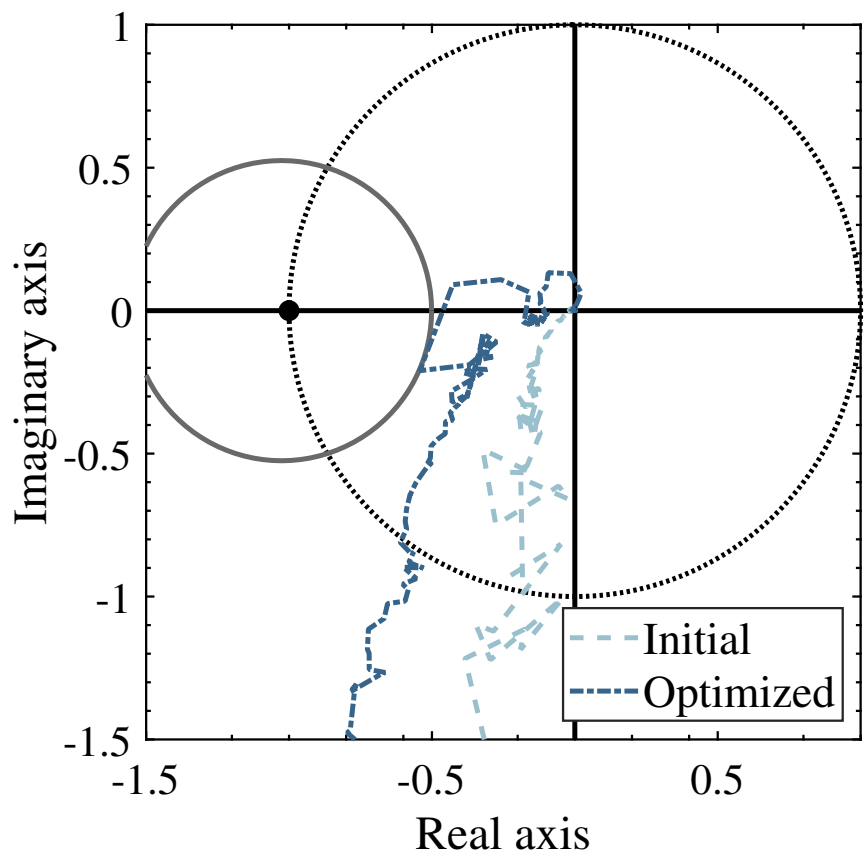

Figure 5.5 Nyquist plots of loop gain (L) (Initial and Optimized) of low pass filter design in discrete domain for a minimum phase plant. Discrete domain design result also makes optimized loop gain (dark blue line) become tangent to the stability circle (gray line) which means the constraint for guaranteeing stability margins has been satisfied.

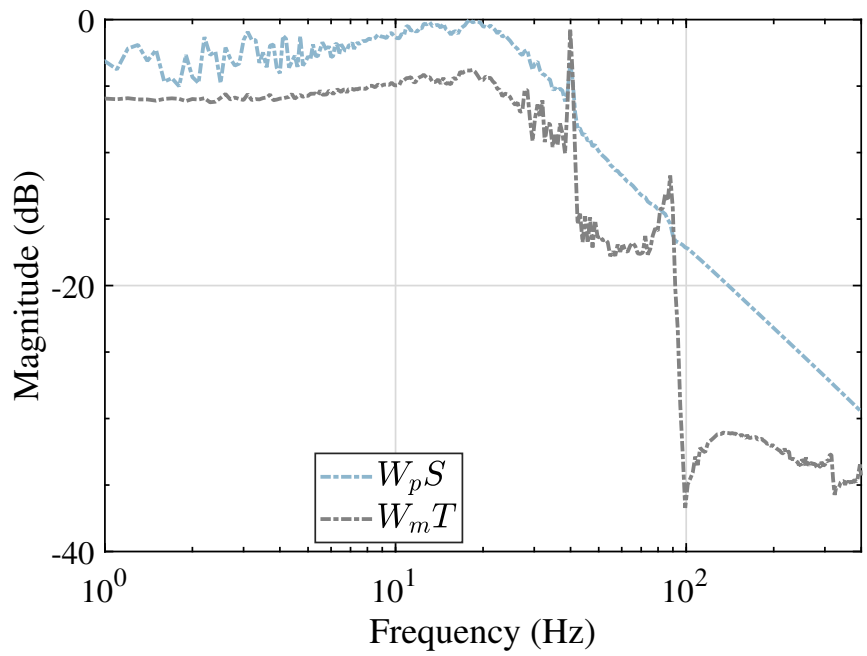

Figure 5.6 Magnitude plots of W_pS and W_mT of low pass filter design in discrete domain for a minimum phase plant. Constraints for sensitivity function and complementary sensitivity function have been satisfied successfully since magnitude plots of W_pS and W_mT are under 0 [dB] line.

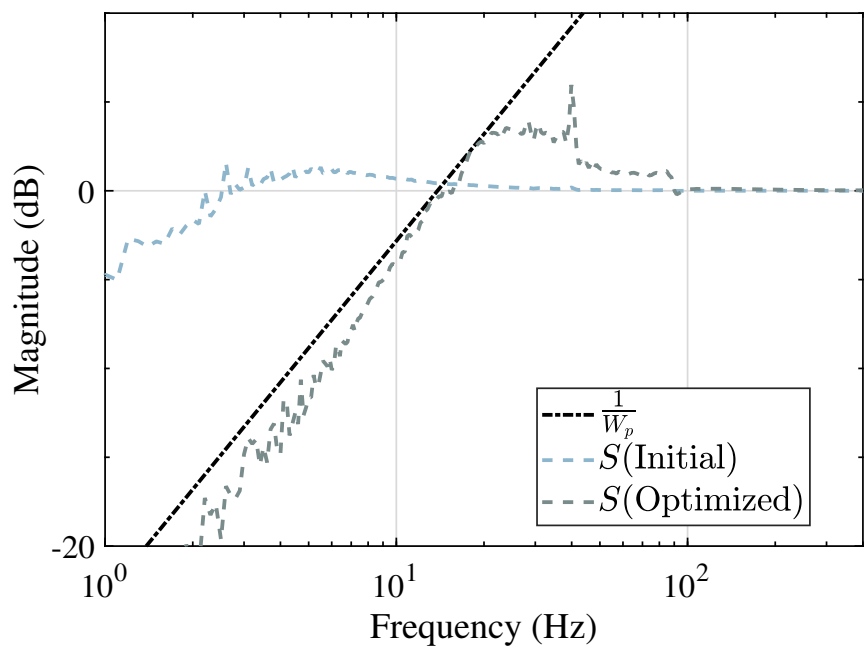

Figure 5.7 Magnitude plots of $\frac{1}{W_p}$, S (initial) and S (optimized) of low pass filter design in discrete domain for a minimum phase plant. Same as in continuous domain design, the design result has made the crossover frequency of sensitivity function (S) increased which represents for better disturbance rejection performance compared to initial condition.

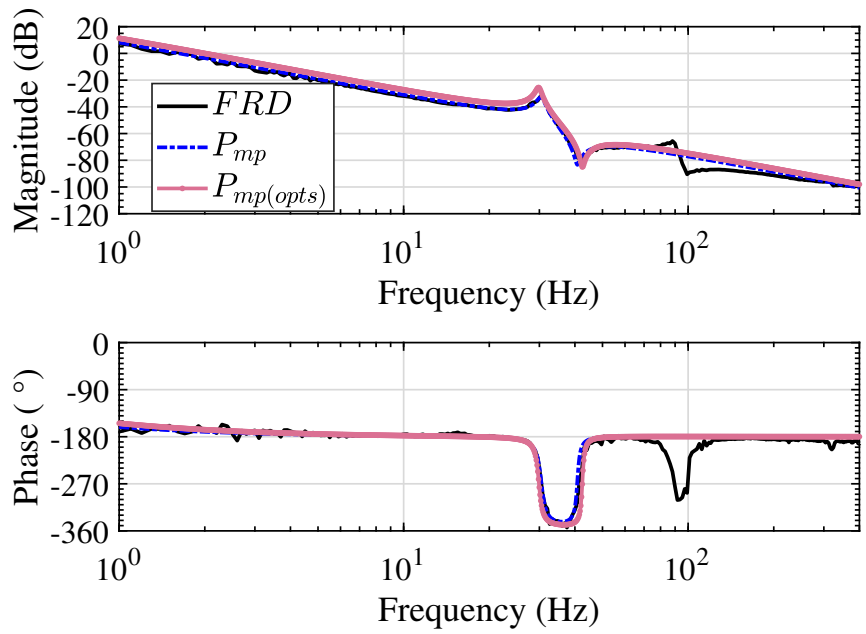

Figure 5.8 Bode plots of frequency response data (FRD), nominal plant model $P_{mp}(s)$ (identified from frequency response data) and optimized nominal plant model $P_{mp(opts)}(s)$ in the simultaneous identification of nominal plant model and design of low pass filter (s domain) for a minimum phase plant.

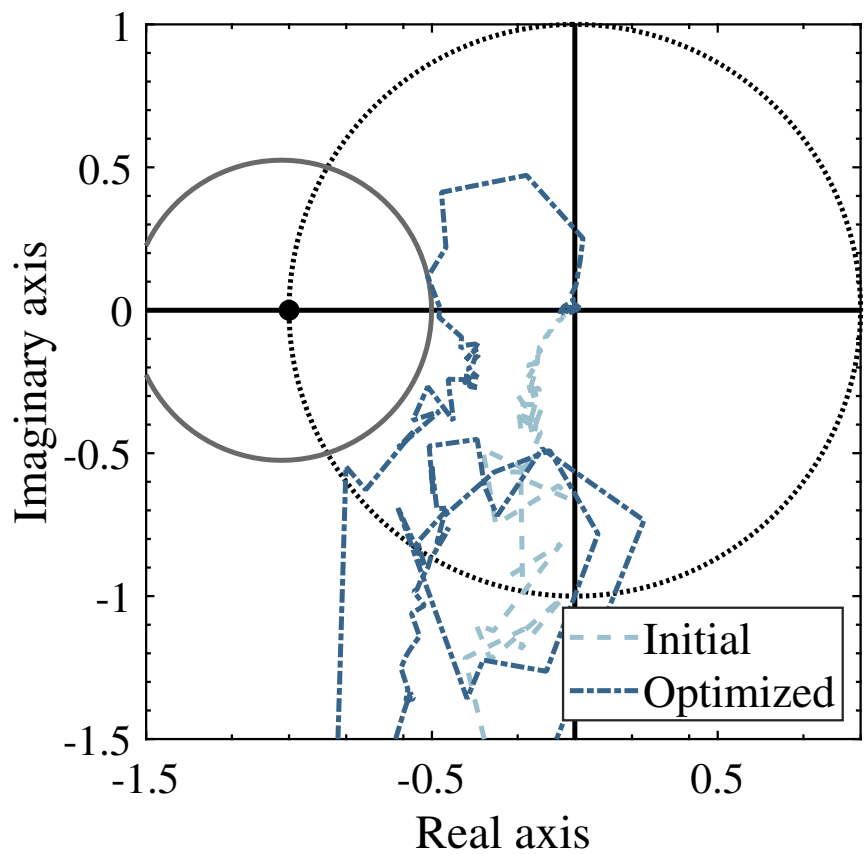

Figure 5.9 Nyquist plots of loop gain (L) (Initial and after optimized) in the simultaneous identification of nominal plant model and design of low pass filter (s domain) for a minimum phase plant in which the constraint for guaranteeing stability margins holds because the optimized loop gain L did not enter the stability circle (gray line).

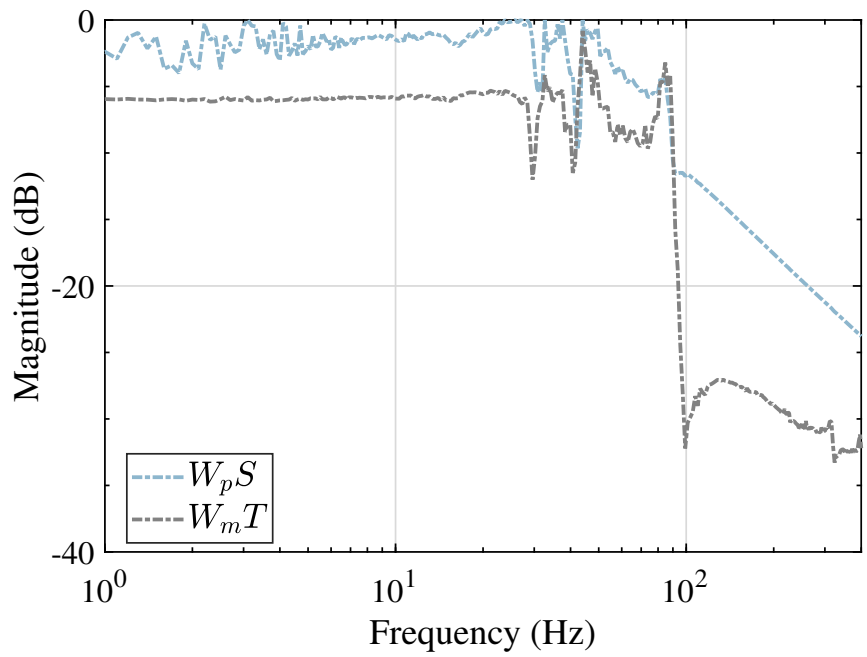

Figure 5.10 Magnitude plots of W_pS and W_mT in the simultaneous identification of nominal plant model and design of low pass filter (s domain) for a minimum phase plant. Constraints for sensitivity function ($|W_pS| \leq 1$) and complementary sensitivity function ($|W_mT| \leq 1$) have been satisfied.

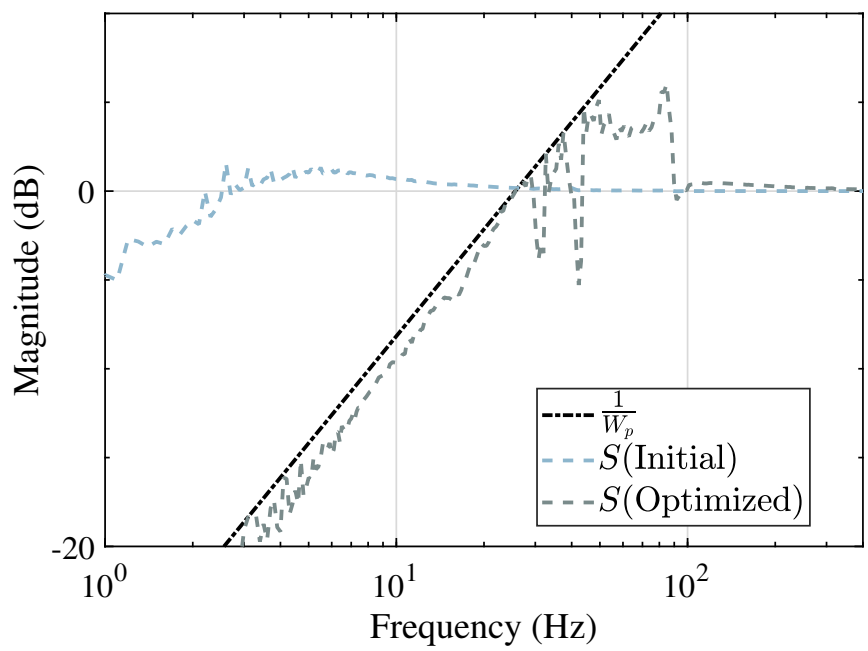

Figure 5.11 Magnitude plots of $\frac{1}{W_p}$, S (initial) and S (optimized) in the simultaneous identification of nominal plant model and design of low pass filter (s domain) for a minimum phase plant. This figure has shown the comparison of initial sensitivity function and optimized sensitivity function.

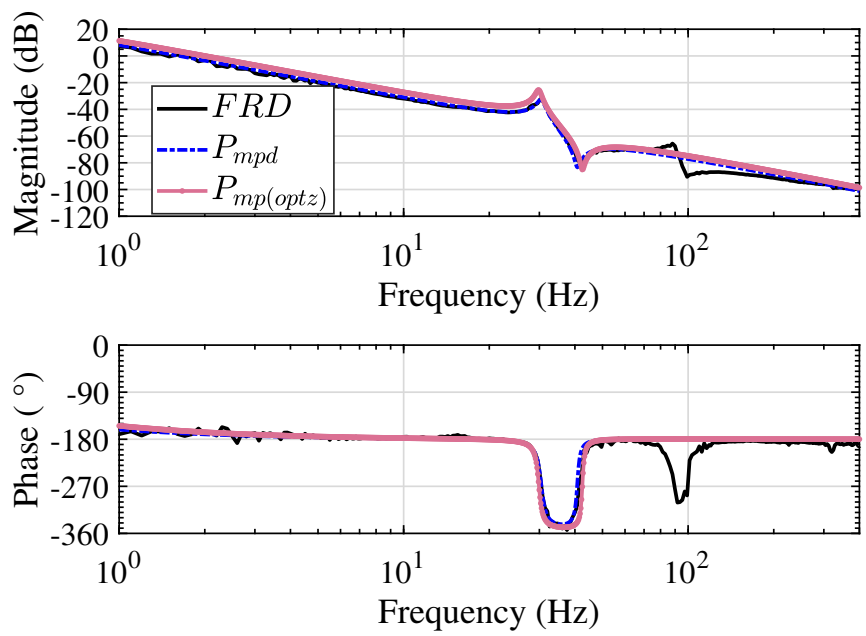

Figure 5.12 Bode plots of frequency response data, nominal plant model P_{mpd} (discretized from P_{mp}) and optimized plant model $P_{mp(optz)}(z)$ in designing low pass filter and identifying nominal plant model simultaneously (z domain) for a minimum phase plant.

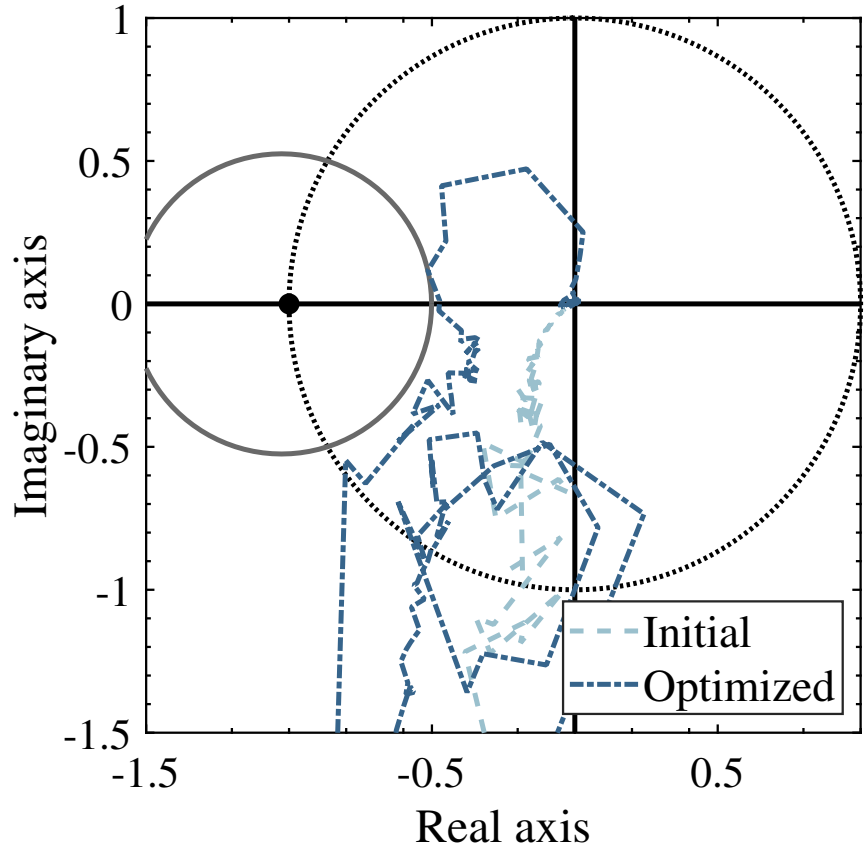

Figure 5.13 Nyquist plots of loop gain (L) (Initial and after optimized) in the simultaneous identification of nominal plant model and design of low pass filter (z domain) for a minimum phase plant. Constraint for guaranteeing stability margins has been satisfied successfully since optimized loop gain (dark blue line) does not invade into the stability circle (gray line).

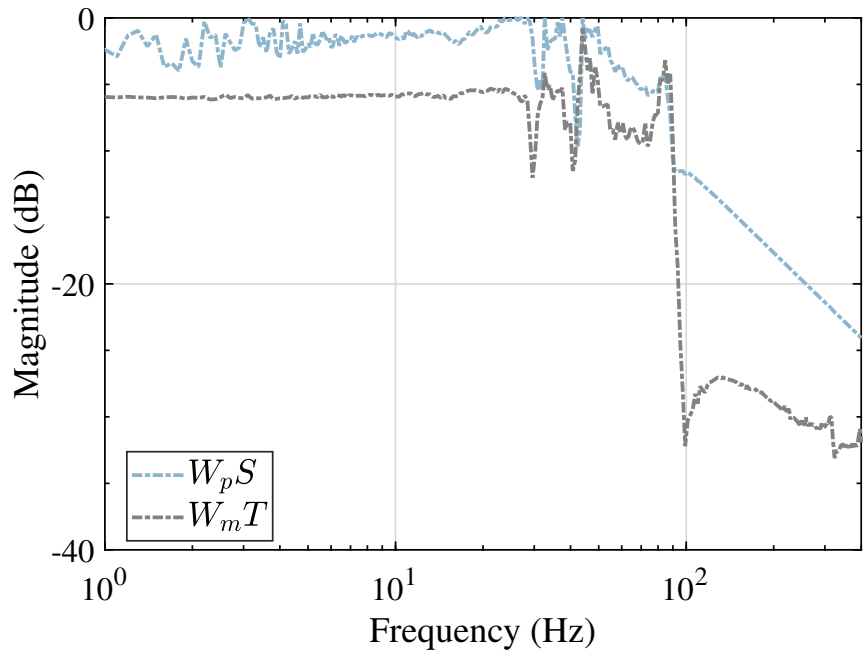

Figure 5.14 Magnitude plots of W_pS and W_mT in the simultaneous identification of nominal plant model and design of low pass filter (z domain) for a minimum phase plant. The satisfication of constraints for sensitivity function ($|W_pS| \leq 1$) as well as complementary sensitivity function $|W_mT| \leq 1$ is verified in this figure.

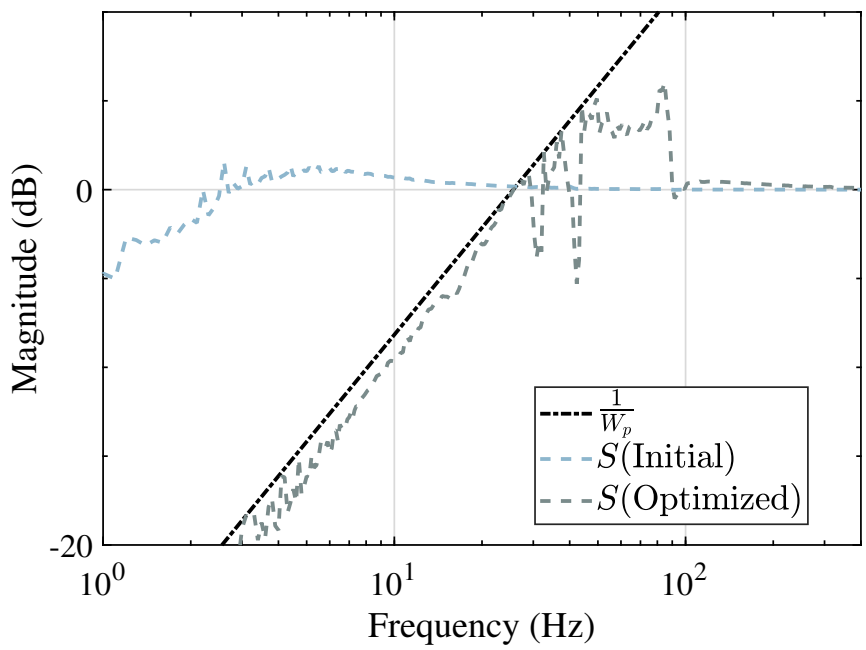

Figure 5.15 Magnitude plots of $\frac{1}{W_p}$, S (initial) and S (optimized) in the simultaneous identification of nominal plant model and design of low pass filter (z domain) for a minimum phase plant. Optimized sensitivity function (S) has larger crossover frequency than initial case which is straightforward.

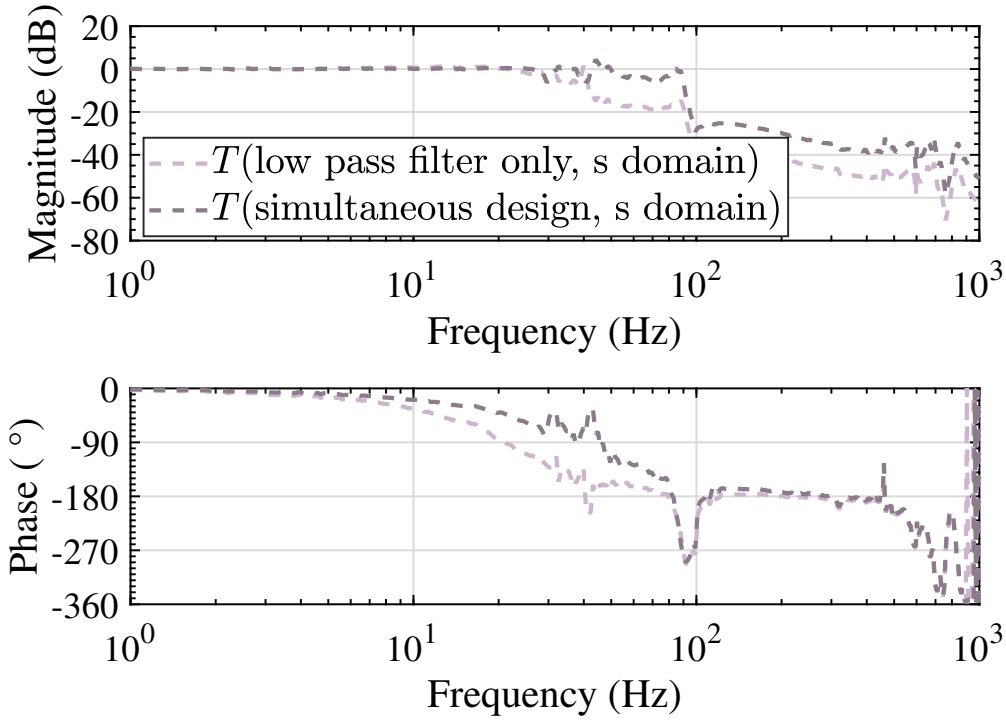

Figure 5.16 Complementary sensitivity function comparison between design low pass filter only and tune plant model and low pass filter altogether. T(simultaneous design, s domain), which represents for the complementary sensitivity function of designing low pass filter and identifying nominal plant model simultaneously case, has larger bandwidth, which reflects the disturbance estimation performance, than T(low pass filter only, s domain) which represents for the complementary sensitivity function of designing low pass filter only case.

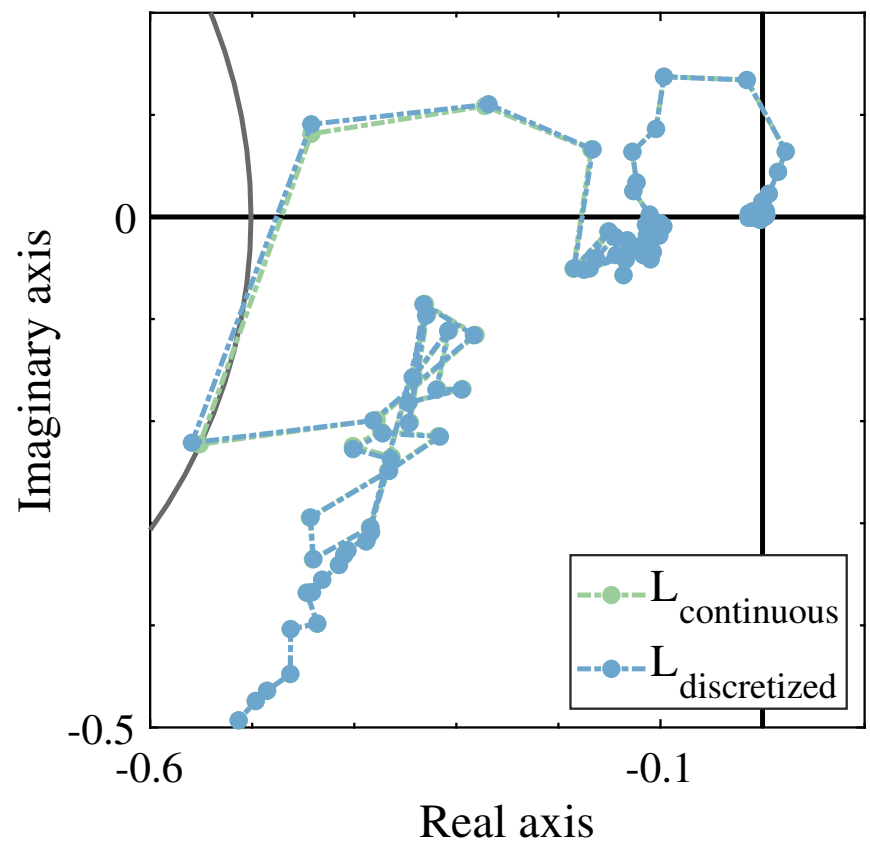

Figure 5.17 Locally-enlarged Nyquist plots of continuous domain loop gain and corresponding discretized loop gain. $L_{\text{continuous}}$ means original continuous version while $L_{\text{discretized}}$ is discretized from the continuous one. The $L_{\text{discretized}}$ has entered stability circle which breaks the constraint for guaranteeing stability margins.

Table 5.2 Summary of case study results for a minimum phase plant

Cases	Constraint	Bandwidth [rad/s]
low pass filter design (s domain) (section 5.3.1)	satisfied	88.6
low pass filter design (z domain) (section 5.3.2)	satisfied	87
nominal plant model identification and low pass filter design (s domain) (section 5.3.3)	satisfied	**160.9**
nominal plant model identification and low pass filter design (z domain) (section 5.3.4)	satisfied	**160.9**
trial-and-error method (section 5.4)	satisfied	65

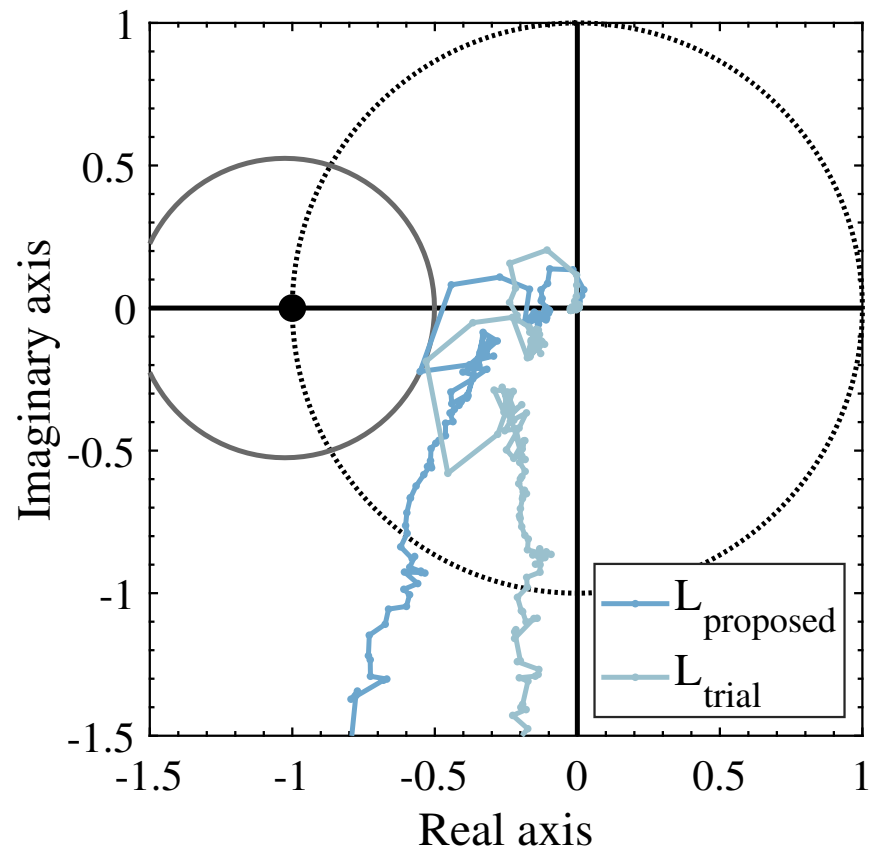

Figure 5.18 Comparison of Nyquist plots of loop gain L obtained by trial-and-error method (L_{trial}) and proposed method of designing low pass filter only in s domain for a minimum phase plant (L_{propsoed}). The proposed method has gained larger bandwidth than trial-and-error method although both methods have satisfied the constraint for guaranteeing stability margins since both Nyquist plots stay outside of stability circle (gray line).

Chapter 6

Numerical case study results of FRD-based DOB design for a non-minimum phase plant

6.1 Overview

This chapter is to show case study results of proposed methods in Chapter 3 and Chapter 4 for a non-minimum phase plant who is a motion stage and has one real unstable zero.

When building a DOB configuration for a non-minimum phase plant, the internal stability problem appears (QP_n^{-1}) due to the unstable inversion caused by the existence of unstable zero(s). To deal with this problem, two different types of methods have been employed which can both be handled by proposed methods.

One way is to approximate the nominal plant model into a minimum phase one, and in this Chapter, second order approximation, zero magnitude error approximation and zero phase error approximation have been employed in designing low pass filter. The other is to make low pass filter contain the same unstable zero(s) as non-minimum phase nominal plant has. Additionally, for a non-minimum phase plant, identifying nominal plant model and designing low pass filter simultaneously have also been investigated. Therefore, case studies have been classified as shown in Table 6.1. Furthermore, discrete domain design results have also been discussed.

Same as in minimum phase plant case, Nyquist plots of open loop function (constraint for guaranteeing margins) and magnitude plots of W_pS and W_mT (constraints for sensitivity function as well as the complementary sensitivity function) are provided to verify the satisfaction of constraints for each case study. Furthermore, the comparison between different case studies and analysis on simulation results have been given. Finally, two design methods selected from previous research have been introduced and comparison results are present.

6.2 Simulation conditions

1. Software: Matlab R2020a (Yalmip [103] and Mosek [104] toolboxes)
2. Gain margin 6 [dB], phase margin 30°.
   According to Eq. (3.5), $\sigma = 1.03, r_m = 0.525$ and the stability circle C_s in Fig. 3.2 can be decided.

3. Non-minimum phase plant P_{nmp} ([109]).

$$P_{nmp}(s) = \frac{-40(s+957.6)(s-687.5)}{s(s+8.131)(s^2+20s+5.6\times10^4)}, \tag{6.1}$$

$$P_s(s) = \frac{470.25}{s(s+8.131)}, \tag{6.2}$$

$$P_{zme}(s) = \frac{40(s+957.6)(s+687.5)}{s(s+8.131)(s^2+20s+5.6\times10^4)}, \tag{6.3}$$

$$P_{zpe}(s) = \frac{1.8906\times10^7(s+957.6)}{s(s+8.131)(s+687.5)(s^2+20s+5.610\times10^4)}, \tag{6.4}$$

in which $P_s(s)$, $P_{zme}(s)$ and $P_{zpe}(s)$ are the second order approximation, zero magnitude approximation (ZME) and zero phase error approximation (ZPE) of P_{nmp}, respectively and Bode plots are shown as Fig. 6.1.

4. Discrete non-minimum phase plant P_{mpd} (discretized from P_{nmp}) and P_{zmed} (discretized from P_{zme}) (discretization method: Tustin transformation, 4 [kHz]).

$$P_{nmpd}(z) = \frac{6.3687\times10^{-7}(z+1)^2(z-1.188)(z-0.7862)}{(z-0.998)(z-1)(z^2-1.992z+0.995)}, \tag{6.5}$$

$$P_{zmed}(z) = \frac{7.5663\times10^{-7}(z-0.8417)(z-0.7862)(z+1)^2}{(z-1)(z-0.998)(z^2-1.992z+0.995)}. \tag{6.6}$$

6.3 Low pass filter design results in continuous domain for a non-minimum phase plant

6.3.1 Case of second order approximation $P_s(s)$

When the second order approximation of nominal plant $P_s(s)$ is selected, the following result is obtained. Furthermore, resultant figures are shown in Fig. 6.2, Fig. 6.3 and Fig. 6.4.

$$P_s(s) = \frac{470.25}{s(s+8.131)}, Q_{nmp(ps)}(s) = \frac{1}{2.59\times10^-4s^2+0.02424s+1},\ \omega_{nmp(ps)} = 30.8\ [\text{rad/s}], \tag{6.7}$$

in which $Q_{nmp(ps)(s)}$ and $\omega_{nmp(ps)}$ represent for the optimized low pass filter and crossover frequency of weighting function of sensitivity function.

6.3.2 Case of fourth order zero magnitude error approximation $P_{zme}(s)$

When the zero magnitude error approximation $P_{zme}(s)$ is employed and $Q_{nmp(zme)}(s)$ is selected as a second order filter to guarantee the causality of the system. The resultant filter ($Q_{nmp(zme)}(s)$) and bandwidth ($\omega_{nmp(zme)}$) are shown in Eq. (6.9). Corresponding figures are present in Fig. 6.5, Fig. 6.6 and Fig. 6.7.

$$P_{zme}(s) = \frac{40(s+957.6)(s+687.5)}{s(s+8.131)(s^2+20s+5.6\times10^4)}, \tag{6.8}$$

$$Q_{nmp(zme)}(s) = \frac{1}{2.839\times10^{-5}s^2+0.0224s+1},\ \omega_{nmp(zme)} = 37.4\ [\text{rad/s}]. \tag{6.9}$$

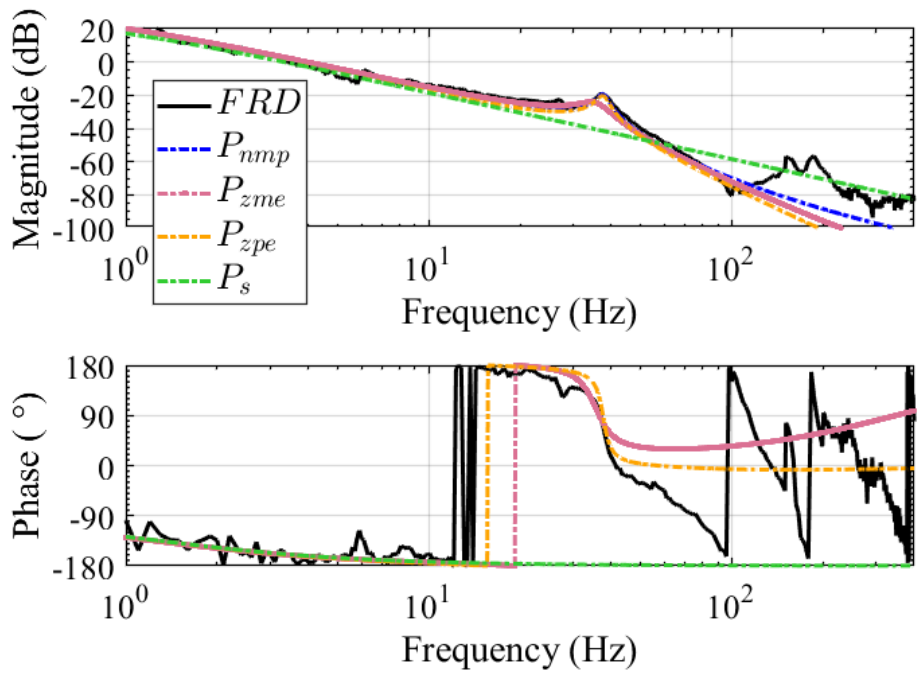

Figure 6.1 Bode plots of frequency response data of a non-minimum phase plant, identified nominal plant model P_{nmp}, P_{zme} (zero magnitude error approximation of P_{nmp}), P_{zpe} (zero phase error approximation of P_{nmp}) and P_s (second order approximation of P_{nmp})

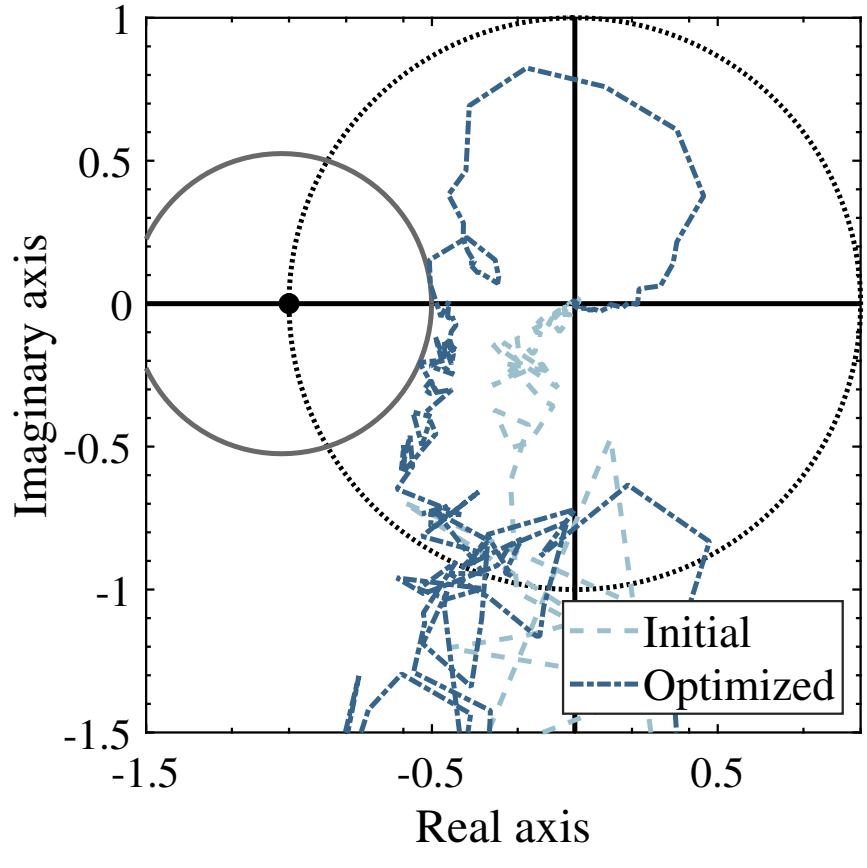

Figure 6.2 Nyquist plots of loop gain (L) (Initial and Optimized) when second order approximation $P_s(s)$ is used in designing low pass filter for a non-minimum phase plant. The tangency to the stability circle of optimized loop gain (dark blue line) has verified that constraint for guaranteeing stability margins has been satisfied.

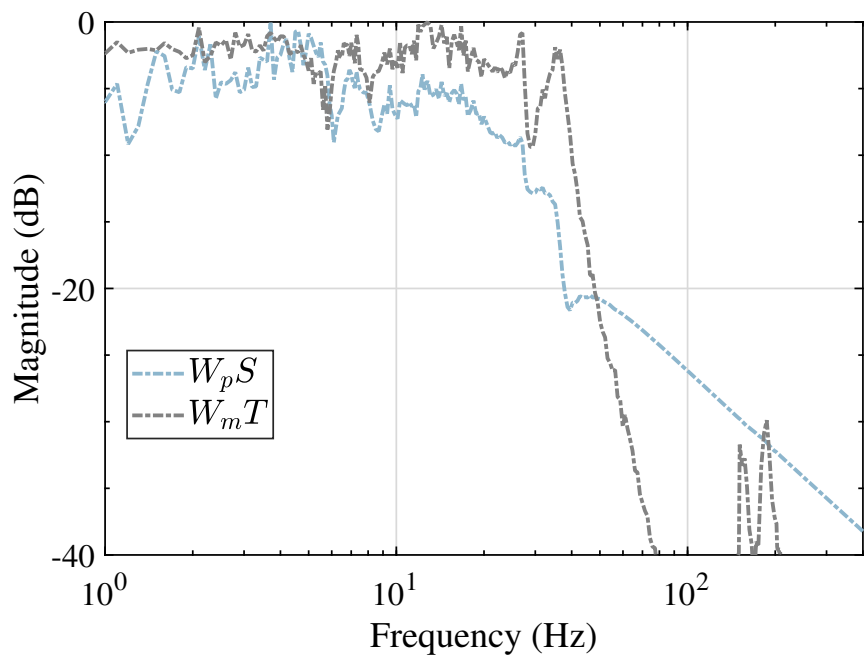

Figure 6.3 Magnitude plots of W_pS and W_mT when second order approximation $P_s(s)$ is used in designing low pass filter for a non-minimum phase plant. Magnitude plots of W_pS and W_mT are under 0 [dB] shows that constraints for sensitivity function ($|W_pS| \leq 1$) and complementary sensitivity function ($|W_mT| \leq 1$) have been satisfied.

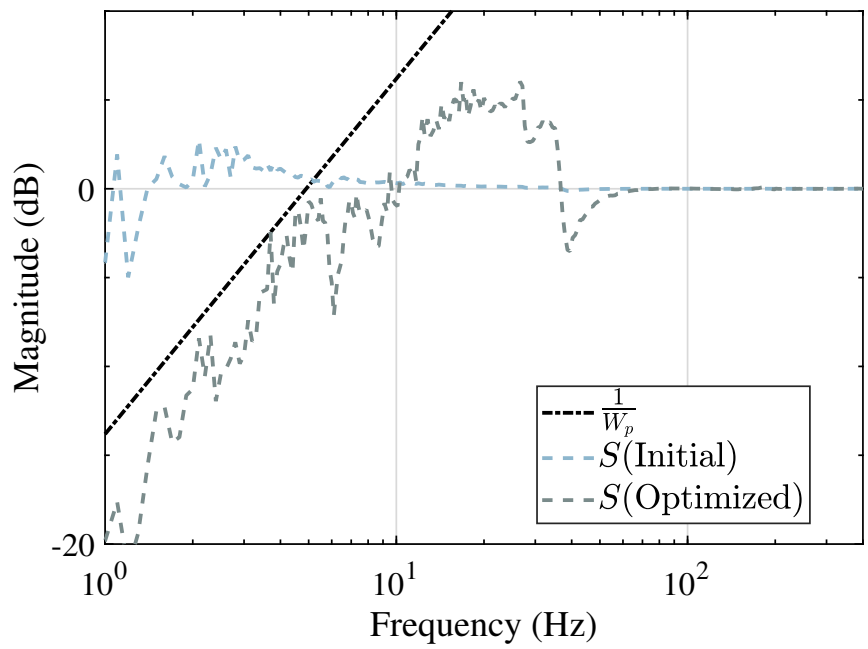

Figure 6.4 Magnitude plots of $\frac{1}{W_p}$, S (Initial) and S (Optimized) when second order approximation $P_s(s)$ is used in designing low pass filter for a non-minimum phase plant. Larger crossover frequency of sensitivity function can be recognized from this figure showing that the optimization process has made the disturbance rejection performance become better.

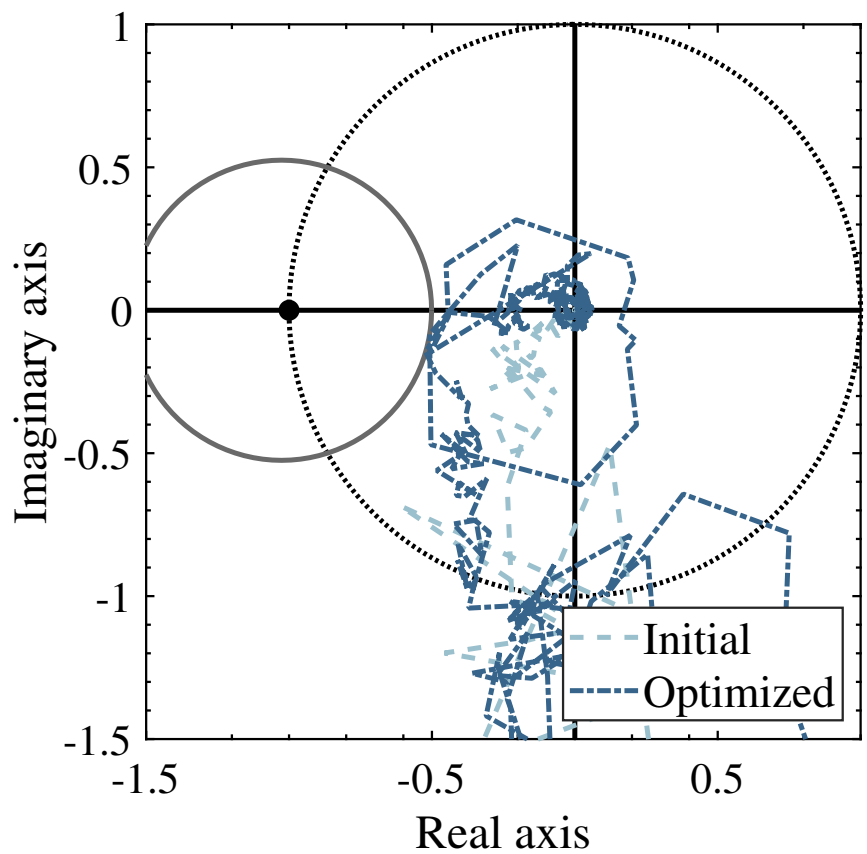

Figure 6.5 Nyquist plots of loop gain (L) (Initial and Optimized) when zero magnitude error approximation $P_{zme}(s)$ is used in designing low pass filter for a non-minimum phase plant. The constraint $|L+\sigma| \geq r_m$ has been satisfied successfully in which $(-\sigma, 0)$ and r_m are center point and radius of stability circle (gray line) respectively.

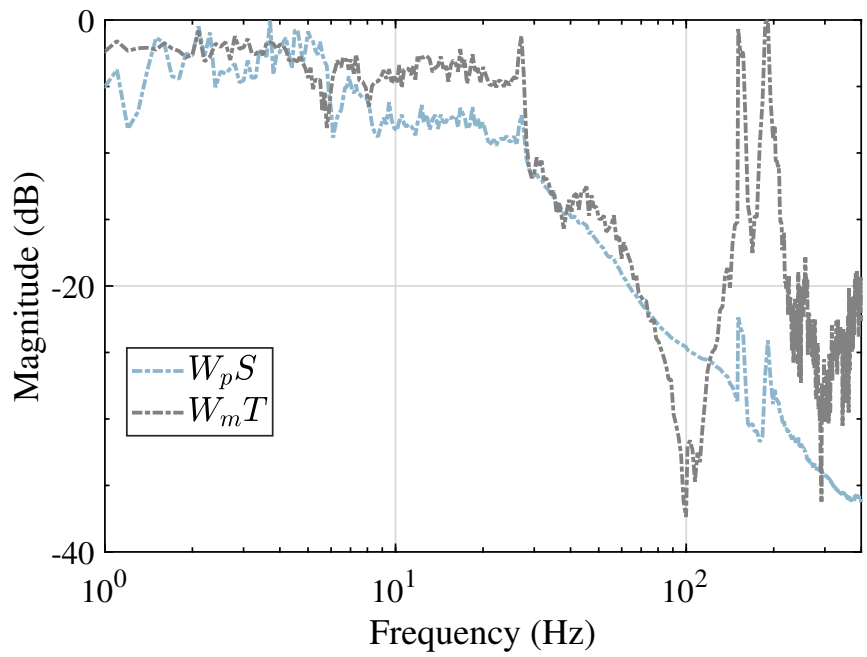

Figure 6.6 Magnitude plots of W_pS and W_mT when zero magnitude error approximation $P_{zme}(s)$ is used in designing low pass filter for a non-minimum phase plant. The optimized low pass filter has made the whole system satisfy constraints $|W_pS| \leq 1$ and $|W_mT| \leq 1$.

6.3.3 Case of fourth order nominal plant $P_{zpe}(s)$

When the zero phase error approximation $P_{zpe}(s)$ is employed and $Q_{nmp(zpe)}(s)$ is selected as a fourth order filter to guarantee the causality of the system. Obtained figures are displayed in Fig. 6.8, Fig. 6.9 and Fig. 6.10.

$$P_{zpe}(s) = \frac{1.8906 \times 10^7 (s + 957.6)}{s(s + 8.131)(s + 687.5)(s^2 + 20s + 5.610 \times 10^4)}, \tag{6.10}$$

$$Q_{nmp(zpe)}(s) = \frac{1}{2.335 \times 10^{-10} s^4 + 4.176 \times 10^{-8} s^3 + 1.212 \times 10^{-4} s^2 + 0.01831 s + 1}, \tag{6.11}$$

$$\omega_{nmp(zpe)} = 43.0 \text{ [rad/s]}, \tag{6.12}$$

in which $Q_{nmp(zpe)}(s)$ and $\omega_{nmp(zpe)}$ are optimized low pass filter and bandwidth, respectively.

6.3.4 Case of fourth order nominal plant $P_{nmp}(s)$

When the non-minimum phase nominal plant model $P_{nmp}(s)$ is utilized, $Q_{nmp(pn)}(s)$ can be obtained as follows. It should be noticed that the obtained filter $Q_{nmp(pn)}(s)$ is also a non-minimum phase one and contains one unstable zero (687.5). Acquired figures are exhibited in Fig. 6.11, Fig. 6.12 and Fig. 6.13.

$$P_{nmp}(s) = \frac{-40(s + 957.6)(s - 687.5)}{s(s + 8.131)(s^2 + 20s + 5.6 \times 10^4)}, \tag{6.13}$$

$$Q_{nmp(pn)}(s) = \frac{-14286(687.5 - s)}{(s + 814.6)(s + 121.9)(s + 98.94)}, \ \omega_{nmp(pn)} = 38.2 \text{ [rad/s]}, \tag{6.14}$$

in which $\omega_{nmp(pn)}$ represents for the optimized bandwidth.

6.4 Low pass filter design result in discrete domain for a non-minimum phase plant

Fourth order discrete nominal plant $P_{zmed}(z)$ (discretized from P_{zme}) is used in the design of low pass filter for a non-minimum phase plant and the optimized results are shown in Eq. (6.16) along with corresponding figures shown in Fig. 6.14, Fig. 6.15 and Fig. 6.16.

$$P_{zmed}(z) = \frac{7.5663 \times 10^{-7} (z - 0.8417)(z - 0.7862)(z + 1)^2}{(z - 1)(z - 0.998)(z^2 - 1.992z + 0.995)}, \tag{6.15}$$

$$Q_{nmp(zmed)}(z) = \frac{z^2 + 2z + 1}{2026z^2 - 3676z + 1655}, \ \omega_{nmp(zmed)} = 36.3 \text{ [rad/s]}. \tag{6.16}$$

6.5 Identification of nominal plant model and design of low pass filter in continuous domain for a non-minimum phase plant

By following procedures in Chapter 4 section 4.2.6, results of designing low pass filter along with identifying nominal plant model for the non-minimum phase plant are shown as follows. To show design

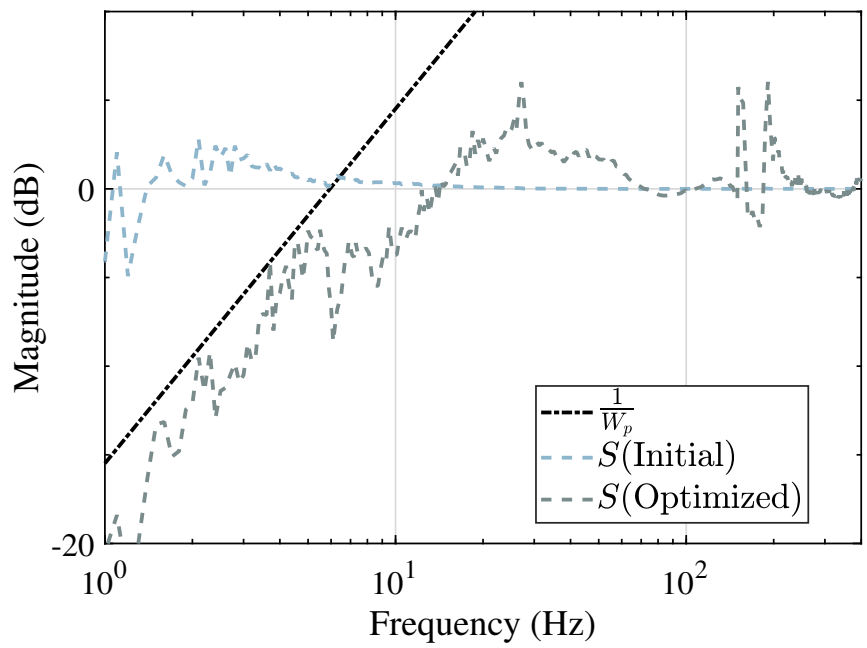

Figure 6.7 Magnitude plots of $\frac{1}{W_p}$, S (Initial) and S (Optimized) when zero magnitude error approximation $P_{zme}(s)$ is used in designing low pass filter for a non-minimum phase plant. The effective disturbance rejection area (the magnitude of sensitivity function S is smaller than 1) has been enlarged after the optimization process.

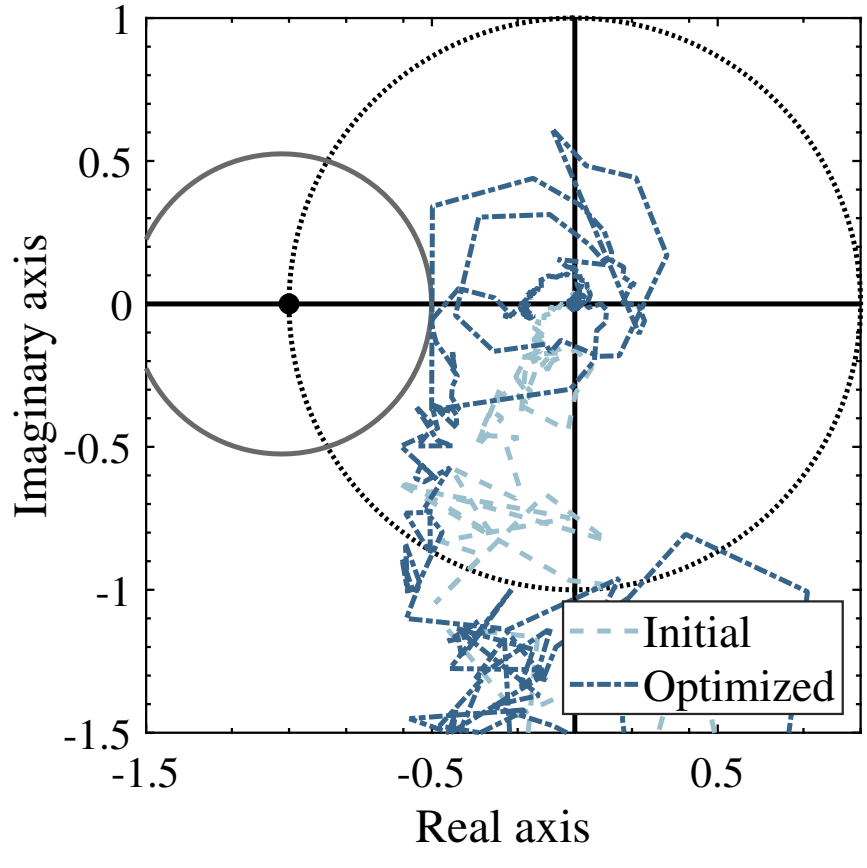

Figure 6.8 Nyquist plots of loop gain (L) (Initial and Optimized) when zero phase error approximation $P_{zpe}(s)$ is used in designing low pass filter for a non-minimum phase plant. The resultant Nyquist plot is tangent to the stability circle (gray line) which indicates that stability margins have been satisfied.

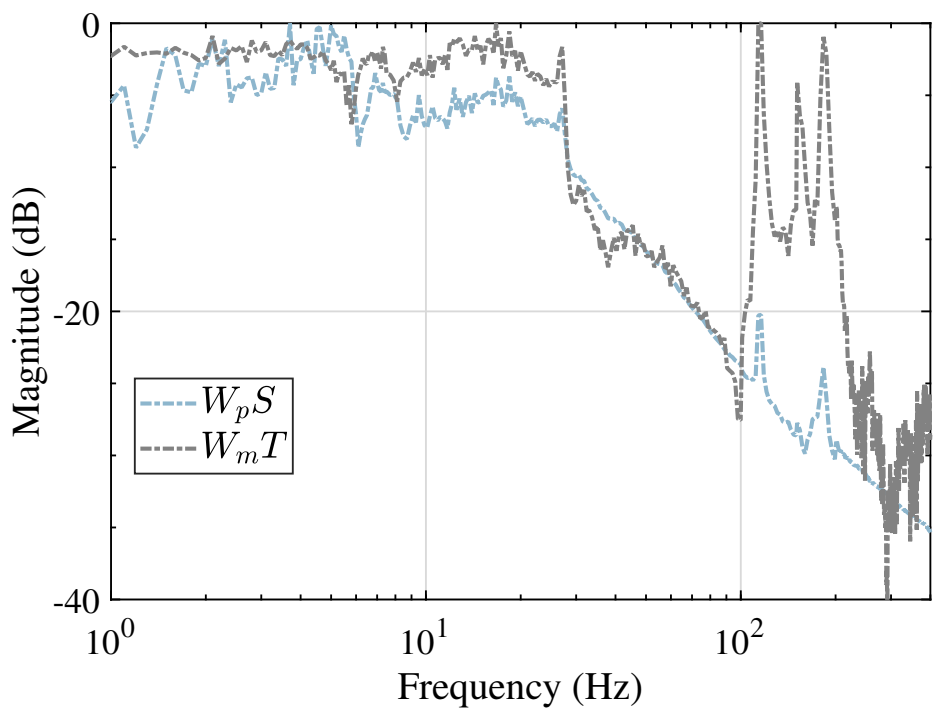

Figure 6.9 Magnitude plots of W_pS and W_mT when zero phase error approximation $P_{zpe}(s)$ is used in designing low pass filter for a non-minimum phase plant. W_p and W_m are weighting functions for sensitivity function (S) as well as complementary sensitivity function (T) respectively and thus, this figure shows that optimized S and T have satisfied the corresponding constraints successfully.

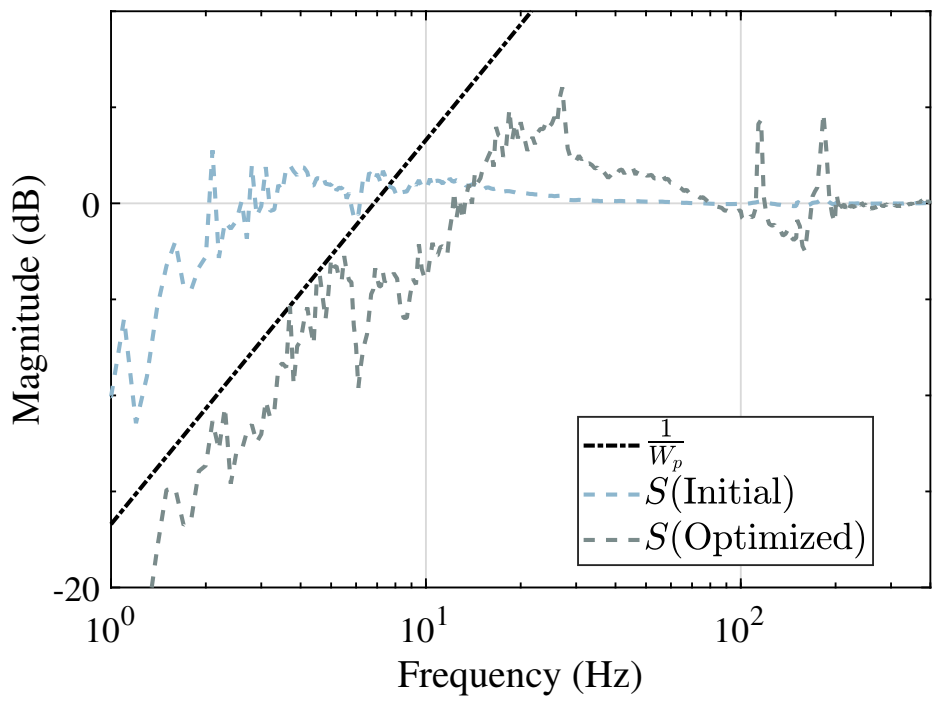

Figure 6.10 Magnitude plots of $\frac{1}{W_p}$, S (Initial) and S (Optimized) when zero phase error approximation $P_{zpe}(s)$ is used in designing low pass filter for a non-minimum phase plant. The optimization process has pushed the sensitivity function (S) to have larger crossover frequency which can be told from this figure.

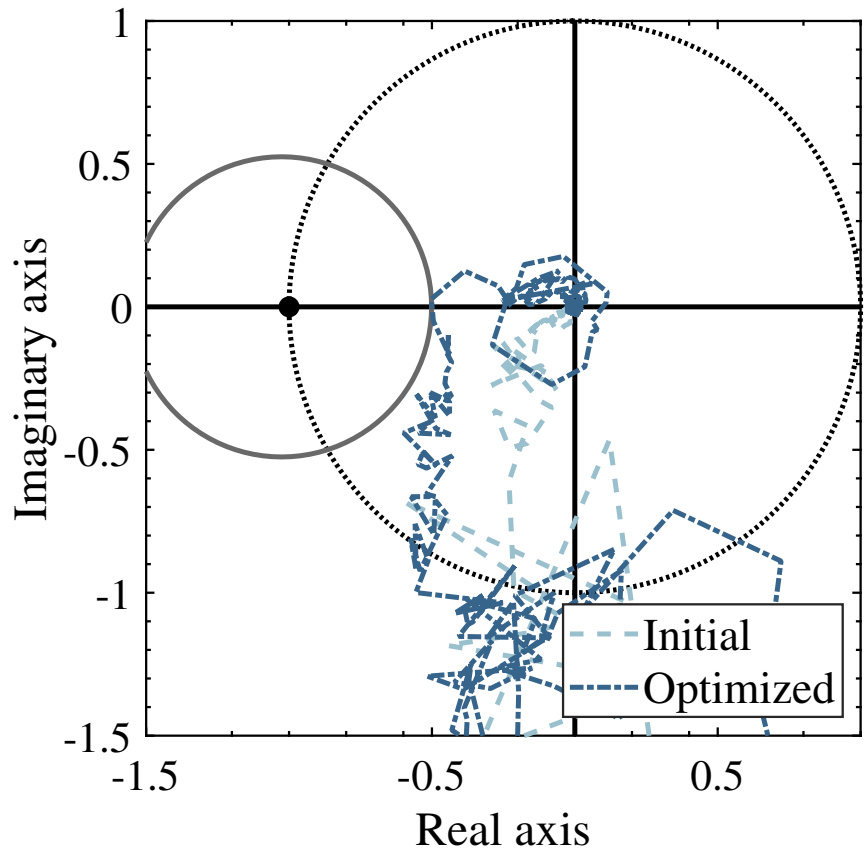

Figure 6.11 Nyquist plots of loop gain (L) (Initial and Optimized) when the non-minimum phase plant $P_{nmp}(s)$ is used in designing low pass filter for a non-minimum phase plant. The dark blue line is the optimized open loop function and since it stays outside of the stability circle (gray line), the constraint for guaranteeing stability margins holds straightforwardly.

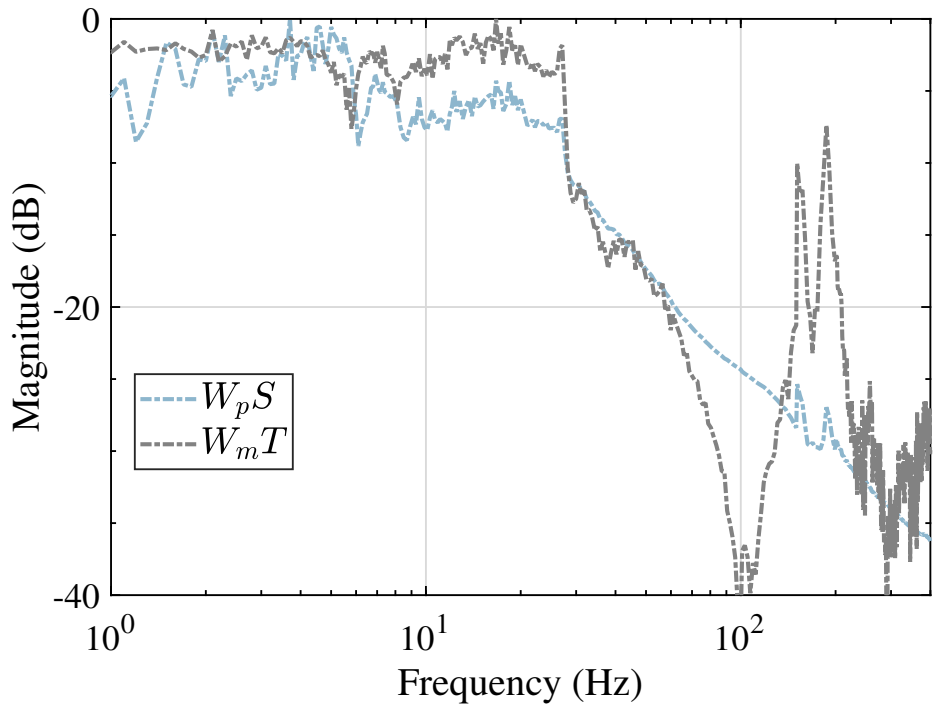

Figure 6.12 Magnitude plots of W_pS and W_mT when the non-minimum phase plant $P_{nmp}(s)$ is used in designing low pass filter for a non-minimum phase plant. This figure is to show that constraints $|W_pS| \leq 1$ and $|W_mT| \leq 1$ have been met.

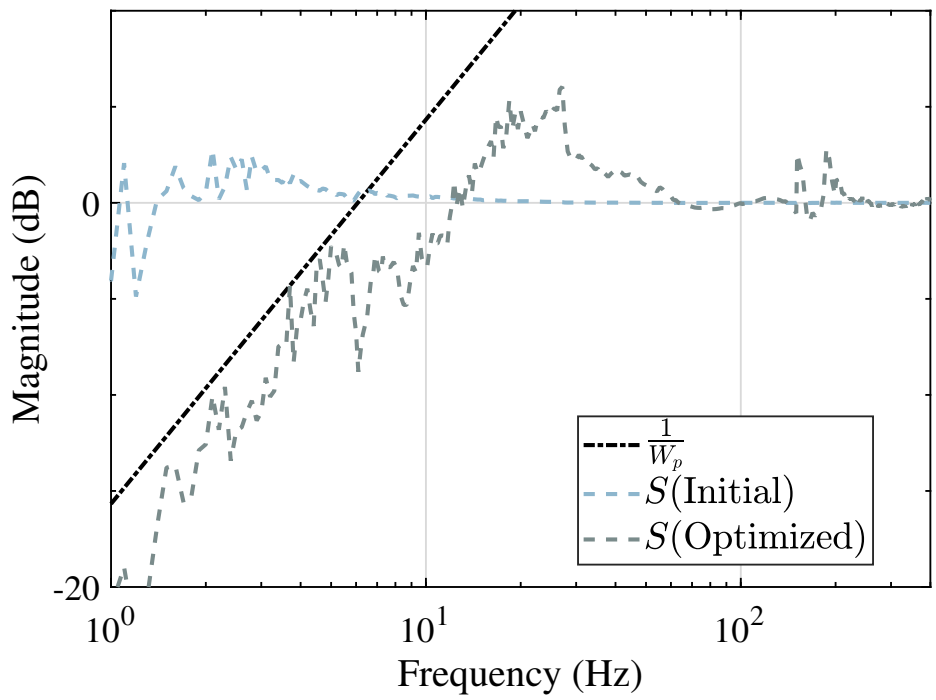

Figure 6.13 Magnitude plots of $\frac{1}{W_p}$, S (Initial) and S (Optimized) when the non-minimum phase plant $P_{nmp}(s)$ is used in designing low pass filter for a non-minimum phase plant. The crossover frequency of optimized weighting function (W_p), which is used in representing the bandwidth of DOB, is larger compared to the initial case.

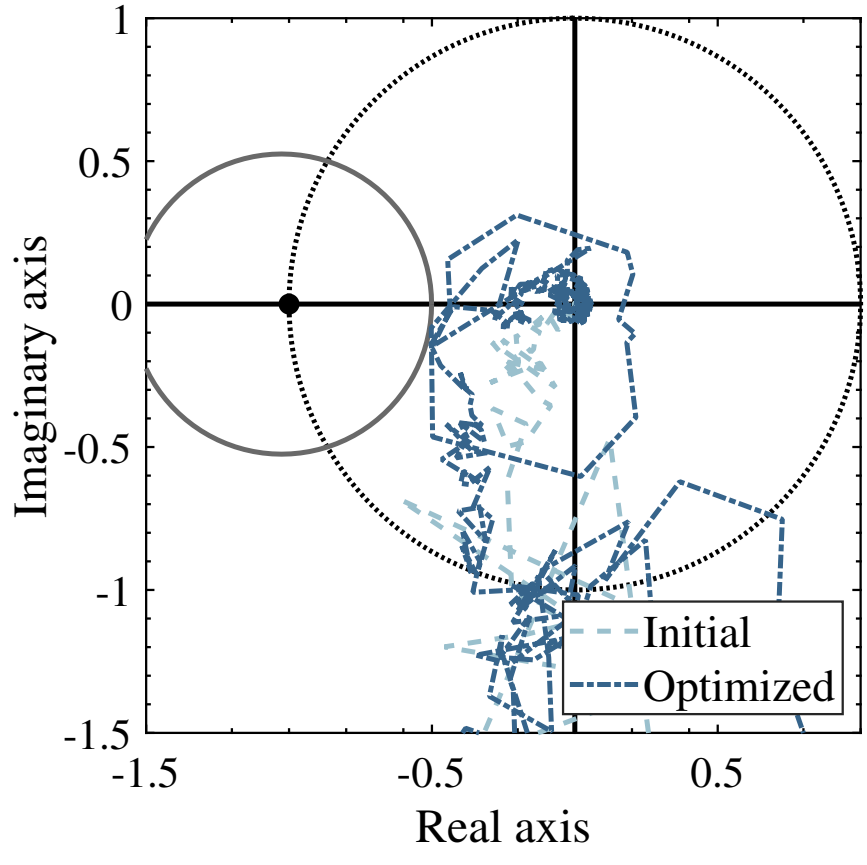

Figure 6.14 Nyquist plots of loop gain (L) (Initial and Optimized) when discrete nominal plant model $P_{zmed}(z)$ (discretized from zero magnitude error approximation P_{zme}) is used in designing low pass filter for a non-minimum phase plant. The design in discrete domain has successfully made the constraint $|L+\sigma| > r_m$ hold in which $(-\sigma, 0)$ and r_m are center point and radius of stability circle (gray line), respectively.

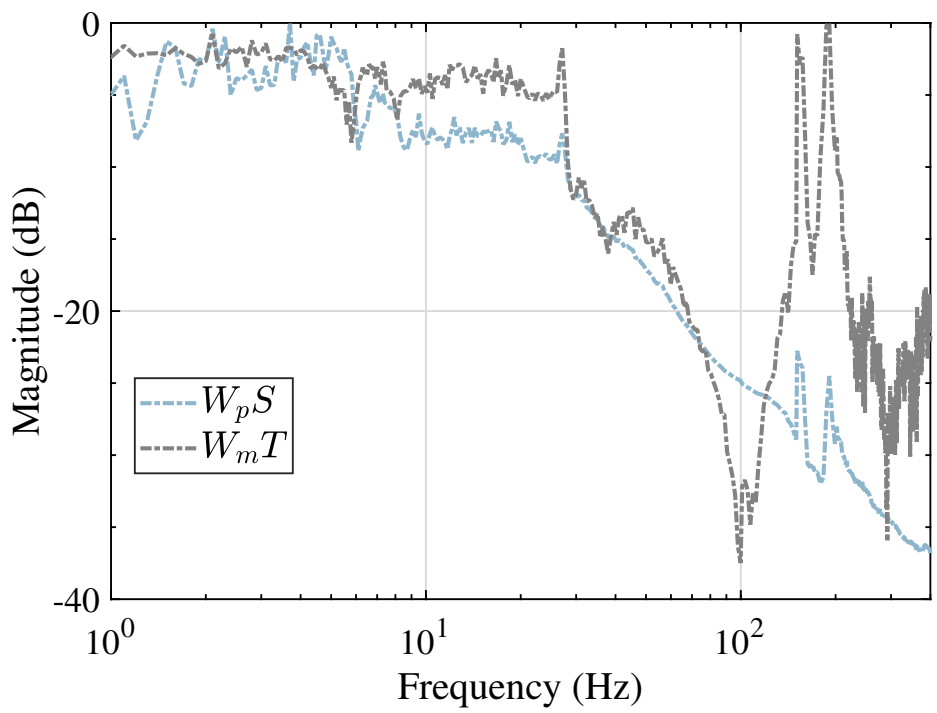

Figure 6.15 Magnitude plots of W_pS and W_mT when discrete nominal plant model $P_{zmed}(z)$ (discretized from zero magnitude error approximation P_{zme}) is used in designing low pass filter for a non-minimum phase plant. From this figure, predefined constraints $|W_pS| \leq 1$ and $|W_mT| \leq 1$ have been satisfied.

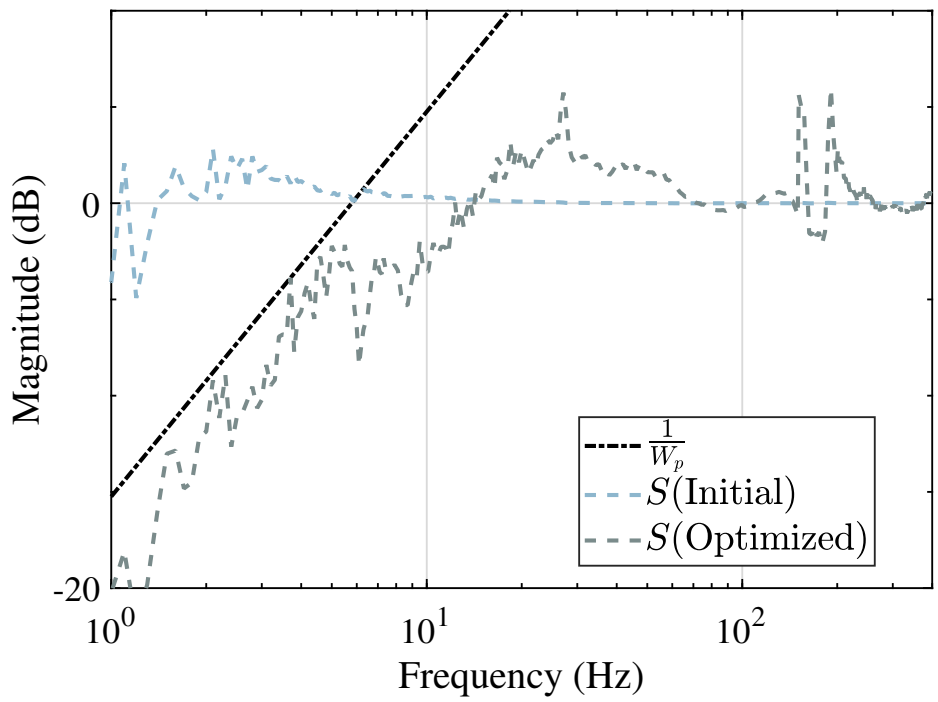

Figure 6.16 Magnitude plots of $\frac{1}{W_p}$, S (Initial) and S (Optimized) when discrete nominal plant model $P_{zmed}(z)$ (discretized from zero magnitude error approximation P_{zme}) is used in designing low pass filter for a non-minimum phase plant. From this figure, the crossover frequency of sensitivity function has become larger which indicates that disturbance rejection performance has been improved.

results straightforwardly, figures Fig. 6.17, Fig. 6.18, Fig. 6.19 and Fig. 6.20 have been present.

$$P_{nmp(pqs)}(s) = \frac{6.410(s^2 + 4129s + 5.021 \times 10^6)}{s(s + 7.776)(s^2 + 48.19s + 5.011 \times 10^4)}, \tag{6.17}$$

$$Q_{nmp(pqs)}(s) = \frac{1.645 \times 10^4}{s^2 + 199.2s + 1.645 \times 10^4},\ \omega_{nmp(pqs)} = 47.8\ [\text{rad/s}]. \tag{6.18}$$

6.6 Identification of nominal plant model and design of low pass filter in discrete domain for a non-minimum phase plant

The identification of nominal plant model and design of low pass filter in discrete domain has also been accomplished and the obtained result is in Eq. (6.20). Correspondingly, obtained figures are present in Fig. 6.21, Fig. 6.22, Fig. 6.23 as well as Fig. 6.24 to analyze the result effectively.

$$P_{nmp(pqz)}(z) = \frac{3.915 \times 10^{-7}(z + 1)^2(z^2 - 1.477z + 0.5576)}{(z - 0.998)(z - 1)(z^2 - 1.986z + 0.9888)}, \tag{6.19}$$

$$Q_{nmp(pqz)}(z) = \frac{2.724 \times 10^{-4}(z + 1)^2}{z^2 - 1.945z + 0.9456},\ \omega_{nmp(pqz)} = 45.6\ [\text{rad/s}]. \tag{6.20}$$

6.7 Analysis on simulation results for a non-minimum phase plant

1. Constraints have all been satisfied.

   For all these case studies, Nyquist plots of loop gain L (Initial and Optimized)), which are shown in Fig. 6.2, Fig. 6.5 and Fig. 6.8, Fig. 6.11, Fig. 6.14, as well as Fig. 6.18, Fig. 6.22, respectively, stay outside of the stability circle (gray line) which implies that the stability margin constraint holds successfully for all these cases. Furthermore, proposed optimization method forces the optimized Nyquist plot to be tangent to the gray circle which implies that the bandwidth of L is maximized under the limitation of constraints. In addition, constraints for sensitivity function and complementary sensitivity function are satisfied as $|W_pS|$ and $|W_mT|$ are always under 0 [dB] as shown in Fig. 6.3, Fig. 6.6, Fig. 6.9, Fig. 6.12 and Fig. 6.15, Fig. 6.19, Fig. 6.23.

2. Comparison of optimized bandwidth results.

   (a) Simultaneous identification of nominal plant model and design of low pass filter (ω_p : over 45 [rad/s]) (s domain and z domain) have obtained larger bandwidth than cases of designing low pass filter only (ω_p : smaller than 44 [rad/s]).

   Same as in the analysis of minimum phase plant, more tuning freedom is in simultaneous design which accounts for such phenomenon.

   (b) Discrete domain design has achieved comparative performance as continuous domain design which can be straightforwardly understood from Fig. 6.25.

   (c) When approximations of non-minimum phase plant are used in the design of low pass filter, zero phase error approximation case has obtained largest bandwidth due to more tuning freedom.

$$\omega_{nmp(zpe)}\ (43.0\ [\text{rad/s}]) > \omega_{nmp(zme)}(37.4\ [\text{rad/s}]) > \omega_{nmp(ps)}\ (30.8\ [\text{rad/s}]) \tag{6.21}$$

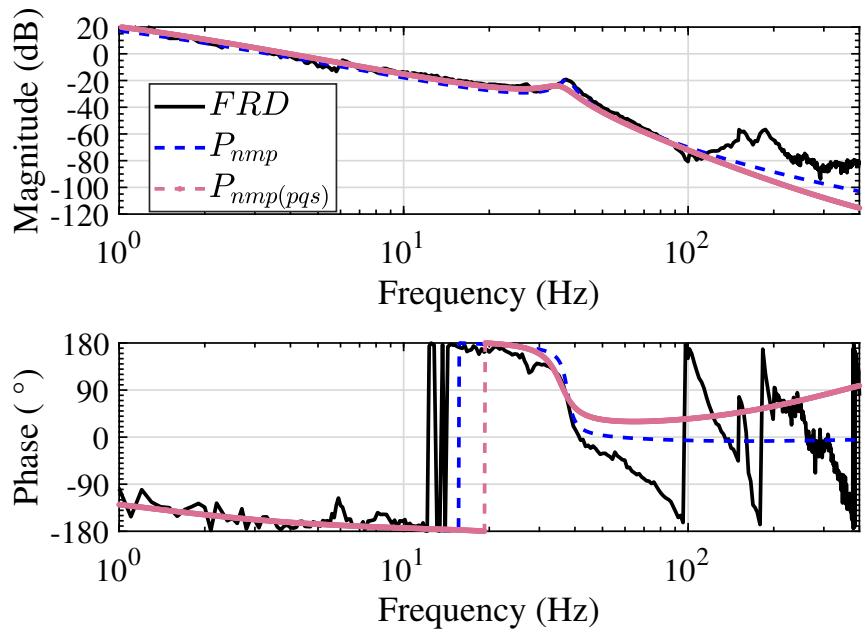

Figure 6.17 Bode plots of frequency response data (FRD), nominal plant model $P_{nmp}(s)$ (identified from FRD) and optimized nominal plant model $P_{nmp(pqs)}(s)$ in the simultaneous identification of nominal plant model and design of low pass filter (s domain) for a non-minimum phase plant.

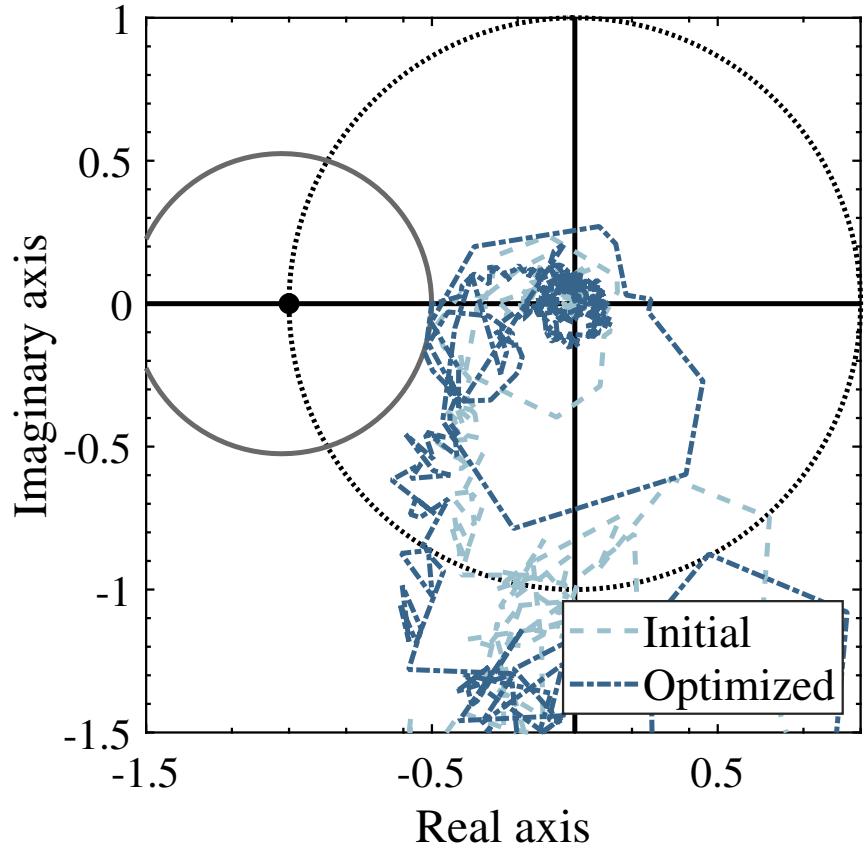

Figure 6.18 Nyquist plots of loop gain (L) (Initial and Optimized) in the simultaneous identification of nominal plant model and design of low pass filter (s domain) for a non-minimum phase plant. This figure is to show that the optimized loop gain has satisfied the constraint for guaranteeing stability margins since it stays outside of the stability circle (gray line).

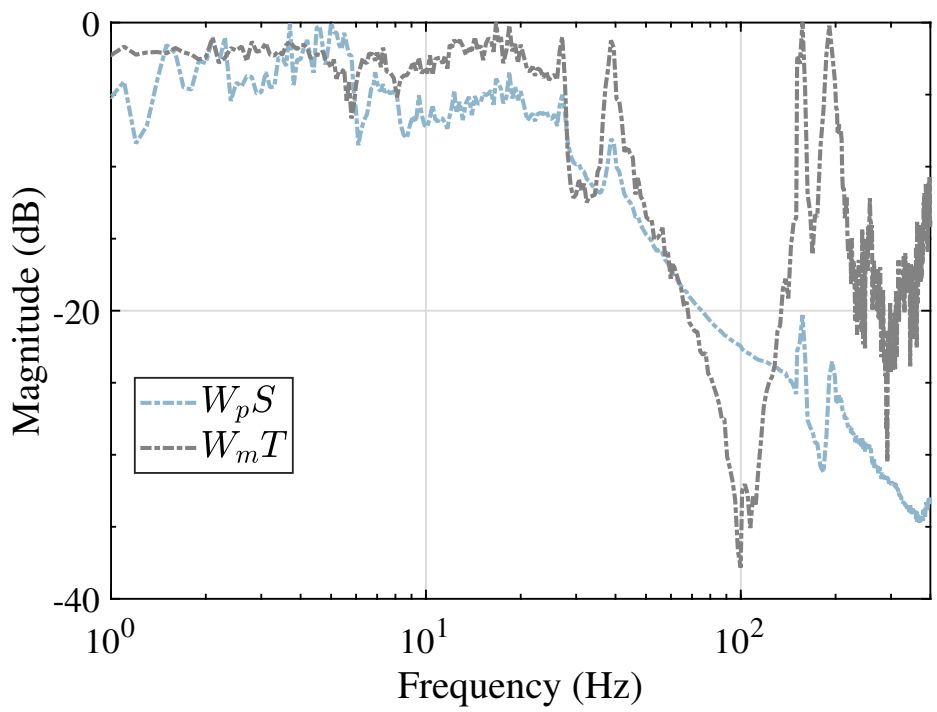

Figure 6.19 Magnitude plots of W_pS and W_mT in the simultaneous identification of nominal plant model and design of low pass filter (s domain) for a non-minimum phase plant. From this figure, $|W_pS| \leq 1$ and $|W_mT| \leq 1$ hold successfully.

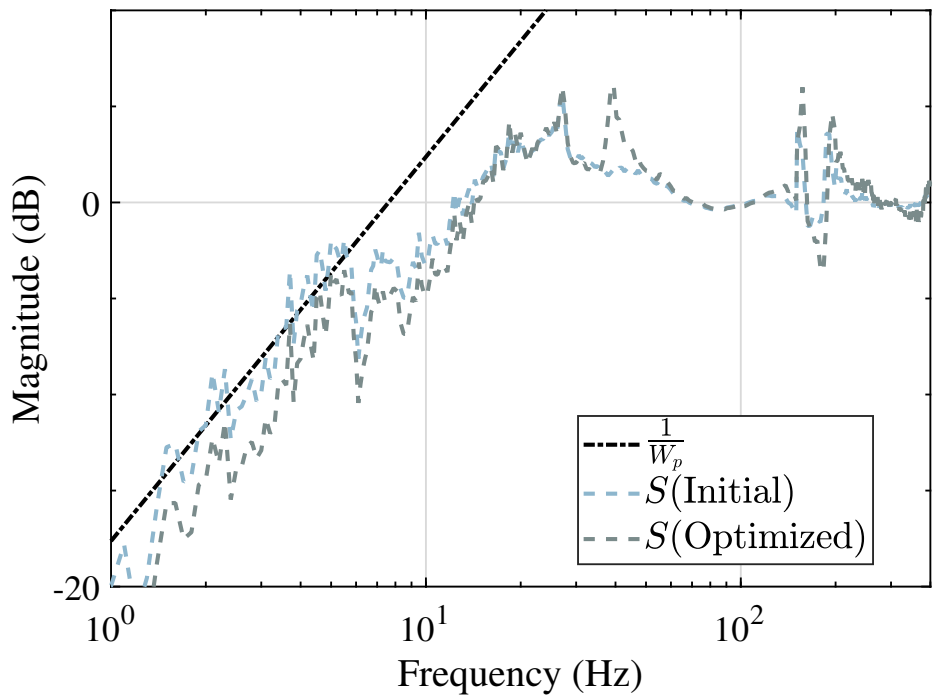

Figure 6.20 Magnitude plots of $\frac{1}{W_p}$, S (Initial) and S (Optimized) in the simultaneous identification of nominal plant model and design of low pass filter (s domain) for a non-minimum phase plant. Optimization process has pushed the sensitivity function to have a larger crossover frequency.

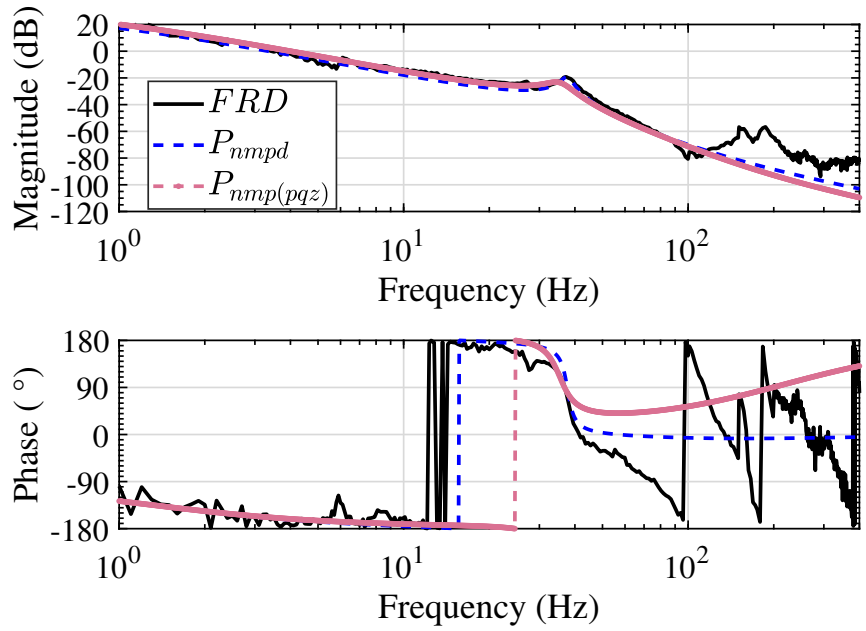

Figure 6.21 Bode plots of frequency response data (FRD), nominal plant model $P_{nmpd}(z)$ (identified from FRD) and optimized nominal plant model $P_{nmp(pqz)}(z)$ in the simultaneous identification of nominal plant model and design of low pass filter (z domain) for a non-minimum phase plant.

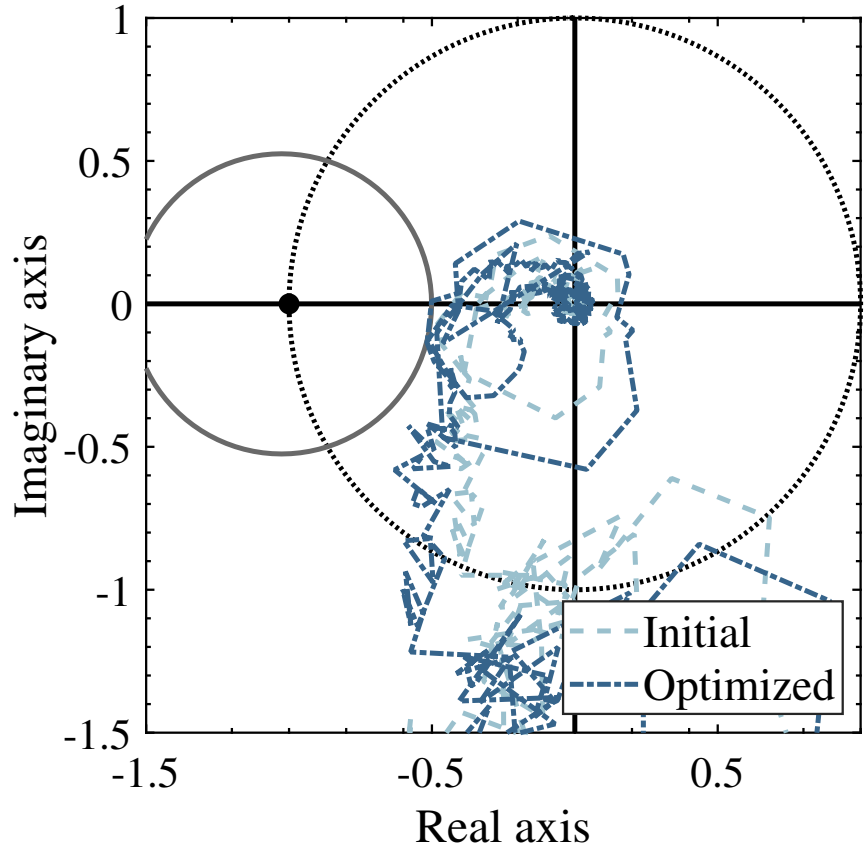

Figure 6.22 Nyquist plots of loop gain (L) (Initial and Optimized) in the simultaneous identification of nominal plant model and design of low pass filter (z domain) for a non-minimum phase plant. The design in discrete domain has achieved a similar Nyquist plot as in continuous domain which satisfies the gain margin and phase margin successfully.

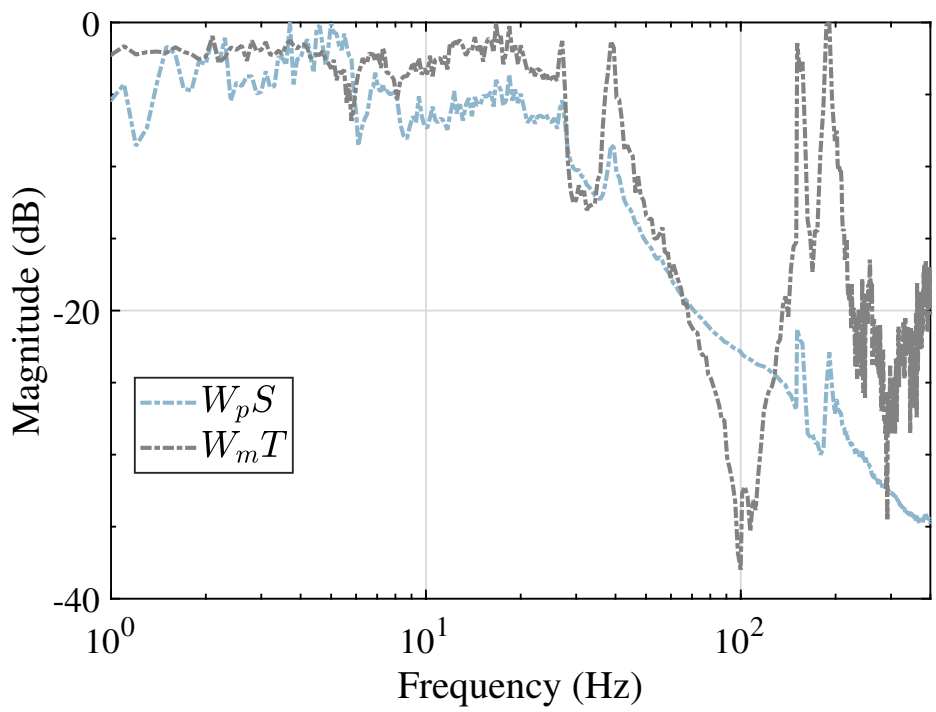

Figure 6.23 Magnitude plots of W_pS and W_mT in the simultaneous identification of nominal plant model and design of low pass filter (z domain) for a non-minimum phase plant. Similar as the result in continuous domain, constraints $|W_pS| \leq 1$ and $|W_mT| \leq 1$ have been met.

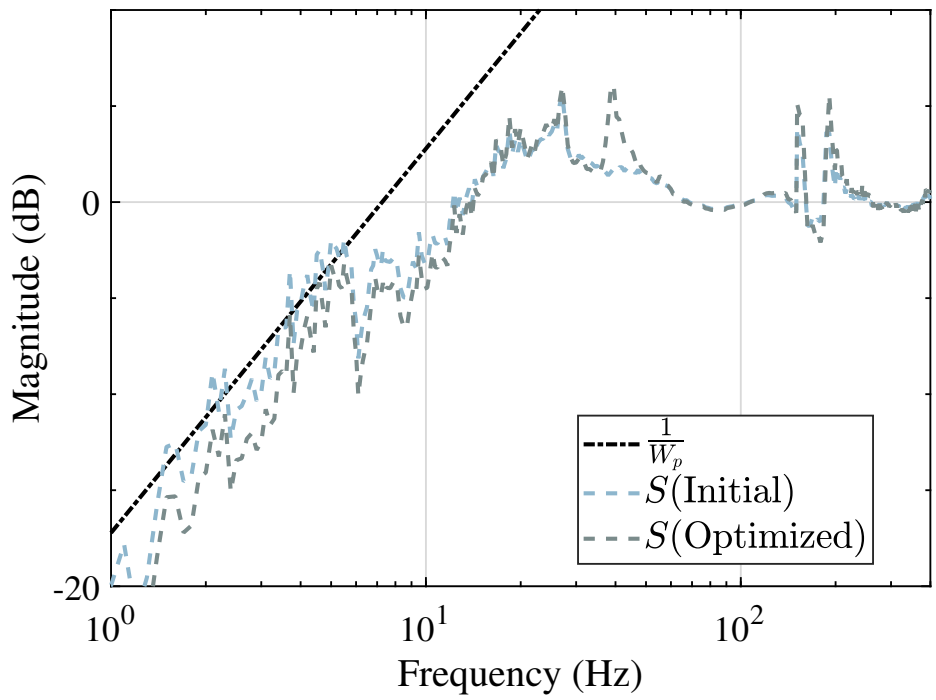

Figure 6.24 Magnitude plots of $\frac{1}{W_p}$, S (Initial) and S (Optimized) in the simultaneous identification of nominal plant model and design of low pass filter (z domain) for a non-minimum phase plant. The crossover frequency has become larger compared to the initial case which means better disturbance rejection performance. Furthermore, sensitivity function (S(Optimized)) is under $\frac{1}{W_p}$ which shows that $|W_pS| \leq 1$ has been satisfied.

(d) Comparison results when same relative order $Q(s)$ filter is designed.

$$\omega_{nmp(pn)}(38.2\ [\text{rad/s}]) > \omega_{nmp(zme)}(37.4\ [\text{rad/s}]) > \omega_{nmp(ps)}(30.8\ [\text{rad/s}]). \tag{6.22}$$

Remark:

1. Qualitative analysis
   Since $L = \underbrace{\overbrace{P(nmp, FRD)}^{FRD}\ \overbrace{P_n^{-1}}^{\text{nominal plant}}}_{\text{approximation error}} Q/(1-Q)$, the approximation error influences the bandwidth of L and $Q/(1-Q)$ part amplifies the gain of approximation error and adds phase delay in the low frequency region while decreases the gain in higher frequency region. The objective for tuning L is to make it have larger gain (qualitatively) in low frequency region .
   As shown in Fig. 6.26, the obtained nominal plant model $P_{nmp(pqs)}$ has less gain approximation error compared with P_{zpe} and phase lead in the high frequency region which is beneficial for gain amplification. Therefore, higher bandwidth of L can be expected.
2. Selection of orders of nominal plant model and low pass filter
   In this thesis, when the nominal plant model is tuned with low pass filter simultaneously, the order of nominal plant model should be decided at first. The typical oscillation modes should be considered in order to obtain satisfactory bandwidth. However, if too many oscillation modes are selected into the nominal plant model, the resultant low pass filter will have high order which adds calculation burden to the optimization software and may lead to numerical problems. Therefore, the selection of order of nominal plant is important but more of experience-based procedure.
3. Variations of frequency response data
   If the frequency response data of system varies as working environment changes, proposed methods can obtain a robust result which satisfies all the constraints by employing all frequency data sets rather than one frequency response data set into proposal.
4. Notes on implementation in optimization software
   Since proposed methods are data-based calculation methods and the value of high order frequency item (*e.g.* $(j\omega)^4$) varies in a large range as the frequency point changes which could become a burden for the optimization software and cause numerical errors or more seriously, solution error. Therefore, the modeling of the problem in software should be adjusted (basic idea and example is shown in Eq. (6.23) and Eq. (6.24)). When ω_k changes from 1 to 400, assuming the range is shown as follows,

$$\begin{aligned} N_1 &= ((j\omega_k)^3 + \epsilon_2(j\omega_k)^2 + \epsilon_1(j\omega_k) + \epsilon_0) \in [0, 10^6], \\ D_1 &= ((j\omega_k)^3 + \epsilon_5(j\omega_k)^2 + \epsilon_4(j\omega_k) + \epsilon_3) \in [0, 10^6]. \end{aligned} \tag{6.23}$$

   Take constraint for stability margins as an example,

$$|\frac{N_1}{D_1} + \sigma| > r_m(\text{original one}) \Leftrightarrow \frac{|N_1 + \sigma D_1|}{10^3} > \frac{r_m|D_1|}{10^3}(\text{adjusted one}). \tag{6.24}$$

   then the adjusted one should be used in optimization. Importantly, such method can only release the calculation burden to some extent. Selection of a very high order low pass filter could lead to such problem which should be paid attention to.

6.8 Comparison with existing methods

To better show the efficacy of the proposal, the following two typical methods are compared with proposed methods. For these two methods, P_{nmp} is selected as the nominal plant. To make a fair comparison, same stability margins as ones used in proposal are guaranteed. To guarantee the internal stability, $Q(s)$ should contain the same unstable zeros as nominal plant model has.

6.8.1 Introduction on existing methods

Trial-and-error method

The $Q_{\text{trial(nmp)}}(s)$ is selected as the following form:

$$Q_{\text{trial(nmp)}}(s) = \frac{1}{(\tau_{nmp}s+1)^{tq}} \frac{(z_0 - s)\cdots(z_{j^*} - s)}{(s+z_0)\cdots(s+z_{j^*})}, \tag{6.25}$$

in which $z_0 \cdots z_{j^*}$ are unstable zeros of nominal plant and τ_{nmp} is the parameter to be designed; tq is the relative order.

Similar as in minimum phase case,the tuning process can be summarized as follows when $P_{(nmp,FRD)}$ and $P_{nmp}(s)$ represent the frequency response data of a non-minimum phase plant and nominal plant model identified from frequency response data, respectively.

1. Give τ_{nmp} a value and plot Nyquist plot of $L_{\text{trial(nmp)}} = P_{(nmp,FRD)}P_{nmp}(s)Q_{\text{trial(nmp)}}(s)(1 - Q_{\text{trial(nmp)}}(s))$ to check whether it satisfies the constraint for stability margins or not.
2. If the $L_{\text{trial(nmp)}}$ in previous step satisfies the constraint, decrease the value of τ_{nmp} and check new $L_{\text{trial(nmp)}}$ again.
3. If the $L_{\text{trial(nmp)}}$ does not satisfy the constraint, increase the value of τ_{nmp} and check new $L_{\text{trial(nmp)}}$ again.
4. Repeat the above steps until the $L_{\text{trial(nmp)}}$ becomes tangent to the stability circle.

Based on the tuning process, $Q_{\text{trial(nmp)}}(s)$ is obtained as in Eq. (6.26).

$$Q_{\text{trial(nmp)}}(s) = \frac{(-s+687.5)}{(9.025\times10^{-3}s+1)^2(s+687.5)},\ \omega_{p\text{trial(nmp)}} = 38.1\ [\text{rad/s}]. \tag{6.26}$$

H_∞ method

By selecting appropriate weighting functions, Q filter design problem has been formulated into Eq. (6.27) and further formulated into Eq. (6.28) which is a standard H_∞ optimization problem [70].

$$\text{Maximize} \qquad \tilde{\lambda} \tag{6.27a}$$

$$\text{s.t. min} \quad \left\| \begin{bmatrix} \tilde{\lambda}W_1(s)(1 - Q_{\text{hinf}}(s)) \\ W_2(s)Q_{\text{hinf}}(s) \end{bmatrix} \right\|_\infty \leq 1. \tag{6.27b}$$

$\Leftrightarrow$

$$\text{Maximize} \qquad \tilde{\lambda} \tag{6.28a}$$

$$\text{s.t. min} \quad \left\| \begin{bmatrix} \tilde{\lambda}W_1(s)(\tilde{P}\tilde{K}+1)^{-1}) \\ W_2(s)\tilde{P}\tilde{K}(\tilde{P}\tilde{K}+1)^{-1}) \end{bmatrix} \right\|_\infty \leq 1. \tag{6.28b}$$

where $W_1(s)$ as well as $W_2(s)$ are weighting functions and

$$Q_{\text{hinf}}(s) = \frac{\tilde{P}(s)\tilde{K}(s)}{\tilde{P}(s)\tilde{K}(s)+1}, \tilde{P}(s) = \tilde{P}_0(s)\tilde{P}_l(s), \tag{6.29}$$

while $\tilde{P}_0(s)$ is a stable transfer function and $\tilde{P}_l(s)$ is an allpass portion with all the unstable zeros of nominal plant which makes the resultant Q filter also contains the same unstable zeros as nominal plant has.

By utilizing H_∞ method introduced above [70], the following Q_{hinf} is obtained.

$$Q_{\text{hinf}}(s) = \frac{-27859(s-687.5)}{(s+820.9)(s+687.3)(s+33.95)},\ \omega_{p\text{hinf}} = 25.5\ [\text{rad/s}]. \tag{6.30}$$

6.8.2 Comparison results of existing methods and proposed methods

Comparison results are shown in Fig. 6.27 and Fig. 6.28. Proposed low pass filter design methods when non-minimum phase nominal plant model P_{nmp} is used (trial-and-error and H_∞ also employed this nominal plant model) as well as when P_{zpe} is used (the largest bandwidth of our proposal in continuous domain when only low pass filter is designed) have been picked out to finish the following analysis.

1. Comparison results of obtained bandwidth when same nominal plant model P_{nmp} is used in design low pass filter.

   $$\omega_{nmp(pn)}(38.2\ [\text{rad/s}]) > \omega_{p\text{trial(nmp)}}(38.1\ [\text{rad/s}]) > \omega_{p\text{hinf}}(25.5\ [\text{rad/s}]). \tag{6.31}$$

   When the same nominal plant, *e.g.* non-minimum phase plant, has been selected, the non-minimum phase Q filter designed by proposal has obtained a slightly larger bandwidth compared to trial-and-error method and a much large bandwidth compared to H_∞ method. Furthermore, proposed methods are an auto-tuning process which saves design effort.
2. Comparison results of obtained bandwidth when minimum phase approximation of plant model P_{nmp} is used in design low pass filter.

   $$\omega_{nmp(zpe)}(43.0\ [\text{rad/s}]) > \omega_{nmp(pn)}(38.2\ [\text{rad/s}]) > \omega_{p(trial)}(38.1\ [\text{rad/s}]). \tag{6.32}$$

   When the approximation of the nominal plant is used, proposed method is applicable and the resultant bandwidth is the largest.
3. Tuning nominal plant model and low pass filter together has the largest bandwidth among all design methodologies.

6.9 Summary

This chapter has presented extensive case study results for a non-minimum phase plant and compared proposed methods with existing methods which can be summarized as Table 6.2.

1. Desired constraints have been satisfied in proposed methods and bandwidth-maximized DOB has been designed successfully for each case which verified the feasibility of the proposed method for non-minimum phase plant.

2. Compared with trial-and-error method and H_∞ method, larger bandwidth has been obtained by utilizing proposed methods which shows the superiority of proposed method. Furthermore, design effort has been decreased since the proposed method is an auto-tuning process rather than experiences-based process.
3. Continuous domain and discrete domain have all been investigated and comparative performance has been achieved. Continuous domain design is more convenient and straightforward and larger bandwidth can be obtained. However, discrete domain design is more promising in terms of implementation.
4. For a non-minimum phase plant, low pass filter can be designed no matter the identified non-minimum phase plant or its approximation is used in the proposal. In this case study, zero phase error approximation case has gained largest bandwidth when only low pass filter is designed.
5. Simultaneous identification of plant model and design of low pass filter has obtained larger bandwidth compared with design low pass filter only.

Table 6.1 Case study summary for the non-minimum phase plant employed in this chapter

	corresponding section of theoretical analysis	employed nominal plant model	number of to-be-decided parameters
low pass filter design (s domain) (section 6.3)	section 3.2	1. second order nominal plant 2. zero magnitude error approximation (ZME, [107]) of non-minimum phase plant 3. zero phase error approximation (ZPE, [108]) of non-minimum phase plant 4. non-minimum phase plant	1. 2 parameters of filter 2. 2 parameters of filter 3. 4 parameters of filter 4. 3 parameters of filter
low pass filter design (z domain) (section 6.4)	section 3.3	discretized from ZME of non-minimum phase plant	2 parameters of filter
nominal plant model identification and low pass filter design (s domain) (section 6.5)	section 4.2	obtained from optimization process	7 parameters of plant and filter
nominal plant model identification and low pass filter design (z domain) (section 6.6)	section 4.3	obtained from optimization process	7 parameters of plant and filter
trial-and-error method (section 6.8)		non-minimum phase plant	1 parameter of filter
H_∞ method (section 6.8)		non-minimum phase plant	

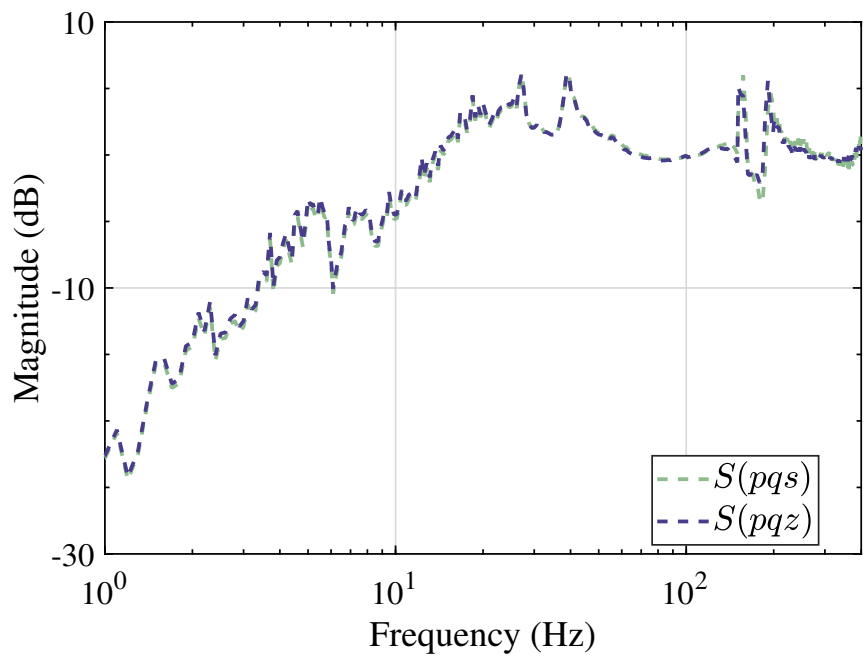

Figure 6.25 Comparison of magnitude plots of optimized sensitivity function in continuous domain $S(pqs)(s)$ and discrete domain $S(pqz)(z)$ when nominal plant model and low pass filter are tuned simultaneously. From this figure, the obtained sensitivity function in continuous domain and discrete domain has comparative crossover frequency (slightly larger in continuous case).

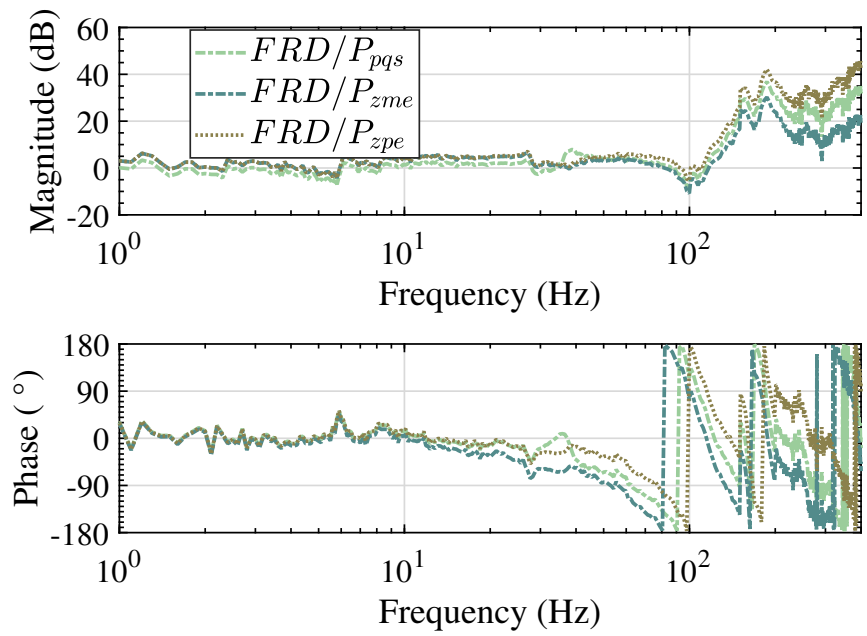

Figure 6.26 Comparison of approximation error of zero magnitude error approximation P_{zme}, zero phase error approximation P_{zpe} and optimized nominal plant model $P_{nmp(pqs)}$.

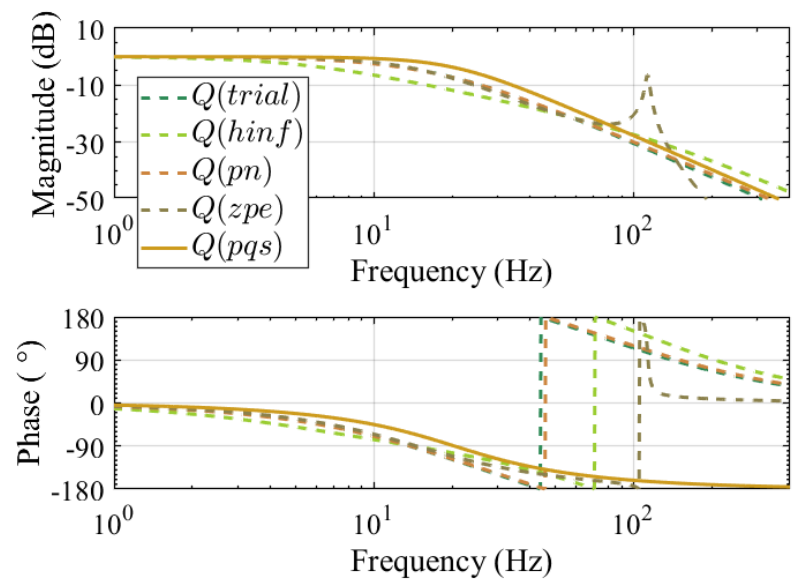

Figure 6.27 Comparison of Q filters designed by proposed methods and existing methods in which $Q(trial)$, $Q(hinf)$, $Q(pn)$, $Q(zpe)$ and $Q(pqs)$ represent for the low pass filter designed by trial-and-error method, H_∞ method, proposed method where non-minimum phase plant is used, proposed method where zero phase error magnitude approximation is used and proposed method in which nominal plant model and low pass filter have been tuned simultaneously, respectively. The $Q(pqs)$ has the largest bandwidth and $Q(zpe)$ has a relatively large bandwidth while a peak appears around 100 Hz which is not friendly to noise suppression around that frequency range.

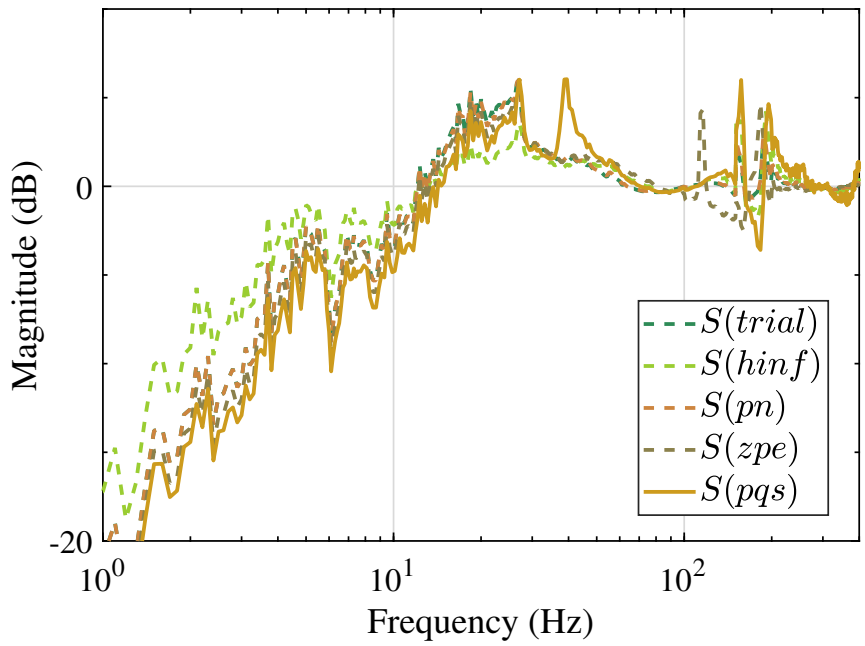

Figure 6.28 Comparison of sensitivity functions of proposed methods and existing methods in which $S(trial)$, $S(hinf)$, $S(pn)$, $S(zpe)$ and $S(pqs)$ represent for the sensitivity function obtained by trial-and-error method, H_∞ method, proposed method where non-minimum phase plant is used, proposed method where zero phase error magnitude approximation is used and proposed method in which nominal plant model and low pass filter have been tuned simultaneously, respectively. From this figure, the crossover frequency of sensitivity function has the largest value in the case of $S(pqs)$.

Table 6.2 Summary of case study results for a non-minimum phase plant

Cases	Nominal plant model	Bandwidth [rad/s]
low pass filter design (s domain) (section 6.3)	1. second order nominal plant (section 6.3.1) 2. ZME of non-minimum phase plant (section 6.3.2) 3. ZPE of non-minimum phase plant (section 6.3.3) 4. non-minimum phase plant (section 6.3.4)	1. 30.8 2. 37.4 3. 43.0 4. 38.2
low pass filter design (z domain) (section 6.4)	discretized form of ZME of non-minimum phase plant	36.3
nominal plant model identification and low pass filter design (s domain) (section 6.5)	obtained from optimization process	**47.8**(largest)
nominal plant model identification and low pass filter design (z domain) (section 6.6)	obtained from optimization process	45.6
trial-and-error (section 6.8)	non-minimum phase plant	38.1
H_∞ (section 6.8)	non-minimum phase plant	25.5

Chapter 7

Experimental verification with a non-minimum phase motion stage

7.1 Overview

In this chapter, experimental results for a non-minimum phase system are presented.

To start with, the structure of the experimental test bench is introduced. Then the detailed system identification process for obtaining frequency response data which has been directly used in the design of DOB has been present. Subsequently, DOBs designed in the case study of Chapter 6 have all been implemented to the test bench and output responses are recorded to analyze the disturbance rejection performance. Finally, experimental results have been compared and analyzed among different cases including proposed methods and previous methods. Design methodology of simultaneous identification of nominal plant model and design of low pass filter has provided the best disturbance rejection performance.

7.2 Experimental test bench introduction

The experimental test bench (left side) and its simplified model (right side) are shown in Fig. 7.1. The test bench constitutes two parts: the linear motor whose stroke is 200mm and the stage which are connected to each other by a leaf spring. Side view of the stage has U-type trough structure and another linear motor which can not be seen from figure is placed at the bottom of it.

Two encoders are used and one of it is for recording linear motor position (has not been marked out in the figure) and the other is to record stage position whose possible positions are shown as the blue dots in the Left side figure of Fig. 7.1. Different positions present different plant dynamics changing from minimum phase one to non-minimum phase one ([17]). In this thesis, the non-minimum phase case, which refers to the highest position (reference point is the desk), is used.

The setup for experimental test bench is shown as Fig. 7.2. Signal transmission is done by Ethercat and the detailed control hardware setup introduction is given in Appendix. In order to obtain the frequency response data from the current reference of linear motor to the stage position, system identification was conducted and the detailed process is introduced as follows.

7.3 System identification process

① System identification condition [110]

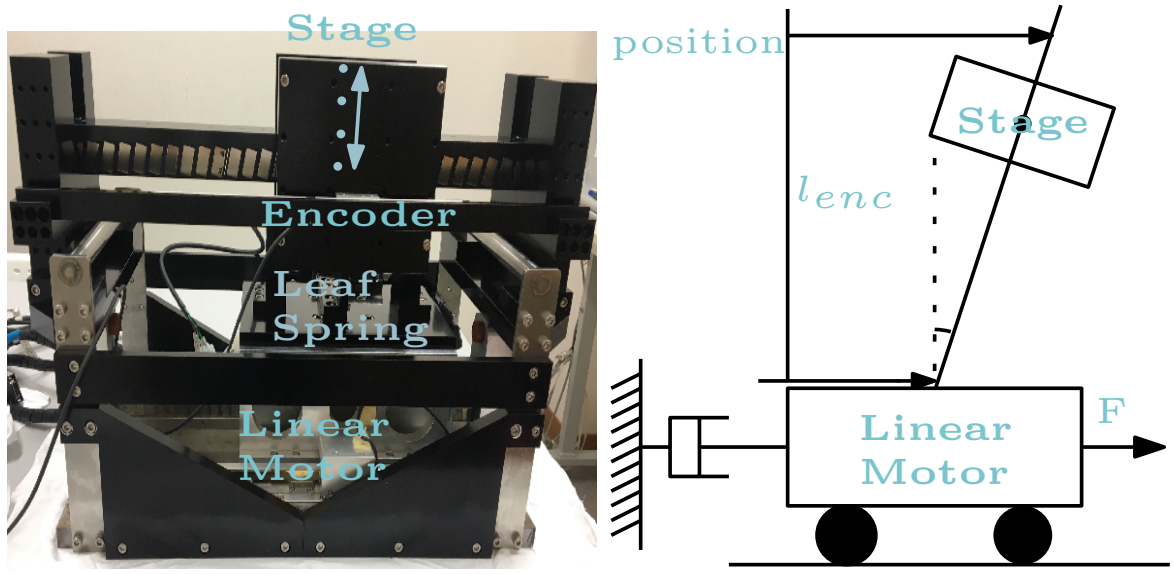

Figure 7.1 Figure of experimental test bench

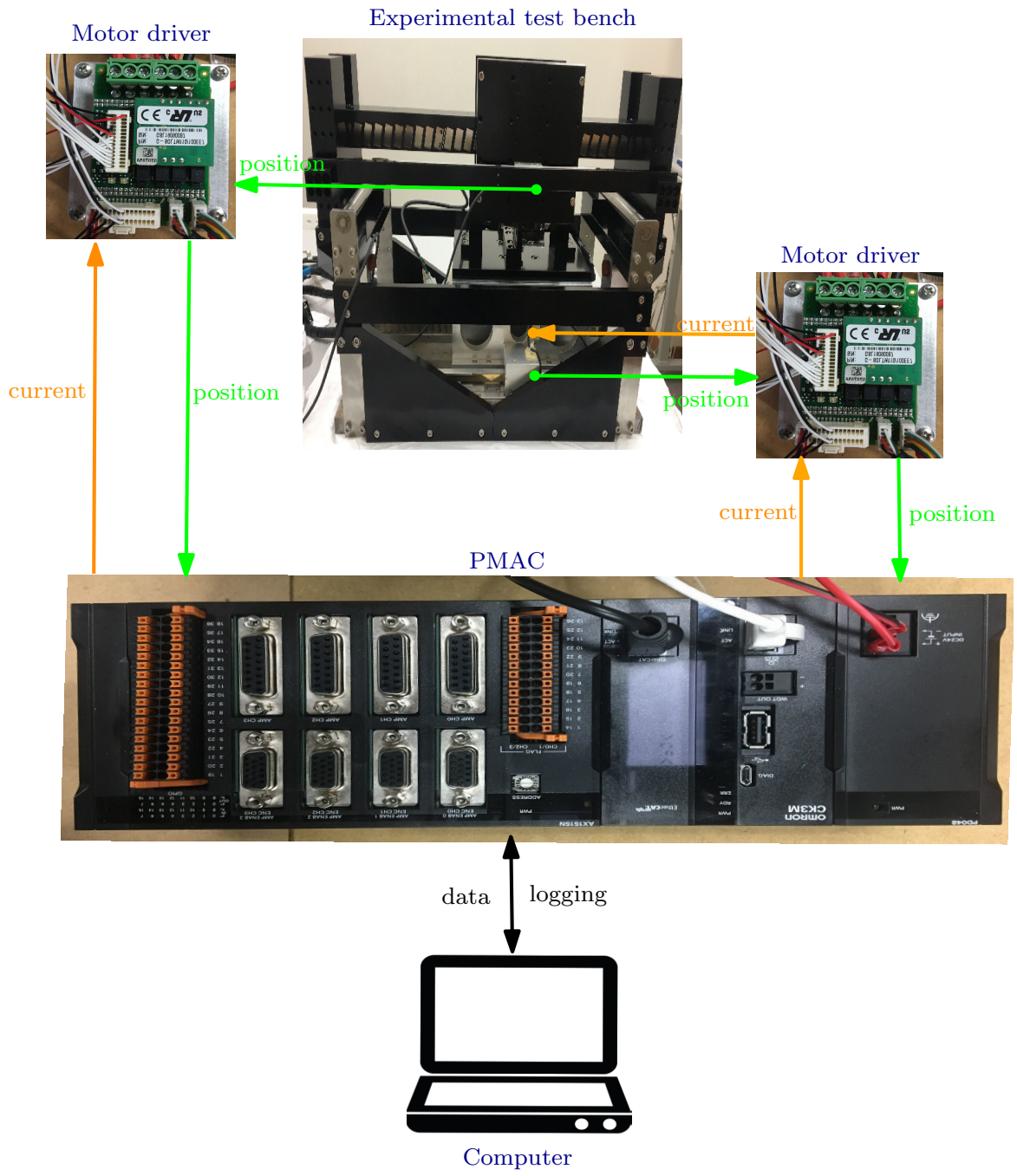

Figure 7.2 Control hardware setup for experiment

1. Objective: obtain the frequency response data from the motor force to the stage position
2. Signals: input signal: current reference; output signal: stage position
3. Excitation signals: multi-sine signals
4. Frequency range: $[1\ [\text{Hz}], 400\ [\text{Hz}]]$
5. Sampling frequency: 4 [kHz]; current controller bandwidth: around 1 [kHz]
6. Excitation methods: divide frequency range into several intervals
   Inject signals which belong to $[1\ [\text{Hz}], 20\ [\text{Hz}]]$, $[21\ [\text{Hz}], 60\ [\text{Hz}]]$, $[61\ [\text{Hz}], 100\ [\text{Hz}]]$, $[101\ [\text{Hz}], 200\ [\text{Hz}]]$, $[201\ [\text{Hz}], 300\ [\text{Hz}]]$, $[301\ [\text{Hz}], 400\ [\text{Hz}]]$ respectively into the system and record stage position and current reference data.
7. Time domain data selection
   After recording the time domain data (position signal and current reference signal) for several periods (in this case, 100 periods are recorded), data which present high repeatability were selected.

After the time domain data (position and current reference) has been selected, the frequency response data can be obtained by Fast Fourier transformation in Matlab. Furthermore, the nominal plant model can be identified based on the frequency response data.

② System identification result

The plant dynamics (from the motor current reference to the stage position) including real plant (FRD, $P_r(j\omega_k)$) and nominal plant (P_{nmp}) are shown in Fig. 7.3. The plant FRD will be directly used in the design of DOB and nominal plant P_{nmp} is intentionally selected as a fourth order non-minimum phase one as represented in Eq. (7.1).

$$P_{nmp} = \frac{-40(s+957.6)(s-687.5)}{s(s+8.131)(s^2+20s+5.6\times10^4)}. \tag{7.1}$$

③ Notes on system identification process

1. Frequency range
   At first, larger frequency range ($[0.1\ [\text{Hz}], 500\ [\text{Hz}]]$) was desired. However, the frequency response data of $[0.1\ [\text{Hz}], 1\ [\text{Hz}])$ and $(400\ [\text{Hz}], 500\ [\text{Hz}]]$ has been abandoned due to the following reasons. When high frequency signals are injected into the system, the movement of motor can barely be recognized and is of less repeatability which means the frequency response data is of large variance. When very low frequency range signals are injected, due to the influence of friction, the accuracy of frequency response data is of less reliability.

7.4 Experiment condition

7.4.1 Block diagram

Fig. 7.4 is used to test the disturbance rejection performance of designed disturbance observers. In Fig. 7.4, C is the current controller inside motor driver and K is the back emf constant of motor. The back emf (the detailed measurement process is shown in Appendix) has been measured and its influence has been compensated by the motor driver. d is the injected disturbance (1.5 [A]) while f is the real friction. If the designed DOB can reach good disturbance (d) rejection performance, then the conclusion of rejection performance of real friction is satisfactory can be made. The reference signal r is set as 0 and

output position signal (y) is recorded to verify the disturbance rejection performance.

7.4.2 PD controller

Reasons for selecting PD controller

PD controller is selected in this experiment and reasons are elaborated as follows:

1. Step disturbance can be rejected without steady state error by using DOB plus PD controller configuration.
   If only DOB part in Fig. 7.5 is considered, $\frac{y}{d} = \frac{P_r(1-Q)}{1-Q+P_rP_n^{-1}Q+C_{fb}P_r}$ holds.
   When $P_r \cong P_n$, $\frac{y}{d} \cong \frac{P_r}{1+C_{fb}P_r}(1-Q)$. Since Q is a low pass filter, $1-Q$ contains one s in numerator.
   e.g. $Q = \frac{b_m s^m + \cdots + b_1 s + 1}{a_n s^m + \cdots + a_1 s + 1}$, $1-Q = \frac{a_n s^n + \cdots + (a_1 - b_1)s}{a_n s^n + \cdots + a_0 + 1}$,
   $\lim_{t\to\infty} y = \lim_{s\to 0} \frac{P_r}{1+C_{fb}P_r} \frac{a_n s^n + \cdots + (a_1 - b_1)s}{a_n s^n + \cdots + a_0 + 1} \frac{1}{s} s = 0.$

2. For mechanical systems with large friction, limit cycle may occur if controller which contains integrator is used, *e.g.* PID controller.
   When motor arrives at point whose velocity is 0 [mm/s], motor stops due to friction, But as time goes on, existence of integrator makes the force become larger and larger and finally win stick-slip friction force and motor will move again. Such process will repeat again and again which is called as limit cycle.

Selection of PD controller

In order to make sure the open loop function L_{cl} for Fig. 7.5 which is shown as Eq. (7.2) has stability margins, the controller is selected and fixed as shown in Eq. (7.3).

$$L_{cl} = \frac{C_{fb}Pr}{1-Q+P_rP_n^{-1}Q}. \tag{7.2}$$

Examples of Nyquist plots of open loop function for different case study results are shown in Fig. 7.6 (cases of when $P_{zme}(s)$ and $P_{zpe}(s)$ are used in designing low pass filter and simultaneous design of plant model and Q filter in s domain case are shown due to their large bandwidth).

$$C_{fb}(s) = 1.05 + \frac{0.049s}{0.0146s+1}. \tag{7.3}$$

7.5 Analysis on experimental results

Experimental results for all the case study results of the non-minimum phase motion stage have been shown in Fig. 7.7.

1. The disturbance has been well-rejected by proposed disturbance observers. Moreover, proposed method of simultaneous identification of nominal plant model and design of low pass filter as well

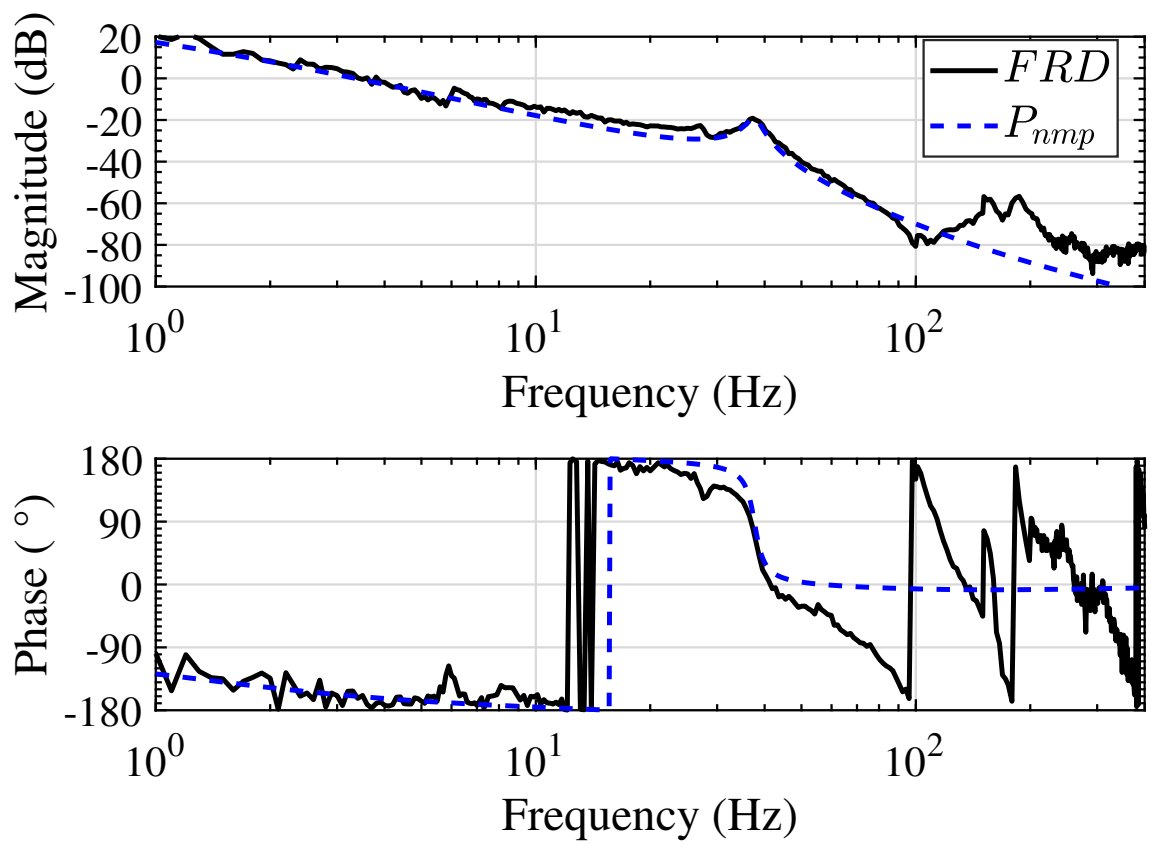

Figure 7.3 Bode plots of plant dynamics (FRD) and identified non-minimum phase nominal plant model (P_{nmp})

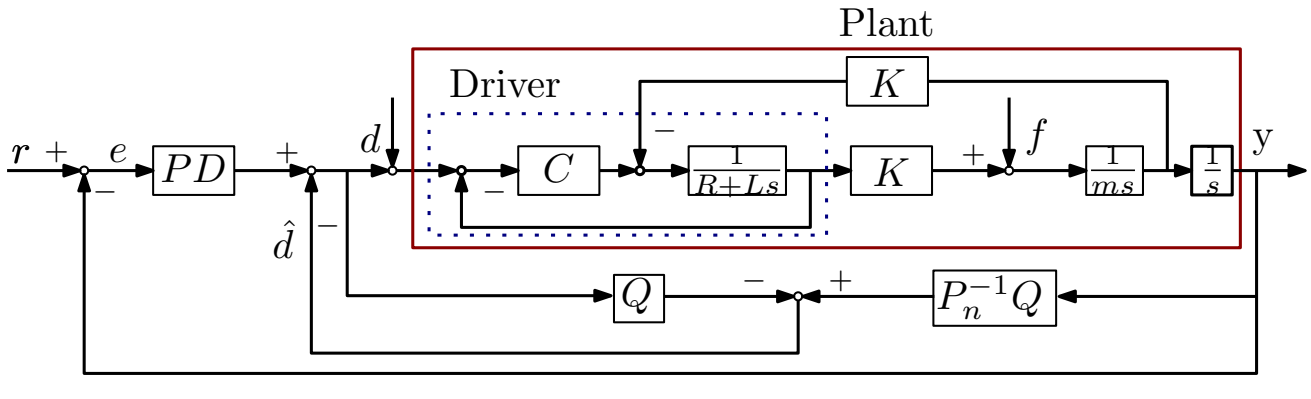

Figure 7.4 Block diagram of experimental block diagram

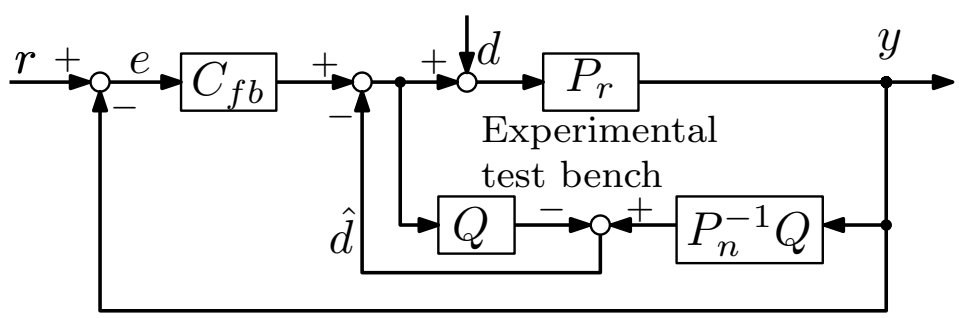

Figure 7.5 Figure of DOB plus outer loop feedback controller

as only low pass filter design when $P_{nmp}(s)$ (non-minimum phase plant) or $P_{zpe}(s)$ (zero phase error approximation) is used have overperformed trial-and-error method along with H_∞ method.

2. The deviation from origin which is reflected by $||e||_\infty$ has matched well with simulation results.

7.6 Summary

In this chapter, the experiment-related introduction has been first given starting from the structure of experimental test bench followed by the process for obtaining frequency response data. Then experimental results for the corresponding numerical case study have been shown and can be summarized as Table 7.1.

1. In system identification process, the measurement of frequency response data is of vital importance. From practical point of view, very low frequency range and very high frequency range have been abandoned due to the influence of friction and encoder resolution. For different application, such issue should be paid attention to.
2. Experimental results have shown that proposed methods have designed larger bandwidth DOBs which have satisfactory disturbance rejection performance.
3. Proposed methods have better disturbance rejection performance compared to existing methods in terms of $||e||_\infty$.

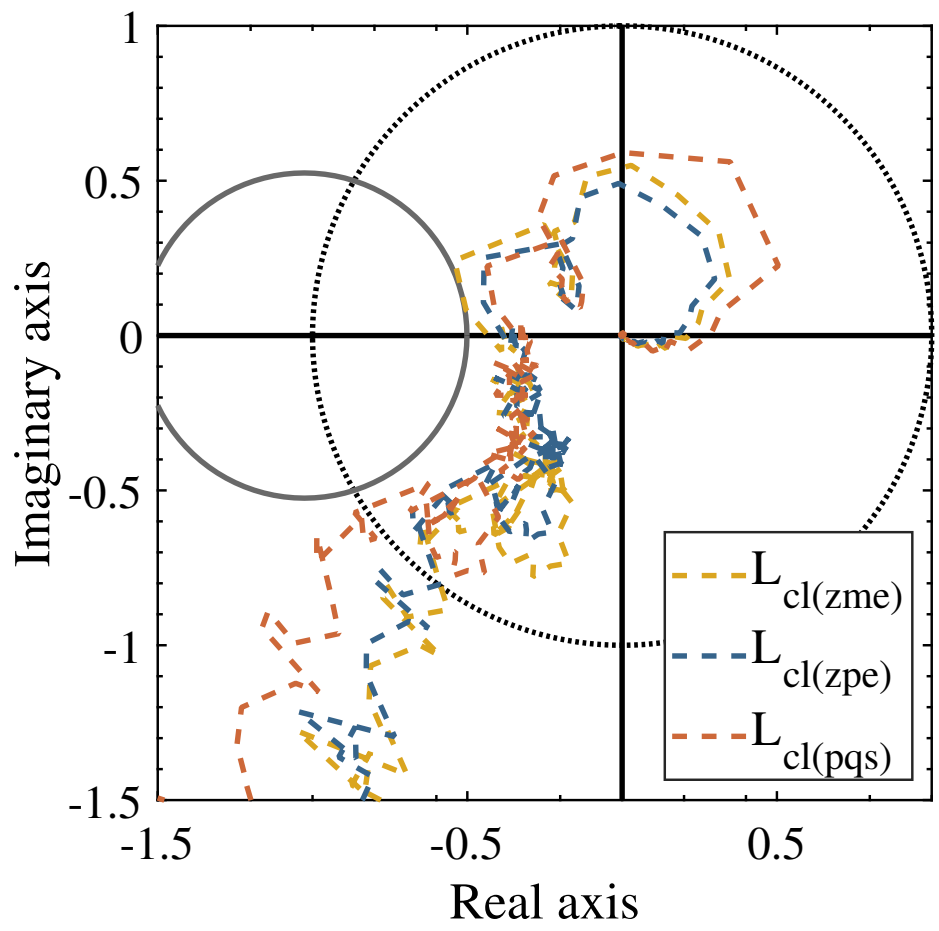

Figure 7.6 Nyquist plots of open loop function for DOB plus outer loop feedback controller in low pass filter design for cases of when $P_{zme}(s)$ and $P_{zpe}(s)$ are used ($L_{cl(zme)}$ and $L_{cl(zpe)}$) and case of tuning nominal plant model and Q filter simultaneously in s domain ($L_{cl(pqs)}$). From this figure, combining employed feedback controller C_{fb} with proposed DOBs does not have any stability problem.

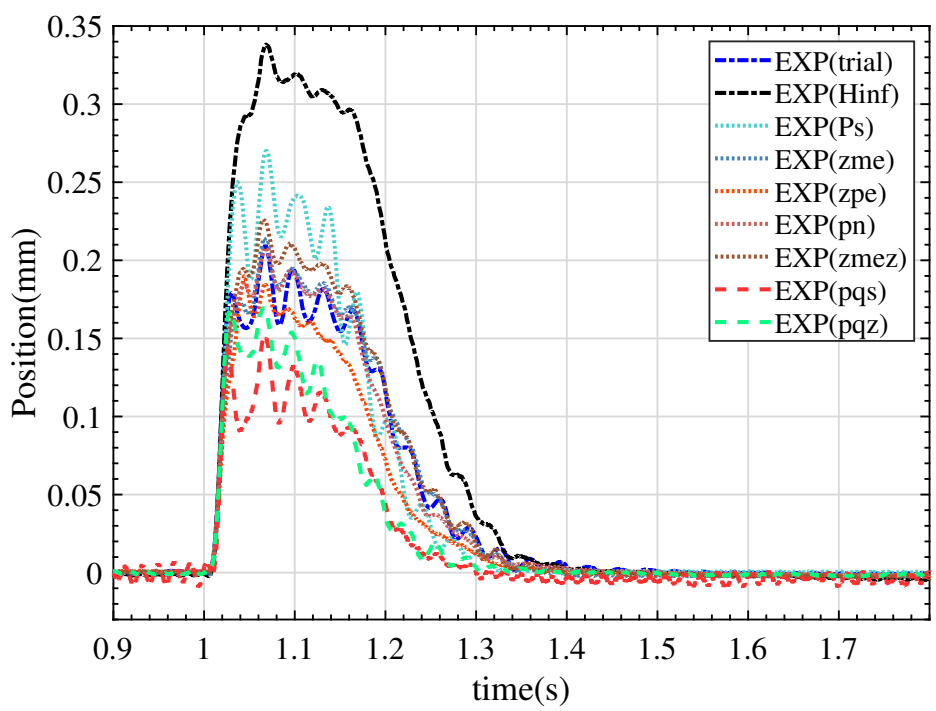

Figure 7.7 Figure of experimental disturbance rejection performance in terms of position response. In this figure, totally nine different cases of experiment have been conducted. Firstly, the DOB designed by trial-and-error method (EXP(trial)) and DOB designed by H_∞ method (EXP(Hinf)) are shown. Thereafter, DOBs designed by proposed methods starting from low pass filter design in continuous domain including case of second order approximation of non-minimum phase plant model is used (EXP(Ps)), case of ZME approximation of non-minimum phase plant model is used (EXP(zme)), case of ZPE approximation of non-minimum phase plant model is used (EXP(zpe)) along with case of non-minimum phase plant model is used (EXP(pn)) have been present. Then DOB designed in discrete domain (EXP(zmez)) is shown. Finally, DOBs designed by tuning the nominal plant model and low pass filter together in continuous domain (EXP(pqs)) as well as in discrete domain (EXP(pqz)) have also been implemented. The best disturbance rejection performance is found in EXP(pqs) case in terms of $||e||_\infty$.

Table 7.1 Summary of experimental results for a non-minimum phase motion stage

Cases	Employed nominal plant	Bandwidth [rad/s]	$\|\|e\|\|_\infty$
low pass filter design (s domain)	1. second order nominal plant 2. ZME of non-minimum phase plant 3. ZPE of non-minimum phase plant 4. non-minimum phase plant	1. 30.8 2. 37.4 3. 43.0 4. 38.2	1. 0.270 2. 0.214 3. 0.190 4. 0.208
low pass filter design (z domain)	discretized from ZME of non-minimum phase plant	36.3	0.226
nominal plant model identification and low pass filter design (s domain)	obtained from optimization process	47.8	**0.151**(smallest)
nominal plant model identification and low pass filter design (z domain)	obtained from optimization process	45.6	0.170
trial-and-error method	non-minimum phase plant	38.1	0.210
H_∞ method	non-minimum phase plant	25.5	0.338

Chapter 8

Conclusion

This thesis has proposed a frequency response data-based auto-tuning method to maximize the bandwidth of disturbance observer by convex optimization in order to reduce the harmful effects of disturbances in applications of precision machine.

FRD-based low pass filter design is investigated in Chapter 3 in which a systematic design methodology has been proposed (design procedures can be found in section 3.2.5). Importantly, proposed methods are also applicable to non-minimum phase plant, which is difficult to handle and has special characteristics, *e.g.* unstable inversion. Thereafter, for the first time in disturbance observer design, identification of nominal plant model and design of low pass filter have been accomplished simultaneously by an auto-tuning process proposed in Chapter 4 (see design procedures in section 4.2.6) irrespective of whether the system is minimum phase or non-minimum phase. Furthermore, the separation method of nominal plant model and low pass filter from optimized open loop function has been presented. Moreover, auto-tuning process to design a large bandwidth disturbance observer in discrete domain has also been investigated which is promising in terms of implementation (see design procedures in section 3.3.5 and 4.3.6).

Proposed methods have turned the original non-convex design problem into a convex optimization problem by transforming original non-convex constraints to convex constraints by mathematical derivation process in Chapter 3 and Chapter 4. Newly-obtained convex constraints are sufficient condition of original constraints and thus, obtained optimal point undoubtedly satisfies the original optimization problem also. By using ordinary optimization software, the bandwidth-maximized disturbance observer can be designed. Additionally, compared to existing methods, proposed methods neither have trial-and-error process nor require repetitive selection process of weighting functions. Moreover, since frequency response data is directly employed in the design process, the effort in careful identification of parametric nominal plant model can be decreased.

Case studies have been conducted to verify the feasibility of proposed methods in Chapter 5 and Chapter 6. For both minimum phase system and non-minimum phase system, optimized DOBs realize the maximized bandwidth and satisfy pre-defined constraints (see Table 5.2 and Table 6.2). Identifying nominal plant model and designing low pass filter at the same time has obtained largest bandwidth due to more tuning freedom and discrete domain design performs comparatively as continuous domain design. Additionally, larger bandwidth has been obtained by proposal compared to existing methods.

Finally, proposed disturbance observers have been implemented to a non-minimum phase motion stage in Chapter 7 and satisfactory disturbance rejection performance has been obtained (results have been summarized in Table 7.1). In terms of $||e||_\infty$, identifying nominal plant model and designing low pass filter

at the same time in continuous domain has provided the minimum value which means best disturbance rejection performance.

In summary, the contributions of this thesis can be enumerated as following:

1. Systematic methodologies with less design effort, which directly employ the numerical data of the frequency characteristics of the control target measured for plant identification rather than an approximate mathematical plant model, have been developed for designing disturbance observer with maximized bandwidth.
2. Identifying the nominal plant model and designing the low pass filter at the same time in an auto-tuning process for obtaining maximal bandwidth disturbance observer has been proposed.
3. Numerical case studies as well as experimental applications to a non-minimum phase motion stage have verified the usefulness of proposed methods.

8.1 Future work

1. Relationship between quality of frequency response data and design result
   Since this thesis is a frequency response data-based research, the quality of frequency response data matters. Quality refers to the range, the density, the influences of noise *etc.* From a practical point of view, low frequency range data may be influenced by friction and high frequency range data may be influenced by the resolution of encoder. The influence of quality issues on disturbance observer design shall be investigated in depth.
2. Outer loop feedback controller design
   This thesis focused on the design of inner loop which is disturbance observer part. However, the selection of outer loop feedback controller has an impact on the performance of whole system. Designing an appropriate controller for realizing good disturbance rejection as well as reference tracking is one direction to extend the current work. The design could use an iterative double-layer nested optimization algorithm in which feedback controller is in the outer layer and DOB design is in the inner layer. In every iteration, inner layer DOB is the first one to be optimized and then outer layer feedback controller is to be optimized.
3. Multi-input-multi-output (MIMO) system design
   This thesis has conducted the DOB design for single-input-single-output (SISO) system. However, many practical applications need to be modeled as MIMO system (*e.g.* load side disturbance rejection problem) and its FRD-based design shall be studied.

Appendix A:

Control hardware setup

① Experimental test bench control hardware introduction

As shown in Fig. A.1, the whole setup contains two motor drivers and a PMAC controller. Two motor drivers (G-SOLTW10/100EE7) belong to Elmo Gold Solo series. PMAC is a CK3M series product and takes position signals from two motor drivers and provides current reference signals to both of them by Ethercat. The sampling frequency of PMAC is set as 4 [kHz] and current controller bandwidth of motor drivers are adjusted as around 1 [kHz]. Two Heidenhain encoders whose resolution are 100 [nm], of which one is absolute type and the other is incremental type, are used to record position signals.

② Notes on setting up machine

1. Measurement of parameter of motor

   Before setting up the motor driver, back emf should be measured. By connecting each phase correctly to the oscilloscope probes and moving the motor by hand, waveforms can be captured on oscilloscope. Since one period of back emf waveform corresponds to a distance of $2\tau_p$ (pole pitch) and the time t_p for one period can be recognized from oscilloscope, velocity can be obtained as $\frac{2\tau_p}{t_p}$. Furthermore, linear relationship exists between back emf and velocity, then back emf corresponds to a velocity of 1 [m/s] can be obtained.

2. Procedures of setting up motor driver

   By connecting a motor driver to a laptop by an USB cable, the motor driver can be well tuned by utilizing an user-friendly interface called as Elmo application studio (EASII) developed by ELMO company as shown in Fig. A.2. By inputting all the necessary information, such as the encoder resolution and current limit, the connection between encoder, motor and motor driver can be well built. Furthermore, the movement of motor can be verified after current controller and position controller have been tuned. Importantly, in our experiment, the torque control mode is selected which means only the designed current controller of motor driver is employed. After finishing all setup procedures of motor drivers, motor drivers should be connected to PMAC rather than the laptop by Ethercat cable.

3. Procedures of setting up PMAC

   The PMAC should be connected to a laptop by an Ethernet cable and setup of PMAC is done by an interface called as PowerPmac IDE.

   Firstly, signals transmission environment which is Ethercat should be built. It is done by appending slaves to master under system item in solution explorer as shown in Fig. A.3. Furthermore, each slave should be connected to one motor. Signals on transmission line should be defined by the user

by setting up PDO mapping (Fig. A.4). In my setting, the position signal is taken from motor driver and control word as well as current reference are sent back to motor driver. The control word signal is of significant importance in protecting motor from over-current damage. Other signals can also be taken, such as current velocity or torque, as long as PDO mapping is well defined. After loading mapping to PMAC and activating the Ethercat, the Ethercat transmission environment can be successfully built.

The next step is to set up the PMAC to recognize position signals which is shown in Fig. A.5. The control type as well as the encoder resolution can be defined. After finishing this step, the PMAC should be able to recognize position signals in defined units, in this case, millimeter.

The final step is to implement the designed disturbance observer as well as the feedback controller by C code written in rticplc.c file (which is in C language item combo box).

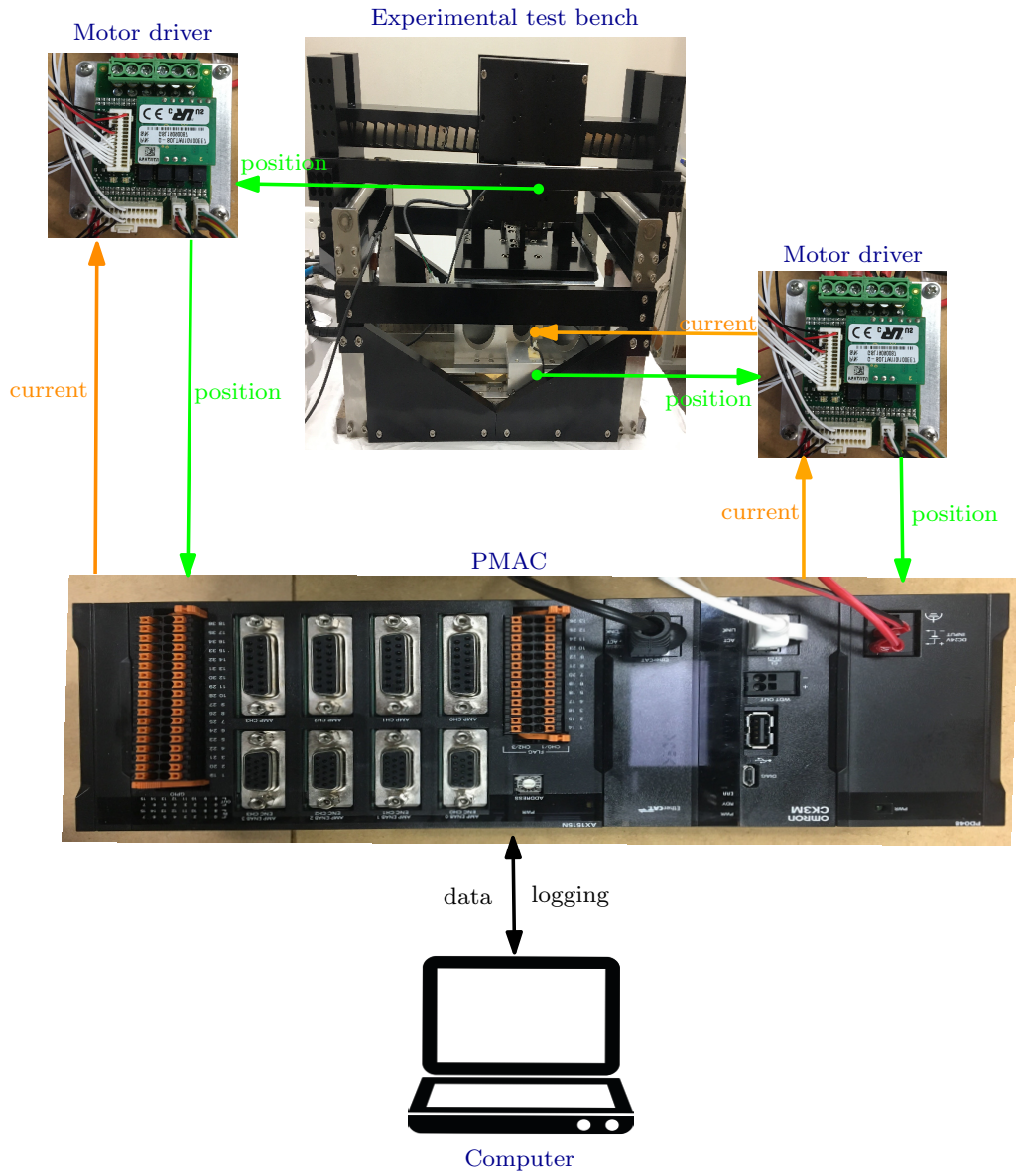

Figure A.1 Control hardware setup for experiment

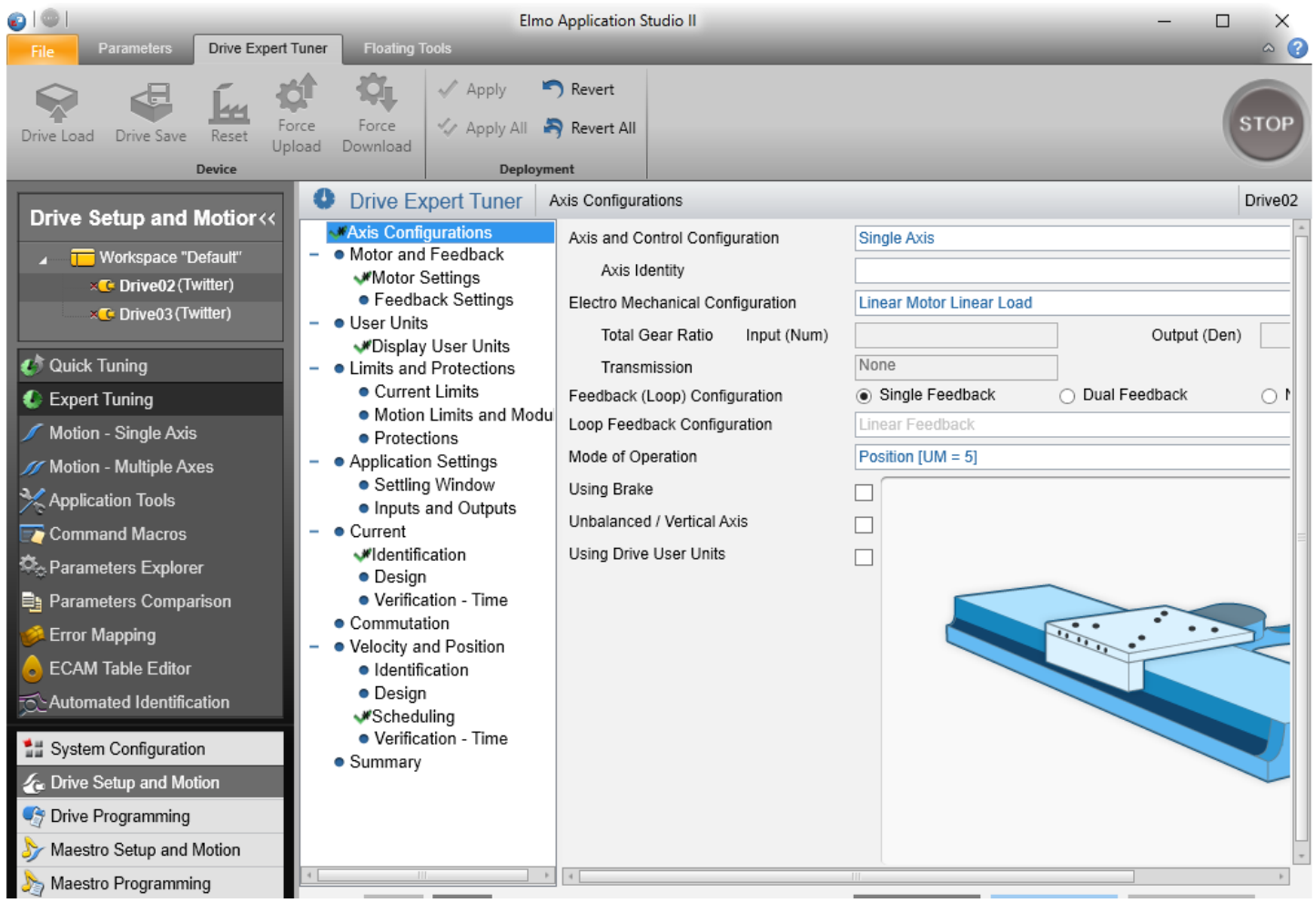

Figure A.2 Interface of EASII

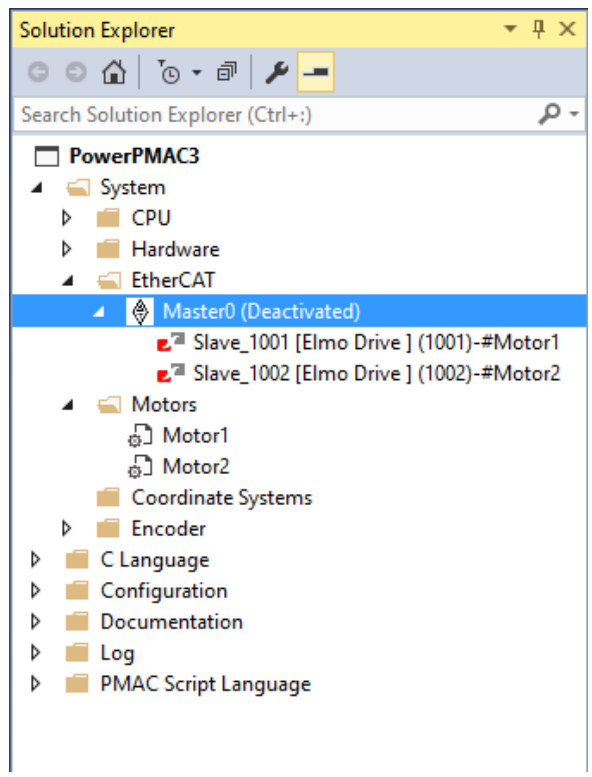

Figure A.3 Interface of IDE

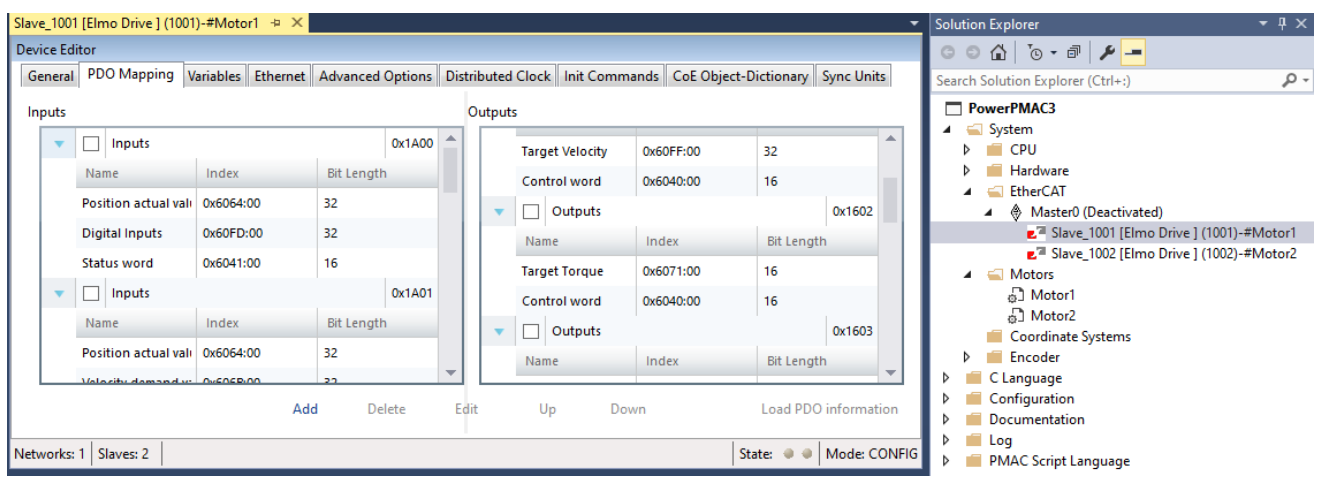

Figure A.5 Figure of PDO mapping

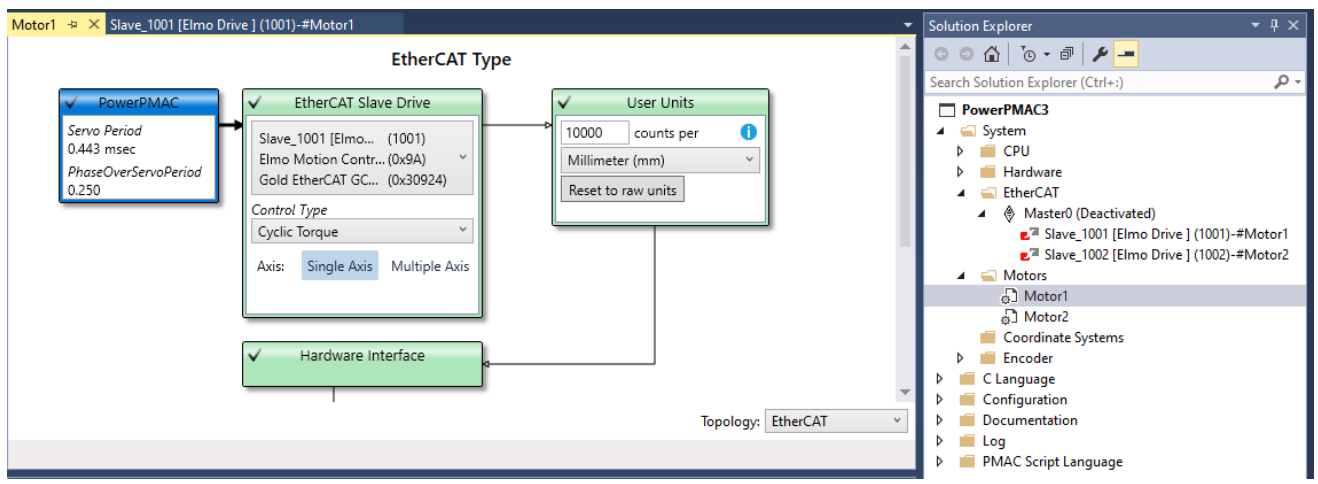

Figure A.5 Figure of motor setup in IDE

References

[1] C. Zhong, Z. Chen and Y. Guo, "Attitude control for flexible spacecraft With disturbance rejection", IEEE Transactions on Aerospace and Electronic Systems, vol. 53, no. 1, pp. 101-110, 2017. doi: 10.1109/TAES.2017.2649259.

[2] P. Albertos, R. Sanz and P. Garcia, "Disturbance rejection: a central issue in process control", Proceedings of International Conference on Systems and Control, pp. 1-8, 2015. doi: 10.1109/I-CoSC.2015.7153309.

[3] T. Umeno and Y. Hori, "Robust speed control of dc servomotors using modern two degrees-of-freedom controller design", IEEE Transactions on Industrial Electronics, vol. 38, no. 5, pp. 363–368, 1991.

[4] T. Umeno, T. Kaneko and Y. Hori, "Robust servosystem design with two degrees of freedom and its application to novel motion control of robot manipulators", IEEE Transactions on Industrial Electronics, vol. 40, no. 5, pp. 473-485, 1993, doi: 10.1109/41.238016.

[5] S. Komada, N. Machii and T. Hori, "Control of redundant manipulators considering order of disturbance observer", IEEE Transactions on Industrial Electronics, vol. 47, no. 2, pp. 413-420, 2000.

[6] C. K. Thum, C. Du, F. L. Lewis, B. M. Chen and E. H. Ong, "$\mathcal{H}_\infty$ disturbance observer design for high precision track following in hard disk drives", IET Control Theory & Applications, vol. 3, no. 12, pp. 1591-1598, 2009, doi: 10.1049/iet-cta.2008.0317.

[7] Z. Gao, "On the centrality of disturbance rejection in automatic control", ISA Transactions, vol. 4, no. 53, pp. 850–857, 2014.

[8] L. L. Xie and L. Guo, "How much uncertainty can be dealt with by feedback?", IEEE Transactions on Automatic Control, vol. 45, no. 12, pp. 2203–2217, 2000.

[9] E. Sariyildiz, R. Oboe and K. Ohnishi, "Disturbance observer-based robust control and its applications: 35th anniversary overview", IEEE Transactions on Industrial Electronics, vol. 67, no. 3, pp. 2042-2053, 2020, doi: 10.1109/TIE.2019.2903752.

[10] B. A. F Francis and W. M. Wonham, "The internal model principle for linear multivariable regulators", Applied Mathematics and Optimization 2, vol. 2, pp. 170–194, 1975.

[11] J. C. Doyle, "Structured uncertainty in control system design", Proceedings of IEEE Conference on Decision and Control, pp. 260–265,1985.

[12] E. Sariyildiz and K. Ohnishi, "Analysis the robustness of control systems based on disturbance observer", International Journal of Control, vol. 86, no. 10, pp. 1733–1743, 2013.

[13] J. Han, "A Class of Extended State Observers for Uncertain Systems" , Control and Decision, vol. 10, no. 1, pp. 85-88, 1995.

[14] Q. C. Zhong, A. Kuperman, and R. K. Stobart, "Design of UDE-based controllers from their two-degree-of-freedom nature", International Journal of Robust Nonlinear Control, vol. 21, no. 17, pp.

1994–2008, 2011.

[15] K. Ohishi, K. Ohnishi, and K. Miyachi, "Torque-speed regulation of DC motor based on load torque estimation method", Proceedings of International Power Electronics Conference, pp. 1209-1218, 1983.

[16] H. Fujimoto, K. Fukushima and S. Nakagawa, "Vibration suppression short-span seeking of HDD with multirate feedforward control", Proceedings of American Control Conference, pp. 582-587, 2006. doi: 10.1109/ACC.2006.1655419.

[17] A. Hara, K. Saiki, K. Sakata, and H. Fujimoto, "Basic examination on simultaneous optimization of mechanism and control for high precision single axis stage and experimental verification", Proceedings of the Conference of IEEE Industrial Electronic, pp. 2509-2514, 2008.

[18] H. Butler, "Position control in lithographic equipment [applications of control]", IEEE Control Systems Magazine, vol. 31, no. 5, pp. 28-47, 2011, doi: 10.1109/MCS.2011.941882.

[19] J. B. Hoagg and D. S. Bernstein, "Nonminimum-phase zeros - much to do about nothing - classical control - revisited part II", IEEE Control Systems Magazine, vol. 27, no. 3, pp. 45-57, 2007, doi: 10.1109/MCS.2007.365003.

[20] T. Mita and H. Yoshida, "Undershooting phenomenon and its control in linear multivariable servomechanisms", IEEE Transactions on Automatic Control, vol. 26, no. 2, pp. 402-407, 1981, doi: 10.1109/TAC.1981.1102601.

[21] M. Vajta, "Some Remarks on Padé-Approximations", 3rd TEMPUS-INTCOM Symposium, pp. 251-256, 2000.

[22] S. Skogestad and I. Postletyhwaite, Multivariable feedback control: analysis and design, Wiley.

[23] G. C. Goodwin, S. F. Graebe and M. E. Salgado, Control system design, Pearson, 2000.

[24] B. A Guvenc, L. Guvenc and S. Karaman, "Robust MIMO disturbance observer analysis and design with application to active car steering", International Journal of Robust and Nonlinear Control, vol. 20, no. 8, pp. 873-891, 2010.

[25] H. Fujimoto, T. Saito, and T. Noguchi, "Motion stabilization control of electric vehicle under snowy conditions based on yaw-moment observer", Proceedings of IEEE International Workshop on Advanced Motion Control, pp. 35–40, 2004.

[26] K. Yang, Y. Choi and W. K. Chung, "On the tracking performance improvement of optical disk drive servo systems using error-based disturbance observer", IEEE Transactions on Industrial Electronics, vol. 52, no. 1, pp. 270-279, 2005.

[27] K. Ohishi, T. Miyazaki and Y. Nakamura,"High performance ultra-low speed servo system based on doubly coprime factorization and instantaneous speed observer", IEEE/ASME Transactions on Mechatronics, vol. 1, no. 1, pp. 89-98, 1996.

[28] L. Wang and J. Su, "Robust disturbance rejection control for attitude tracking of an Aircraft", IEEE Transactions on Control Systems Technology, vol. 23, no. 6, pp. 2361–2368, 2015.

[29] Y. Nakajima, T. Nozaki and K. Ohnishi, "Heartbeat synchronization with haptic feedback for telesurgical robot", IEEE Transactions on Industrial Electronics, vol. 61, no. 7, pp. 3753–3764, 2014.

[30] B. Ugurlu, M. Nishimura, K. Hyodo, M. Kawanishi and T. Narikiyo, "Proof of concept for robot-aided upper limb rehabilitation using disturbance observers", IEEE Transactions on Human-Machine Systems, vol. 45, no. 1, pp. 110–118, Feb. 2015.

[31] https://industrial.panasonic.com/ww.

[32] K. Ohnishi and T. Mizoguchi, "Real haptics and its applications", IEEJ Transactions On Electrical

And Electronic Engineering, vol. 12, pp. 803–808, 2017.

[33] K. Ohishi, T. Miyazaki and Y. Nakamura, "Two-degrees-of-freedom speed controller based on doubly coprime factorization and speed observer", IEEE International Conference on Industrial Electronics, Control, and Instrumentation, pp. 602–608, 2015.

[34] K. Ohnishi, M. Shibata and T. Murakami, 1996, "Motion Control for Advanced Mechatronics", IEEE/ASME Transactions on Mechatronics, vol. 1, no. 1, pp. 56–67, 1996.

[35] W. C. Yang and M. Tomizuka, "Disturbance rejection through an external model for non-minimum phase systems", Journal of Dynamic Systems, Measurement, and control, vol. 116, no. 1, pp. 39–44, 1994.

[36] N. H. Jo, H. Shim and Y. I. Son, "Disturbance observer for nonminimum phase linear systems", International Journal of Control, Automation and Systems, vol. 8, pp. 994–1002, 2010.

[37] X. Chen, G. Zhai and T. Fukuda, "An approximate inverse system for non-minimum-phase systems and its application to disturbance observer", System & Control Letters , vol. 52, no. 3-4, pp. 193–207, 2004.

[38] J. Yang, W. H. Chen and S. Li, "Nonlinear disturbance observer based robust control for systems with mismatching disturbances/uncertainties", IET Control Theory & Applications, vol. 5, no. 18, pp. 2053-2062, 2011.

[39] W. H. Chen, D. J. Ballance, P. J. Gawthrop and J. O'Reilly, "A nonlinear disturbance observer for robotic manipulators", IEEE Transactions on Industrial Electronics, vol. 47, no. 4, pp. 932-938, 2000, doi: 10.1109/41.857974.

[40] X. K. Chen, T. Fukuda and K. D. Young, "A new nonlinear robust disturbance observer Systems", System & Control Letters, vol. 41, no. 3, pp. 189-199, 2000.

[41] W. H. Chen, "Disturbance observer based control for nonlinear systems", IEEE/ASME Transactions on Mechatronics, vol. 9, no. 4, pp. 706–710, 2004.

[42] W. H. Chen, J. Yang, L. Guo and S. Li, "Disturbance-observer-based control and related methods —an overview", IEEE Transactions on Industrial Electronics, vol. 63, no. 2, pp. 1083-1095, 2016.

[43] S. Li, J. Yang, W. H. Chen and X. Chen, Disturbance observer based control: methods and applications, CRC Press, 2014.

[44] H. Shim and N. H. Jo, "An almost necessary and sufficient condition for robust stability of closed-loop systems with disturbance observer", Automatica, vol. 45, no.1, pp. 296–299, 2008.

[45] E. Schrijver and D.V. Johannes, " Disturbance observers for rigid mechanical systems: equivalence, stability, and design", Journal of Dynamic Systems, Measurement, and Control, vol. 124, no. 4, pp. 539-548, 2002.

[46] Y. Choi, K. Yang, W. K. Chung, H. R. Kim and I. H. Suh, "On the robustness and performance of disturbance observers for second-order systems", IEEE Transactions on Automatic Control, vol. 48, pp. 315-320, 2003.

[47] K. Yang, Y. Choi, W. K. Chung, I. L. Suh and S. R. Oh, "Robust tracking control of optical disk drive systems using error based disturbance observer and its performance measure", Proceedings of the American Control Conference, pp. 1395-1400, 2002.

[48] K. Kong and M. Tomizuka, "Nominal model manipulation for enhancement of stability robustness for disturbance observer-based control systems", International Journal of Control, Automation and Systems, vol. 11, pp. 12–20, 2013.

[49] N. Yun and J. Sun, "Design of a disturbance observer for a two-link manipulator with flexible joints", IEEE Transactions on Control Systems Technology, vol. 22, no. 2, pp. 809-815, 2014, doi: 10.1109/TCST.2013.2248733

[50] C. C. Wang and M. Tomizuka, "Design of robustly stable disturbance observers based on closed loop consideration using $\mathcal{H}_\infty$ optimization and its applications to motion control systems", Proceedings of the American Control Conference, pp. 3764-3769, 2004.

[51] E. Sariyildiz and K. Ohnishi, "Bandwidth Constraints of Disturbance Observer in the Presence of Real Parametric Uncertainties", European Journal of Control, vol. 19, no. 3, pp. 199-205, 2013, https://doi.org/10.1016/j.ejcon.2013.03.009

[52] S. Hyungbo and J. Young-Jun, "State space analysis of disturbance observer and a robust stability condition", Proceedings of IEEE Conference on Decision and Control, pp. 2193-2198, 2007.

[53] N. H. Jo, C. Jeon and H. Shim, "Noise reduction disturbance observer for disturbance attenuation and noise suppression", IEEE Transactions on Industrial Electronics, vol. 64, no. 2, pp. 1381-1391, 2017, doi: 10.1109/TIE.2016.2618858.

[54] J. Han, H. Kim, Y. Joo, N. H. Jo and J. H. Seo, "A simple noise reduction disturbance observer and Q-filter design for internal stability", Proceedings of International Conference on Control, Automation and Systems, pp. 755-760, 2013, doi: 10.1109/ICCAS.2013.6704014.

[55] X. Chen and M. Tomizuka, "Optimal plant shaping for high bandwidth disturbance rejection in discrete disturbance observers", Proceedings of the American Control Conference, pp. 2641-2646, 2010.

[56] I. Godler, H. Honda and K. Ohnishi, "Design guidelines for disturbance observer's filter in discrete time", International Workshop on Advanced Motion Control, pp. 390-395, 2002.

[57] G. Park and H. Shim, "A generalized framework for robust stability analysis of discrete-time disturbance observer for sampled-data systems: a fast sampling approach", Proceedings of International Conference on Control, Automation and Systems, pp. 295-300, 2015.

[58] T. Uzunovic, E. Sariyildiz and A. Sabanovic,"A discussion on discrete implementation of disturbance-observer-based control", International Workshop on Advanced Motion Control, pp. 613-618, 2018.

[59] C. Kempf and S. Kobayashi, "Disturbance observer and feedforward design for a high-speed direct-drive positioning table", IEEE Transactions on Control Systems Technology, vol. 7, no. 5, pp. 513-526, 1999, doi: 10.1109/87.784416

[60] E. Sariyildiz and K. Ohnishi, "A new solution for the robust control problem of non-minimum phase systems using disturbance observer", IEEE International Conference on Mechatronics, pp. 46-51, 2013.

[61] E. Sariyildiz and K. Ohnishi, "A Guide to design disturbance observer", Journal of Dynamic Systems, Measurement, and Control, vol. 136, no. 2, 021011, 2014.

[62] E. Sariyildiz, S. Hangai, T. Uzunovic, T. Nozaki and K. Ohnishi, "Stability and robustness of the disturbance observer-based motion control systems in discrete-time domain", IEEE/ASME Transactions on Mechatronics, doi: 10.1109/TMECH.2020.3032115.

[63] H. Shim, N. H. Jo and Y. Son, "A new disturbance observer for non-minimum phase linear systems", Proceedings of American Control Conference, pp. 3385-3389, 2008.

[64] Y. I. Son, Hyungbo Shim, N. H. Jo and Sung Jong Kim, "Design of disturbance observer for non-minimum phase systems using PID controllers", SICE Annual Conference, pp. 196-201, 2007, doi:

10.1109/SICE.2007.4420976.

[65] A. Tesfaye, H. S. Lee and M. Tomizuka, "A sensitivity optimization approach to design of a disturbance observer in digital motion control systems", IEEE/ASME Trans. Mechatron, vol. 5, no. 1, pp. 32-38, 2000.

[66] X. Chen, J. Yang, S. Li and Q. Li , "Disturbance observer based multi-variable control of ball mill grinding circuits", Journal of Process Control, vol. 19, no. 7, pp. 1205-1213, 2009.

[67] P. Zhou, T. Chai and J. Zhao, "DOB design for nonminimum-phase delay systems and its application in multivariable MPC control", IEEE Transactions on Circuits and Systems II: Express Briefs, vol. 59, no. 8, pp. 525-529, 2012, doi: 10.1109/TCSII.2012.2204844.

[68] J. Yang, S. Li, X. Chen and Q. Li, "Disturbance rejection of dead-time processes using disturbance observer and model predictive control", Chemical Engineering Research and Design, vol. 89, no. 2, pp. 125-135, 2011.

[69] J. Su, L. Wang and J. N. Yun, "Disturbance rejection control for non-minimum phase systems with optimal disturbance observer", ISA Transactions, vol. 57, pp. 1-9, 2015.

[70] L. Wang and J. Cheng, "Robust disturbance rejection methodology for unstable non-minimum phase systems via disturbance observer", ISA Transactions, vol. 100, pp. 1-12, 2020.

[71] Z. S. Hou and Z. Wang, "From model-based control to data-driven control: Survey, classification and perspective", Information Sciences, vol. 253, no. 20, pp. 3-35, 2013. https://doi.org/10.1016/j.ins.2012.07.014.

[72] S. Yin, X. Li, H. Gao and O. Kaynak, "Data-based techniques focused on modern industry: an overview", IEEE Transactions on Industrial Electronics, vol. 62, no.1, pp. 657–667, 2015.

[73] A. S. Bazanella, L. Campestrini and D. Eckhard, Data-driven Controller Design: The $\mathcal{H}_2$ Approach, Springer Netherlands, 2012.

[74] S. Formentin, K. van Heusden and A. Karimi, "A comparison of model-based and data-driven controller tuning", International Journal of Adaptive Control and Signal Processing, vol. 28, no. 10, pp. 882–897, 2014.

[75] M. Campi, A. Lecchini and S. Savaresi, "Virtual reference feedback tuning: a direct method for the design of feedback controllers", Automatica, vol. 38, no. 8, pp. 1337-1346, 2002.

[76] M. Safonov and T. C. Tsao, "The unfalsified control concept: A direct path from experiment to controller", Feedback Control, Nonlinear Systems, and Complexity, pp. 196-214, 1994.

[77] H. Hjalmarsson, S. Gunnarsson and M. Gevers, "A convergent iterative restricted complexity control design scheme", IEEE Conference on Decision and Control, vol. 2, pp. 1735-1740, 1994, doi: 10.1109/CDC.1994.411185.

[78] Z. Hou, Nonparametric models and its adaptive control theory, Science Press, 1999.

[79] K. Moore, "Iterative learning control for deterministic systems", Automatica, vol. 6, no. 32, pp. 948-949.

[80] A. Karimi, L. Miskovic and D. Bonvin, "Convergence analysis of an iterative correlation-based controller tuning method", IFAC Proceedings Volumes, vol.35, no. 1, pp. 413-418, 2002.

[81] I. M. Horowitz, Quantitative feedback theory, Publications Boulder, Colorado, 1993.

[82] R. Hoogendijk, A. den Hamer, G. Angelis, R. van de Molengraft and M. Steinbuch, "Frequency response data based optimal control using the data based symmetric root locus", IEEE International Conference on Control Applications, pp. 257-262, 2010, doi: 10.1109/CCA.2010.5611199.

[83] L. H. Keel and S. P. Bhattacharyya, "Controller Synthesis Free of Analytical Models: Three Term Controllers", IEEE Transactions on Automatic Control, vol. 53, no. 6, pp. 1353-1369, 2008, doi: 10.1109/TAC.2008.925810.

[84] A. Karimi, M. Kunze and R. Longchamp, "Robust controller design by linear programming with application to a double-axis positioning system", Control Engineering Practice, vol. 15, no. 2, pp. 197-208, 2007.

[85] M. Saeki, "Data-driven loop-shaping design of PID controllers for stable plants", International Journal of Adaptive Control and Signal Processing, vol. 28, no. 12, pp. 1325-1340, 2014.

[86] A. Karimi and G. Galdos, "Fixed-order $\mathcal{H}_\infty$ controller design for nonparametric models by convex optimization", Automatica, vol. 46, pp. 1388-1394, 2010.

[87] M. Hast, K. J. Åström, B. Bernhardsson, and S. Boyd, "PID design by convex-concave optimization", Proceedings of the European Control Conference, pp. 4460-4465, 2013.

[88] K. Nakamura, K. Yubai, D. Yashiro, and S. Komada, "Controller design method achieving maximization of control bandwidth by using Nyquist diagram", Proceedings of the International Automatic Control Conference, pp. 35-40, 2016.

[89] A. Karimi, A. Nicoletti, and Y. Zhu, "Robust $\mathcal{H}_\infty$ controller design using frequency-domain data via convex optimization", International Journal of Robust and Nonlinear Control, vol. 28, no. 12, pp. 3766-3783, 2018.

[90] A. Nicoletti, M. Martino and A. Karimi, "A data-driven approach to power converter control via convex optimization", IEEE Conference on Control Technology and Applications, pp. 1466-1471, 2017, doi: 10.1109/CCTA.2017.8062665.

[91] G. Galdos, A. Karimi and R. Longchamp, "$\mathcal{H}_\infty$ controller design for spectral MIMO models by convex optimization", Journal of Process Control, vol. 20, pp. 1175-1182, 2010.

[92] A. Karimi, "Frequency-domain robust control toolbox", IEEE Conference in Decision and Control, pp. 3744–3749, 2013.

[93] M. Saeki, M. Ogawa and N. Wada, "Low-order $\mathcal{H}_\infty$ controller design on the frequency domain by partial optimization", International Journal of Robust and Nonlinear Control, vol. 20, no. 3, pp. 323-333, 2010.

[94] S. Shinoda, K. Yubai, D. Yashiro and J. Hirai, "Fully parameterized multivariable controller design minimizing closed-loop interaction by iterative LMI optimization", IEEJ international workshop on Sensing, Actuation, and motion Control, TT3-6, 2016.

[95] A. Karimi and C. Kammer, "A data-driven approach to robust control of multivariable systems by convex optimization", Automatica, vol. 85, pp. 227-233, 2017.

[96] A. J. Den Hamer, S. Weiland and M. Steinbuch, "Model-free norm-based fixed structure controller synthesis", Proceedings of the IEEE Conference on Decision and Control held jointly with Chinese Control Conference, pp. 4030-4035, 2009.

[97] S. Khadraoui, H. Nounou, M. Nounou, A. Datta and S. Bhattacharyya, "A measurement-based approach for designing reduced order controllers with guaranteed bounded error", International Journal of Control, vol. 86, no.9, pp. 1586-1596, 2013.

[98] S. Boyd and L. Vandenberghe, Convex Optimization, Cambridge University Press, 2004.

[99] S. Boyd, L. El Ghaoui, E. Feron, and V. Balakrishnan, Linear Matrix Inequalities in System and Control Theory, Society for Industrial and Applied Mathematics, 1994.

[100] S. Boyd. Sequential Convex Programming, 2013.

[101] A.L. Yuille and A. Rangarajan. "The concave-convex procedure", Neural Computation, vol. 15, no. 4, pp. 915-936, 2003.

[102] S. Boyd, M. Hast and K. J. Åström, "MIMO PID tuning via iterated LMI restriction", International Journal of Robust and Nonlinear Control, vol. 26, no. 8, pp. 1718-1731, 2016.

[103] J. Löfberg, "YALMIP : a toolbox for modeling and optimization in MATLAB", IEEE International Conference on Robotics and Automation, pp. 284-289, 2004.

[104] MOSEK ApS, MOSEK optimization toolbox for MATLAB manual, 2019.

[105] W. Ohnishi, T. Beauduin and H. Fujimoto, "Preactuated multirate feedforward control for independent stable inversion of unstable intrinsic and discretization Zeros", IEEE/ASME Transactions on Mechatronics, vol. 24, pp. 863-871, 2019.

[106] X. Wang, W. Ohnishi and T. Koseki, "Bandwidth maximization of disturbance observer based on experimental frequency response data", SICE Journal of Control, Measurement, and System Integration, vol. 13, no. 6, pp. 257-264, 2020.

[107] J. T. Wen and B. Potsaid, "An experimental study of a high performance motion control system", Proceedings of the American Control Conference, pp. 5158-5163, 2004.

[108] M. Tomizuka, "Zero phase error tracking algorithm for digital control", Journal of Dynamic Systems, Measurement, and Control, vol. 109, pp. 65-68, 1987.

[109] X. Wang, W. Ohnishi and T. Koseki, "Data-based simultaneous design of plant model and robust filter in disturbance observer", Proceedings of the American Control Conference, 2021.

[110] R. Pintelon and J. Schoukens, System Identification: A Frequency Domain Approach, 2nd ed. Wiley-IEEE Press, 2012

Publications

Journals

X. Wang, W. Ohnishi, T. Koseki, Bandwidth maximization of disturbance observer based on experimental frequency response data, SICE Journal of Control, Measurement, and System Integration, vol. 13, no. 6, pp. 257-264, 2020

X. Wang, W. Ohnishi, T. Koseki, Linear matrix inequality based data-driven disturbance observer design: With application to a non-minimum phase motion stage, Mechatronics (under review)

X. Wang, W. Ohnishi, T. Koseki, Frequency response data-based disturbance observer design: With application to a non-minimum phase motion stage, IEEE/ASME Transactions on Mechatronics (under review)

International Conferences

X. Wang, W. Ohnishi, T. Koseki, Frequency response data based disturbance observer design applicable to non-minimum phase systems, Annual Conference of the Society of Instrument and Control Engineers of Japan, 358-363, 2019 (published)

X. Wang, W. Ohnishi, T. Koseki, Frequency response data-based disturbance observer design via convex optimization, IFAC world congress, 2020 (accepted)

X. Wang, W. Ohnishi, T. Koseki, A summary of disturbance observer design methodology for non-minimum phase system, IEEJ international workshop on sensing, actuation, motion control, and optimization, 2021 (accepted)

X. Wang, W. Ohnishi, T. Koseki, Data-based simultaneous design of plant model and robust filter in disturbance observer, American control conference, 2021 (accepted)

Domestic Conferences

X. Wang, W. Ohnishi, T. Koseki, Causal design of Taylor series approximation in a disturbance observer for a non-minimum phase system, メカトロニクス制御研究会, 2018.

X. Wang, W. Ohnishi, T. Koseki, Experimental verification of FRD-based disturbance observer design for the non-minimum phase system compared with $\mathcal{H}_\infty$-based design, メカトロニクス制御研究会, 2020.